Physics – Uspekhi **62** (3) 215 – 248 (2019)

REVIEWS OF TOPICAL PROBLEMS PACS numbers: 03.75.Hh, **67.10. – j**, **74.20. – z**, 74.25.Uv

BCS – BEC crossover, collective excitations, and hydrodynamics of superfluid quantum liquids and gases

M Yu Kagan, A V Turlapov

DOI: https://doi.org/10.3367/UFNe.2018.10.038471

Contents

Abstract. A Fermi gas described within the Bardeen–Cooper–Schrieffer (BCS) theory can be converted into a Bose – Einstein condensate (BEC) of composite molecules (dimers) by adiabatically tuning the interaction. The sequence of states that emerge in the process of such a conversion is referred to as the BCS – BEC crossover. We here review the theoretical and experimental results obtained for the BCS – BEC crossover in three- and quasi-two-dimensional quantum gases in the limiting geometry of traps and on optical lattices. We discuss nontrivial phenomena in the hydrodynamics of superfluid quantum gases and fluids, including the collective excitation spectrum in the BCS – BEC crossover, the hydrodynamics of rotating Bose condensates containing a large number of quantized vortices, and the intriguing problem of the chiral anomaly in the hydrodynamics of superfluid Fermi systems with an anisotropic p-wave pairing. We also analyze spin-imbalanced quantum gases and the potential to realize the triplet p-wave pairing via the Kohn–Luttinger mechanism in those gases. Recent results on two-dimensional Fermi-gas preparation and the observation of fluctuation phenomena related to the Berezinskii–Kosterlitz–Thouless transition in those gases are also reviewed. We briefly discuss the recent experimental discovery of the BCS – BEC crossover and anomalous superconductivity in bilayer graphene and the role of graphene, other Dirac semimetals (for example, bismuth), and 2D optical lattices as potential reference systems that exhibit all of the effects reviewed here.

Keywords: BCS–BEC crossover, hydrodynamics of superfluid quantum fluids, Feshbach resonance, composite fermions and bosons, rotating Bose condensates, chiral anomaly, fermion Goldstone mode, collective excitation spectrum, imbalanced Fermi gas, anomalous pairing, Kohn–Luttinger mechanism, Berezinskii–Kosterlitz–Thouless transition, bilayer graphene

M Yu Kagan[(1, 2, *)], **A V Turlapov**[(3, †)]
[(1)] National Research University "Higher School of Economics," ul. Myasnitskaya 20, 101000 Moscow, Russian Federation
[(2)] Kapitza Institute for Physical Problems, Russian Academy of Sciences, ul. Kosygina 2, 119334 Moscow, Russian Federation
[(3)] Institute of Applied Physics, Russian Academy of Sciences, ul. Ul'yanova 46, 603950 Nizhny Novgorod, Russian Federation
E-mail: * kagan@kapitza.ras.ru, † turlapov@appl.sci-nnov.ru

Received 18 January 2018, revised 3 October 2018
Uspekhi Fizicheskikh Nauk **189** (3) 225 – 261 (2019)
DOI: https://doi.org/10.3367/UFNr.2018.10.038471
Translated by M Zh Shmatikov; edited by A M Semikhatov

1. Introduction

The physics of Bose condensation in ultracold quantum gases has been rapidly developing in recent decades, being explored using both experimental [1] and theoretical [2, 3] methods and attracting the attention of the scientific community both in Russia and abroad. The aim of this review is to present some interesting phenomena in this area, focusing primarily on the problem of the BCS–BEC crossover for extended and local pairs [4–12] and nontrivial hydrodynamic phenomena in superfluid Fermi–Bose gases and mixtures [13–18] (here and below, BCS is an abbreviation

for Bardeen–Cooper–Schrieffer and BEC is an abbreviation for Bose–Einstein condensate). We plot the global phase diagrams of three-dimensional and quasi-two-dimensional Fermi gases [19–22] in the Feshbach resonance regime [23] and analyze the spectrum of collective excitations [24–27] (sound and orbital waves, breathing modes in traps) and the contribution of those excitations to the thermodynamic properties (in particular, thermal capacity and normal density) in the fermion and boson areas of the phase diagram for superfluid s-wave and p-wave pairing [18]. We also determine critical velocities at which superfluidity breaks up by applying the Landau criterion [28] for extended (Cooper) and local pairs. In interconnecting the physics of high-temperature superfluidity and superconductivity, we solve the problem of composite fermions and bosons in resonance quantum gases and mixtures and plot corresponding phase diagrams [29–32].

We also review the BCS–BEC crossover scenario for the pairing of two composite holes (two spin polarons or two strings) in the d-wave channel for weakly doped cuprates [33]. Another bridge connecting the physics of ultracold gases and the physics of electrons in metals is the concept of a spatially separated Fermi–Bose mixture that was proposed by an author of this review to describe superconducting bismuth oxides in [34, 35]. In passing from the thermodynamic description to the hydrodynamic one, we outline the concept of Landau's classical approach to deriving hydrodynamic equations based on conservation laws written in differential form. In developing this approach, we work out the quantum hydrodynamics of rapidly rotating superfluid condensates [36] that contain a large number of quantum vortices [37–43] and analyze the interesting phenomena (in particular, the second-sound spectrum [16, 44] and the friction force between normal excitations and vortices [40, 42, 43]) that occur in that hydrodynamic system.

We outline other approaches to the development of complex hydrodynamic systems based, in particular, on applying generalized Poisson brackets [45, 46]. We explore the spectrum of Tkachenko waves [47, 48] and Lord Kelvin bending vibrations [49] specific to vortex lattices in rotating superfluid helium and analyze the behavior of the displacement correlator of vortex lines and the vortex-fluid–vortex-crystal transition in rotating Bose condensates with various densities and dimensions [18]. In applying this to anisotropic p-wave pairing in the A-phase of superfluid He-3 [50, 51] and in 100% polarized triplet Fermi gases, we explore in detail the involved and still unresolved problem of chiral anomaly [52–56] and the failure of the momentum conservation law for the superfluid component in fermionic systems with a nontrivial symmetry and zeros of the superfluid gap [52, 53] (see also later studies and monographs [18, 25, 50, 57–59]). In this context, we discuss two approaches to solve the problem. One is based on adding the fermionic Goldstone mode to the set of quantum hydrodynamic equations, and the other is based on a formal analogy between Bogoliubov–de Gennes equations [60, 61] for fermionic quasiparticles in the nonuniform distribution texture (liquid-crystal type [62]) of the orbital momentum vector $\mathbf{l}$ of a Cooper pair and the Dirac equation [63] for massless particles in the magnetic field $\mathbf{B} = \mathrm{rot}\,\mathbf{l}$.

From an experimental perspective, we review, in some detail, the significant progress made recently in designing traps for 2D Fermi gases [21, 22], the new options provided by those traps, and a class of problems that have not yet been resolved experimentally but will be in the future. In particular, we expect to obtain an experimental confirmation of the occurrence of Kohn–Luttinger anomalous superconductivity [64] for triplet p-wave pairing [65, 66] in a quasi-two-dimensional Fermi gas with strongly imbalanced 'up' and 'down' spins [67–69]. We also plan to experimentally determine the regions where nonuniform Larkin–Ovchinnikov–Fulde–Ferrell superconducting states [70, 71] and clustering and phase separation [72, 73] occur in imbalanced quasi-two-dimensional Fermi gases [74, 75].

Finally, we explore regions in the phase diagram of quasi-two-dimensional resonance gases where the Berezinskii–Kosterlitz–Thouless fluctuation corrections [76–82] to mean-field results [79, 83–85] for the BCS–BEC crossover manifest themselves most conspicuously. In responding to the problem of topological insulators and Dirac semimetals (in particular, graphene), which is currently enjoying great popularity, we briefly discuss the problems of how special (highly symmetric) Dirac points appear and vanish in quasi-two-dimensional hexagonal optical lattices [86] and how superconductive p-wave pairing [87, 88] occurs, induced by the proximity effect [89], in a graphene monolayer in contact with a bulk superconductor. We conclude this review with a brief discussion of the anomalous superconductivity and the BCS–BEC crossover in a twisted graphene bilayer [90], which have been discovered recently in experiments.

2. Feshbach resonance

One of the most significant events in condensed matter physics was the discovery in the 1990s of the BEC phenomenon [7] in bosonic ^{87}Rb, ^{23}Na, and ^{7}Li isotopes [1, 91, 92] in the restricted geometry of magnetic traps [93]. At the beginning of this century, in experiments performed in the Feshbach resonance regime [23] in dipole optical traps, Jin's [94], Grimm's [95], Ketterle's [96], and Salomon's [97] groups also discovered the Bose condensation of molecules (composite bosons) $^{40}K_2$ and $^{6}Li_2$ consisting of two fermionic atoms $(f_\uparrow f_\downarrow)$ with spins directed 'up' and 'down'. The experiments also discovered composite fermion molecules (fb) that consist of the ^{40}K fermionic isotope and ^{87}Rb bosonic isotope [98].

We recall that the magnitude and sign of the quantum mechanical s-wave scattering length rapidly vary in the Feshbach resonance if the external magnetic field B comes close to the resonance field B_{res} (see, e.g., [18, 99, 100]). The effective scattering lengths a can be represented in this case as

$$a(B) = a_{\mathrm{bg}}\left(1 + \frac{\Delta_{\mathrm{res}}}{B - B_{\mathrm{res}}}\right), \qquad (1)$$

where a_{bg} is the 'bare' scattering length and Δ_{res} is the effective width of the resonance. Rather frequently, even in the absence of the external magnetic field, the absolute value of the bare scattering length (for quasiresonance vibration levels in a two-atom interaction potential) is rather large and has characteristic values $|a_{\mathrm{bg}}| \approx 15-20$ Å. At the same time, in magnetic fields B whose strength is close to that of the resonance field B_{res}, the characteristic values of the effective scattering length can be as large as 2000–3000 Å. The effective scattering length tends to infinity in the very important unitary limit where $B = B_{\mathrm{res}}$, and hence $1/a \to 0$ [101]. It is noteworthy that the bare scattering length for a quasiresonance level in the absence of a field $a_{\mathrm{bg}} < 0$, while the effective length $a < 0$ if $\Delta B = B - B_{\mathrm{res}} > 0$ and $a > 0$ if $\Delta B = B - B_{\mathrm{res}} < 0$ (Fig. 1).

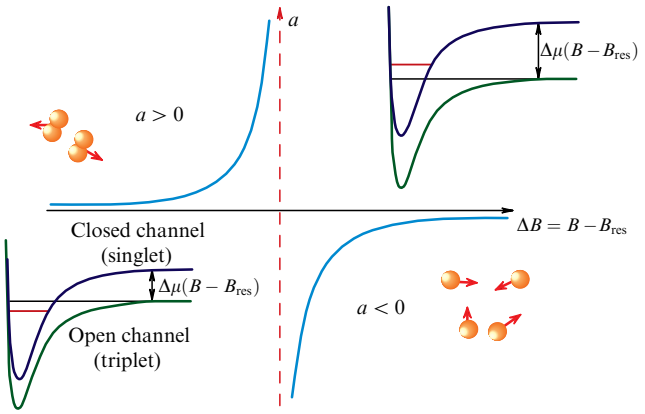

Figure 1. Feshbach resonance describing the s-wave scattering length a as a function of the magnetic field $\Delta B = B - B_{\rm res}$ [19, 21, 22, 33, 100]. If a magnetic field is applied, two terms in open and closed channels cross. As a result, the bound state in the system (in the closed channel) at $a > 0$ is replaced with a virtual level at $a < 0$. $B_{\rm res}$ is the resonance magnetic field, and μ_0 is the magnetic moment of the atom.

In Fig. 1, an analogy with the Heitler–London theory for a hydrogen molecule [102] (that describes the two-particle singlet and triplet terms) is used to depict the closed (singlet) channel (or term) and the open (triplet) channel; it is of importance that a two-particle bound state occurs in the closed singlet state alone, while there is no such state in the open channel. The energies of the terms behave differently depending on the applied magnetic field B. The Feshbach resonance can then be interpreted as the crossing of the singlet and triplet terms in the resonance field $B_{\rm res}$. Consequently, if concentrating on the closed channel alone, in fields $B > B_{\rm res}$, we have the effective length $a < 0$ and the singlet term contains only a virtual bound state. But if $B < B_{\rm res}$, we have the effective length $a > 0$, and a real bound state or molecule occurs in the closed channel, with the biding energy $|E_{\rm b}| = \hbar^2/ma^2$ for two particles with the same mass. Consequently, the following is observed in substance (3D Fermi gas) in the $B < B_{\rm res}$ region. Local pairs or molecules consisting of two elementary fermions with opposite spin projections first emerge at higher temperatures $T_* \sim |E_{\rm b}|$, and then, at lower temperatures $T_{\rm c}^{\rm BEC}$, they experience Bose condensation. However, if $B > B_{\rm res}$, both the extended Cooper pairs and Bose condensate emerge at the same temperature $T_{\rm c}^{\rm BEC}$.

If the magnetic field varies adiabatically slowly, a smooth transition, or crossover, between the local pairs (molecules) and extended (Cooper) pairs is observed. This is the essence of the BCS–BEC crossover phenomenon in a resonance Fermi gas. We stress that such a simplified single-channel approach is only applicable if the system is not too close to the unitary limit where the two-channel nature (related to decays in the open channel of two-particle bosonic states into two single-particle fermionic states and inverse processes of conversion of two Fermi particles into composite bosons or molecules) is of importance. If the Feshbach resonance is explored in more detail [103], a situation actually occurs that is described by the Alexandrov–Ranninger theory of a Fermi–Bose mixture [104, 105]. Our consideration is limited in this review to the single-channel approach, which brings the physics of resonance quantum gases close to the physics of high-temperature superconductivity (if described using models similar to the Hubbard model [106]). We stress that the Feshbach resonance [99, 103, 107] (or, more accurately, the Fano–Feshbach resonance [108, 109]) is currently under intense scrutiny in different areas of solid state and plasma physics, including the physics of electron correlations in the tunnel density of micro-contact states [110].

3. BCS – BEC crossover in 3D systems

The theory of BCS–BEC crossover and experimental results for three- and quasi-two-dimensional resonance Fermi systems are reviewed in detail in numerous classic [8–11] and more recent [78, 79, 83–85, 101, 103–105, 111–124] publications, including our papers [19, 20], reviews [21, 22, 31–33, 88], and monographs [18, 100]. To avoid repetition, we briefly discuss only the most important aspects here.

A global phase diagram of the BCS–BEC crossover for a 3D resonance Fermi gas is shown in Fig. 2. The vertical axis shows the dimensionless temperature $T/\varepsilon_{\rm F}$, and the horizontal axis, the inverse gas parameter $1/ap_{\rm F}$. The BCS region of extended Cooper pairs corresponds to negative values of the scattering length $a < 0$ and a positive value of the chemical potential $\mu > 0$. At the same time, in the BEC region (for local pairs), we have the scattering length $a > 0$ and chemical potential $\mu < 0$.

In the weak correlation region (in the dilute BCS limit as $1/ap_{\rm F} \to -\infty$), Cooper pairing occurs close to the Fermi surface, and hence $\mu \approx \varepsilon_{\rm F} = p_{\rm F}^2/2m$ in that case. The critical temperature in the BCS region can be determined using the well-known Gor'kov–Melik-Barkhudarov formula [12]

$$T_{\rm c}^{\rm BCS} \approx 0.28\varepsilon_{\rm F} \exp\left(-\frac{\pi}{2|a|p_{\rm F}}\right). \qquad (2)$$

As $1/ap_{\rm F} \to 0$, we come close to the so-called unitary limit [101]. In this limit, the system does not have any small parameter, and therefore all the quantities, including the total energy of the system, the chemical potential, and the critical temperature, can be expressed in terms of only the Fermi energy [125]. The chemical potential and critical temperature calculated using the quantum Monte Carlo method are as follows: $\mu = 0.44\varepsilon_{\rm F} > 0$ and $T_{\rm c}^{\rm BCS} = 0.15\varepsilon_{\rm F}$ [126–128]. These values imply that we are still in the region of positive μ values characteristic of extended Cooper pairs. The chemical potential μ at the critical temperature $T_{\rm c}$ vanishes (and then changes its sign) only if the gas parameter value is $ap_{\rm F} \approx 2.5$ ($1/ap_{\rm F} \approx 0.4$) [19], i.e., in the positive scattering length region, $a > 0$. It is noteworthy that for intermediate gas parameter values $1 \leqslant ap_{\rm F} \leqslant 3$ ($1/3 \leqslant 1/ap_{\rm F} \leqslant 1$), we have the dimensionless fermion

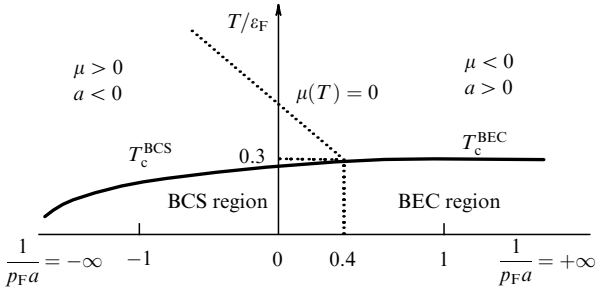

Figure 2. Global phase diagram of a resonance 3D Fermi gas. The BCS region corresponds to Cooper pairing, and the BEC region to Bose condensation of local pairs [19, 21, 88, 100].

density $na^3 = p_F^3 a^3/3\pi^2 \leqslant 1$, which means that the overlap of quasilocal pairs in this intermediate region is not yet strong (unlike the dilute BCS limit), and the pairs only touch each other. We can assert that, in a sense, we are dealing with a Fermi–Bose mixture of quasilocal pairs and unpaired fermions [18, 104, 105]. If $1/ap_F > 0.4$, we pass to the BEC region. The critical temperature of Bose–Einstein condensation can be found in this region in the limit of weak correlations (in the dilute BEC limit at $1/ap_F \gg 1$) using the Einstein formula [7] with the nontrivial corrections calculated in [116]:

$$T_c^{BEC} = 0.2\varepsilon_F\left[1 + 1.3a_{2-2}n^{1/3}\right]. \quad (3)$$

We note that Eqn (3) contains an important quantity: the scattering length of a local pair (molecule or composite boson) on a molecule (another composite boson) a_{2-2}. We show in Section 4 that $a_{2-2} = 0.6|a| > 0$, where a is the scattering length for an elementary fermion on a fermion [31, 32, 114]. We also note that $0.2\varepsilon_F = 3.31(n/2)^{2/3}/2m$, in accordance with the standard formula for the temperature of Bose–Einstein condensation in a gas of composite bosons with the density $n/2 = p_F^3/6\pi^2$ and mass $2m$. We stress that another temperature is specific to the dilute BEC region, which is determined using the Saha formula [129]; this temperature describes a smooth crossover between local pairs and unpaired fermions:

$$T_* = \frac{|E_b|}{(3/2)\ln\left(|E_b|/2\varepsilon_F\right)} \gg T_c^{BEC}, \quad (4)$$

where $|E_b|$ is the absolute value of the binding energy of the composite boson (or molecule). This temperature can be found from the condition of thermodynamic equilibrium between the unpaired fermions n_F and molecules (composite bosons) n_B:

$$n_F(T_*) = 2n_B(T_*). \quad (5)$$

We observe a new interesting state of matter in the intermediate temperature range $T_c^{BEC} < T < T_*$: a normal (nonsuperfluid) Bose gas of composite bosons (molecules) with the mass $2m$ and density $n/2$ [18–20]. A Bose gas of charged particles (local electron pairs or bipolarons with charge $2e$ in a normal, nonsuperconducting, state) exhibits nontrivial dependences of the thermal capacity and resistance on temperature and a tunnel contact with nontrivial properties (in particular, transparency) between the normal (nonsuperconducting) gas of local electron pairs and a standard BCS superconductor with extended Cooper pairs.

4. BCS – BEC crossover in quasi-two-dimensional systems

The kinematic dimension available for observing the BCS–BEC crossover and studying collective mode spectra and similar phenomena in experiments with ultracold gases [130, 131] chronologically varied as follows: first, gases were fabricated with the dimension $D = 3$ in spindle-shaped traps with the harmonic potential near the bottom and the frequencies $\omega_x, \omega_y \gg \omega_z$; next, gases with the dimension $D = 1$ in similar traps with only the lower level of motion along x and y populated; and only recently did a transition to the dimension $D = 2$ occur (disc-shaped traps with frequencies $\omega_x, \omega_y \ll \omega_z$) [22, 132–134]. Thermodynamic and transport properties in quasi-two-dimensional layered systems, thin films, and purely two-dimensional electron monolayers have been explored in depth in the physics of high-temperature superconductivity and strongly correlated Fermi systems for many years, at least since the early 1980s, when the quantum Hall effect was discovered [135, 136] and, not infrequently, significantly earlier. The origin of these experimental studies dates to times when the semiconductor industry for microelectronics was being built and superlattices, inverse layers in heterostructures, interfaces, twinning layers, etc. were explored in depth.

Also beginning in the early 1990s, He-3 monolayers on Andreev levels on the free surface of thin superfluid He-4 films or on the free surface of graphoil (peeling off graphite) were created and studied in depth (from the perspective of thermodynamic properties), using both experimental and theoretical methods, in the physics of quantum liquids and crystals [18, 68, 137–143]. The interest in 2D systems in condensed matter physics has lately been related to studies of transport, elastic, and thermodynamic properties and possible anomalous superconductivity of graphene mono- and bilayers and graphene heterostructures (and similar structures) such as h-BN (boron nitride or 'white graphite') and interfaces such as that of $SrTiO_3/LaAlO_3$ heterostructures [87–89, 144–149].

To return to the physics of ultracold gases with 2D kinematics, we note that a number of experimental issues had to be resolved to have them obtained and studied. The main issue is how motion along the z axis can be excluded. This can be done by placing the gas into a heavily anisotropic potential

$$V(\mathbf{x}) = \frac{m\omega_z^2 z^2}{2} + \frac{m\omega_\perp^2(x^2+y^2)}{2}, \quad \omega_z \gg \omega_\perp, \quad (6)$$

where m is the fermion atom mass. A sequence of potentials like (6) can be obtained using a standing electromagnetic wave created by two counter-propagating laser beams whose frequency is tuned to be far below electric dipole transitions in the atom. The standing wave in the case of Gaussian-mode beams generates the potential

$$V(\mathbf{x}) = sE_{rec}\left[1 - \exp\left(-\frac{m\omega_\perp^2(x^2+y^2)}{2sE_{rec}}\right)\cos^2(kz)\right], \quad (7)$$

where k is the wave vector of the electromagnetic wave, $E_{rec} = \hbar^2k^2/2m$ is the photon recoil energy, and s is the dimensionless depth. The shape of the potential near an antinode is close to (6) with the frequency along the tight confinement direction $\omega_z = 2\sqrt{sE_{rec}}/\hbar$. Trapping of the atomic gas in antinodes is schematically shown in Fig. 3a. Such potentials were created in [132, 133] using lasers with wavelengths of 10.6 μm and 1.064 μm. The gas cloud in each antinode is an isolated 2D system.

The requirement of kinematic two-dimensionality for the Fermi gas of N_1 noninteracting identical fermions at $T = 0$ is equivalent to the condition $\varepsilon_F < \hbar\omega_z$ for the Fermi energy (Fig. 3b). Because $\varepsilon_F = \hbar\omega_\perp\sqrt{2N_1}$, the maximum number of atoms that can be located in the trap without violating the two-dimensionality requirement is $N_{1\,max} = \omega_z^2/(2\omega_\perp^2)$. It is therefore desirable to increase the ratio of frequencies $\omega_z/\omega_\perp$. While in [132] $\omega_z/\omega_\perp = 54.6$, thus allowing $N_{1\,max} = 1490$, the ratio $\omega_z/\omega_\perp = 640$ was attained in

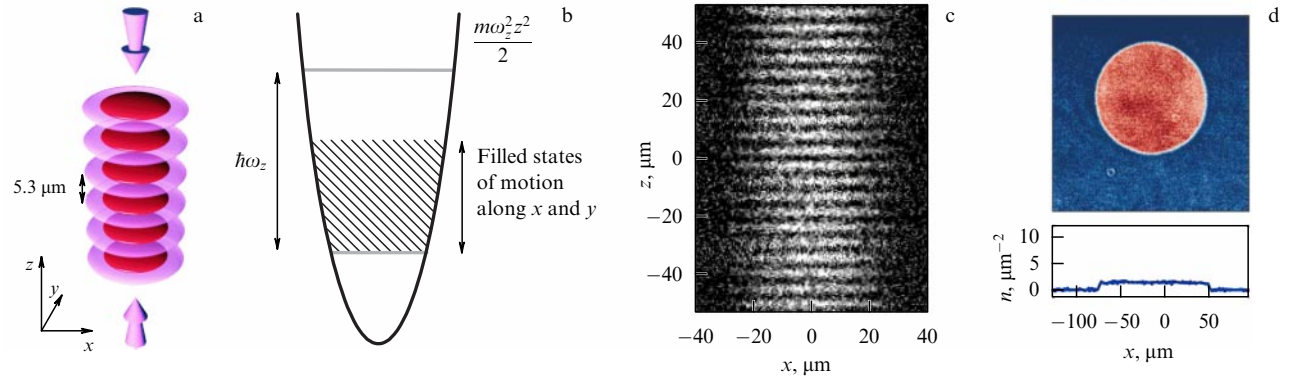

Figure 3. (Color online.) (a) Confinement of 2D gas clouds at antinodes of a standing electromagnetic wave. The gas is displayed in dark-red color, and the intensity distribution of radiation with a wavelength of 10.6 μm in light magenta. (b) 2D ideal Fermi gas at $T = 0$ whose motion along the z axis is limited to a single state, while its motion along x and y is almost free. (c) Image of gas clouds along the y direction presented in [132]. (d) Homogeneous Fermi gas. Gas concentration distribution in the plane (above) averaged over several dozen repeated experiments and the concentration along the diameter cross section (below) (reported in [150]).

subsequent studies [133, 151], enabling the number of particles to be increased to $N_{1\,\max} = 2 \times 10^5$.

The requirement of the maximum possible ratio $\omega_z/\omega_\perp$ can be fulfilled by increasing ω_z; however, this makes the requirement regarding the stability of trapping radiation intensity more stringent. Intensity fluctuations are known to result in gas heating with a rate $\sim \omega_z^2$ [152, 153]. We note that rather deep degeneracy was attained in the above-mentioned experiment [132] with a relatively small value $\omega_z/(2\pi) = 5.57$ kHz, and gas was cooled to the temperature $T = 0.1\varepsilon_F$. However, at a higher frequency $\omega_z/(2\pi) = 78.5$ kHz, this deep degeneracy was not observed, and the temperature was $T = 0.27\varepsilon_F$ [151]. The directional stability of the beams that create the standing wave is also of importance, because angular instability easily results in swinging oscillations of the centers of mass of clouds in the xy plane.

Two-dimensionality breakup can be caused, apart from the chemical potential exceeding $\hbar\omega_z$, by thermal excitation, interactions, or the nonequilibrium population of energy levels in the process of preparation. For example, an excited Bloch band can be filled in a gas with a small number of collisions when the standing wave is activated if, prior to activation, the chemical potential exceeds the recoil energy E_{rec}.

The breakup of two-dimensionality by interaction between particles remains an involved issue [21, 154–156]. Even an insignificant interaction between two atoms mixes the states of the atom motion along the z axis. At the same time, the motion of the pair of atoms remains strictly two-dimensional, because the problems of the center-of-mass motion and pairwise interaction are separated in the harmonic potential. The contribution from three-, four-, and multiparticle interactions to the kinematic dimension has to be clarified. Such interactions are apparently effective in the strong-coupling regime, i.e., if the energy of interaction between particles is of the order of the kinetic energy. Experimental data reported in [155] indicate a breakup of kinematic two-dimensionality in the case of strong attraction between atoms. However, the same data can be explained without involving the breakup of kinematic two-dimensionality [21]. The effect of kinematic two-dimensionality and interactions on the atom spin flip in a high-frequency magnetic field was explored in [157].

Another important issue in the experimental setup was taking images of gas directly in traps without deactivating the trapping potential and the subsequent flying apart. If flying apart continues for a long time, particles from clouds with different populations (and hence, presumably, occupying different collective states) become intermixed, thus complicating the interpretation of data. Figure 3c shows images of the gas in a series of traps [132] obtained without deactivating the trapping potential. The images were taken along the plane of 2D systems.

Images taken along the z direction yield more profound information about the properties of the system and, in particular, enable measuring correlation properties and searching for the vortices that are supposed to emerge if, for example, superfluidity breaks up in accordance with the Berezinskii–Kosterlitz–Thouless mechanism [76, 77]. A single system has to be fabricated to make such images. A single trap close to potential (6) was created in the flattened focus of a laser beam with a short Rayleigh distance [134]. Another way to create a single system is to fill only one minimum in the standing wave [155, 158]. Images were taken in [155, 158] along the z direction. We note that the number of atoms in the 2D gas was significantly increased in these studies, which made the system more macroscopic. Reportedly, $N \sim 10^5$ atoms have been prepared, compared with $N \sim 1000$ involved in earlier experiments [122, 132–134, 151, 154, 159].

An important step that has been made recently was to create a homogeneous 2D Fermi gas [150] in which weak parabolic confinement in the xy plane was substituted with a rectangular potential. An image of the homogeneous Fermi gas is shown in Fig. 3d. The removal of inhomogeneous confinement is of interest for a number of reasons. First, the absence of homogeneity limits correlation radii near phase transitions. Second, such a trap enables observing Fulde–Ferrell–Larkin–Ovchinnikov superfluidity [70, 71] and pairing in the p-wave channel according to the Kohn–Luttinger mechanism [64–66] for partly spin-polarized Fermi gases, problems that are discussed in Section 9.

Quasi-two-dimensional traps are of interest in the theoretical context owing to the manifestation of the fluctuation corrections [18, 21, 78, 79, 88] related primarily to the nature of the Berezinskii–Kosterlitz–Thouless mechanism in 2D systems [76–82, 160–163] and the nontrivial power-law decrease of phase correlators in those systems [164–169]. We

first summarize the main results of the mean-field theory for the BCS–BEC crossover in the 2D system obtained in [83–85] as part of the Leggett self-consistent theory [9] and in [78], where a special Hartree–Fock ansatz was used for the chemical potential of a weakly nonideal 2D Bose gas with repulsion. We note that two phenomena concurrently exist for symmetric attractive potentials in 2D Fermi systems regardless of the potential strength $|U|$ (without the occurrence of a threshold): pairing of two particles in a vacuum (in real space) and Cooper pairing of two particles on the background of the filled Fermi sphere in the momentum space. This is the most substantial manifestation of the difference between the 2D world and the 3D world (where a bound state of two particles only emerges for sufficiently strong potentials with the amplitude $|U| \geqslant W$, where $W \sim \hbar^2/mr_0^2$ is the characteristic energy of zero-point oscillations and r_0 is the range of the potential). Miyake's results [83] show that the mean-field critical temperature in the BCS region (at $|E_b| \leqslant 2\varepsilon_F$) can be calculated using the formula

$$T_c^{BCS} = \sqrt{2\varepsilon_F |E_b|}\,. \tag{8}$$

Consequently, at low temperatures $T \ll |E_b| \leqslant 2\varepsilon_F$, the chemical potential has the form

$$\mu \simeq \varepsilon_F - \frac{|E_b|}{2} \geqslant 0\,. \tag{9}$$

The mean-field temperature in the BEC region (at $|E_b| > 2\varepsilon_F$) according to the results in [78] is

$$T_c^{BEC} = \frac{\varepsilon_F}{4\ln(1/f_{2-2})}\,, \tag{10}$$

where f_{2-2} corresponds again (as in the correction to Einstein formula (3) in the 3D system) to the scattering amplitude of a dimer (composite boson or molecule) on a molecule. We show in Section 5 that in accordance with [113],

$$f_{2-2} \approx \frac{1}{\ln\left(1.6|E_b|/2\varepsilon_F\right)}\,. \tag{11}$$

We note that in 2D systems, the Galitskii–Bloom standard dimensionless gas parameter [170, 171], which is related to the scattering amplitude of the elementary fermion on a fermion, has the form

$$f_0(p_F a_{2D}) = -\frac{1}{2\ln\left(p_F a_{2D}\right)} = \frac{1}{\ln\left(|E_b|/2\varepsilon_F\right)}\,, \tag{12}$$

where a_{2D} is the 2D scattering length. Equation (12) correctly describes both the BEC region with strong attraction, where $|E_b| > 2\varepsilon_F$, and the BCS region with weak attraction, where $|E_b| \leqslant 2\varepsilon_F$. As a result, to plot the phase diagram of the BCS–BEC crossover for 2D systems (by analogy with the inverse gas parameter $1/(ap_F)$ in the 3D case), it is helpful to introduce another dimensionless parameter

$$g = \frac{1}{2f_0(p_F a_{2D})} = \frac{1}{2}\ln\left(\frac{|E_b|}{2\varepsilon_F}\right). \tag{13}$$

Equations (8) and (10) for the critical temperature in the BCS and BEC regions can be expressed as $T_c^{BCS}/\varepsilon_F \sim 2\exp g$ and $T_c^{BEC}/\varepsilon_F \sim 1/[4\ln(6.4g)]$, and we can qualitatively plot the mean-field phase diagram of the BCS–BEC crossover in 2D system using variables T/ε_F and g [21]. The global phase diagram of the BCS–BEC crossover in the 2D system is shown in Fig. 4. We note that the chemical potential in the BEC region at low temperatures and in the intermediate case $|E_b| \geqslant 2\varepsilon_F$ is still controlled (up to small corrections) by Eqn (9). A very unusual pseudogap phase of the normal (nonsuperfluid) gas of composite bosons emerges in this region, totally similarly to the situation in weakly doped superconducting cuprates at higher temperatures $T \geqslant T_c$ [112]. But the chemical potential in the dilute BEC region at $|E_b| \gg \varepsilon_F$ takes the value $\mu \simeq -|E_b|/2$ or, more accurately, if scattering of a dimer on a dimer in the 2D case is taken into account, we obtain

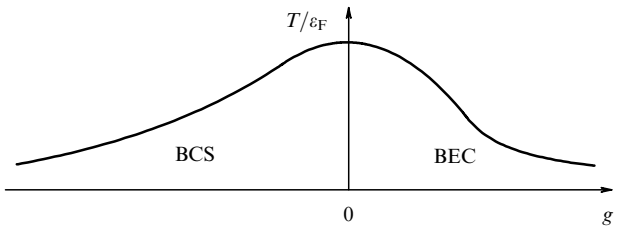

Figure 4. Global phase diagram of the BCS–BEC crossover for 2D systems plotted in the mean-field approximation [21]. The vertical axis shows the dimensionless temperature T/ε_F, and the horizontal axis the dimensionless parameter $g = (1/2)\ln(|E_b|/2\varepsilon_F)$, which is convenient for describing 2D situations. The left-hand part of the phase diagram at $g < 0$ (and, consequently, at $|E_b| < 2\varepsilon_F$) shows the BCS region for extended Cooper pairs, and, located in the right-hand side of the phase diagram at $g > 0$ and $|E_b| > 2\varepsilon_F$, is the BEC region of local pairs. The intermediate region of strong fluctuations corresponds to absolute values of the binding energy $|E_b| \sim 2\varepsilon_F$.

$$\mu \approx -\frac{|E_b|}{2} + \frac{\pi n_{2D}}{2m} f_{2-2}\,, \tag{14}$$

where n_{2D} is the 2D concentration. Hence, for the boson chemical potential we have

$$\mu_{Bose} \approx 2\mu + |E_b| \approx \frac{\pi n_{2D}}{m} f_{2-2} > 0\,, \tag{15}$$

as it should be in a weakly nonideal gas of repulsing composite bosons. We also note that similarly to the 3D case, there is one more characteristic temperature of the smooth crossover between the paired and unpaired fermions in the dilute BEC region, which is determined by the Saha formula. In 2D systems, this temperature has the form

$$T_* = \frac{|E_b|}{\ln\left(|E_b|/2\varepsilon_F\right)}\,. \tag{16}$$

If $T_c^{BEC} < T < T_*$, the normal Bose gas phase reemerges in 2D systems with an unusual behavior of the thermal capacity and other thermodynamic and transport characteristics.

5. Fluctuation corrections and the Berezinskii–Kosterlitz–Thouless transition

Important estimates have been obtained in [78, 79] for the difference between the exact Berezinskii–Kosterlitz–Thouless critical temperatures T_c^{BKT} and the mean-field temperatures in the BCS and BEC regions for a 2D Fermi gas. The results in [78] show that the difference between the exact and mean-field critical temperatures in the dilute BEC region of local pairs (at

$|E_b| \gg \varepsilon_F$) is small in the 2D case and can be calculated using the formula

$$\frac{|T_c^{BEC} - T_c^{BKT}|}{T_c^{BEC}} \sim f_{2-2} \ll 1 . \quad (17)$$

The difference between the exact and mean-field temperatures in the dilute BCS region of extended Cooper pairs at $|E_b| \ll \varepsilon_F$ is again small and, according to [79], is

$$\frac{|T_c^{BKT} - T_c^{BCS}|}{T_c^{BCS}} \sim \frac{T_c^{BCS}}{\varepsilon_F} \sim \sqrt{\frac{|E_b|}{\varepsilon_F}} \ll 1 . \quad (18)$$

The difference between the exact and mean-field temperatures (and hence the effective width of the fluctuation region) becomes significant in the intermediate region at $|E_b| \sim 2\varepsilon_F$ [21]. It is noteworthy that the region of strong fluctuations coincides well with the pseudogap phase region in the BCS–BEC global phase diagram, where $T \geqslant T_c$. We stress that the additional suppression of fluctuations in the quasi-two-dimensional situation, where the trap effectively contains two or more 2D layers, can be related to Josephson tunneling between the layers [172, 173], a phenomenon that can result in the transformation of the standard 2D quadratic form for the fermionic spectrum $\varepsilon(p_\parallel) = p_\parallel^2/2m$ to $\varepsilon(p_\parallel, p_z) = p_\parallel^2/2m + J[1 - \cos(p_z d)]$, where d is the distance between the layers and J is the amplitude of tunneling between the layers. Owing to the emergence of an additional term, proportional to J, in the fermion spectrum, the spectrum rather rapidly becomes a 3D spectrum and thus suppresses the fluctuations [174]. We note that the emergence and dissociation of a vortex–antivortex pair characteristic of the Berezinskii–Kosterlitz–Thouless transition and the specific power-law decrease in the phase correlator are primarily exhibited near the exact critical temperature, while at low temperatures these features are manifested much more weakly, as a result of which the accuracy of the mean-field approximation is much better [18, 21, 88]. The interesting experiment [148] where the layered (bilayer) $LaAlO_3 - SrTiO_3$ system was explored should be noted in this context.

The emergence [165] and pairing [167] of vortices have been experimentally observed in weakly nonideal Bose gases of atoms. Similar effects have not yet been observed for either Fermi atoms or even two-atom molecules on the boson asymptote of the BCS–BEC crossover. At the same time, another specific signature of the Berezinskii–Kosterlitz–Thouless transition has been discovered: the correlation decrease law changes with temperature from a power-law dependence to an exponential one [164]. In [164], a gas consisting of $N = 10^5$ ^{6}Li atoms equally distributed between two spin states was explored experimentally. The s-wave interaction was controlled using an external magnetic field, which was selected to be in the vicinity of the Feshbach resonance, located at $B_{res} = 832$ G. The 2D kinematics was ensured by confining particles in a disc-shaped trap with the frequency ratio $\omega_z/\omega_\perp \simeq 310$. The first-order correlation function $g_1(\mathbf{r})$ was obtained from the experimentally measured momentum distribution $\tilde{n}_{2D}(\mathbf{k})$:

$$g_1(\mathbf{r}) = \int \tilde{n}_{2D}(\mathbf{k}) \exp(i\mathbf{k}\mathbf{r})\, d^2k . \quad (19)$$

The distribution $\tilde{n}_{2D}(\mathbf{k})$ was measured using the focusing technique, which we now describe. After the gas had been prepared at a given level of s-wave attraction, the magnetic field was rapidly, during a time $\ll 1/\omega_\perp$, decreased to $B = 692$ G, a value that corresponds to the Bose side of the resonance, and $l_z/a = 7.11$, where $l_z = \sqrt{\hbar/(m\omega_z)}$ is the characteristic thickness of the 2D system. The radial size of the gas does not change during the switching, and the atoms, at least those initially paired, form compact molecule dimers. Immediately after the interaction is tuned, the optical trap is switched off. As a result, trapping vanishes in the longitudinal direction and weakens in the radial direction, and the cloud begins flying apart along the z axis. The particles move in radial directions in the residual magnetic potential with a frequency $\omega_{exp}/(2\pi) \simeq 10$ Hz. An image of the cloud is taken after a quarter of the period $\tau/4 \equiv \pi/(2\omega_{exp})$, owing to which this observation method is referred to as focusing. If interaction between the particles can be disregarded, the residual potential in the radial direction acts as a lens, under the effect of which the 2D concentration distribution after flying apart, $n_{2D}(\mathbf{r}, t = \tau/4)$, coincides up to a factor with the initial momentum distribution $\tilde{n}_{2D}(\mathbf{k}, t = 0)$. It was assumed in [164] that the obtained image of density distribution corresponds to the momentum distribution immediately before the release. Interpretation of the images is therefore dependent on the assumption about the collisionless motion of particles after the optical potential is switched off. An argument in favor of this assumption is that the weakening of the interaction as a result of a decrease in B and flying apart along the z axis crucially diminish the collision rate.

The measured correlation function $g_1(\mathbf{r})$ [164] is shown in Fig. 5. The measurements were made for the same interaction parameter $\ln(k_F a_{2D}) \simeq -0.5$ that corresponds to the strong-coupling regime and, at various values of the dimensionless temperature $t = T/T_{BEC}^0$, where $T_{BEC}^0 = \varepsilon_F\sqrt{3}/\pi$ is the ideal Bose-gas condensation temperature. We can see that the correlation function decreases at rather low temperatures in accordance with the power law $g_1(r) \propto r^{-\eta(T)}$ with an exponent $\eta(T)$, while at higher t it decreases exponentially. Switching from the exponential decrease to a power-law behavior manifests the emergence of superfluidity. It is noteworthy that the measured exponent $\eta = 0.6-1.4$ is significantly higher than the value $\eta \leqslant 0.25$ that would be expected for a homogeneous gas. A Monte Carlo simulation confirms that η can increase as a result of inhomogeneity [164].

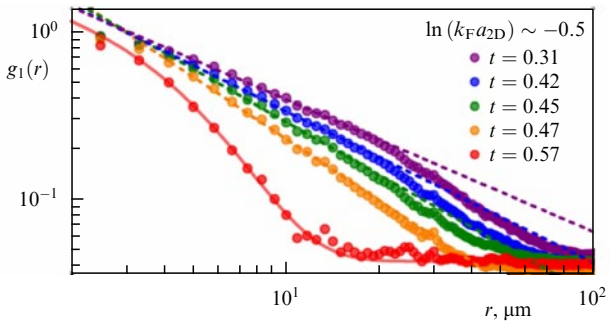

Figure 5. (Color online.) First-order correlation function $g_1(r)$ at various temperatures and $\ln(k_F a_{2D}) = -0.5$. The $t = T/T_{BEC}^0$ temperature scale is used. At temperatures above a certain value, the correlation function decreases exponentially, as is expected for a normal gas. At lower temperatures, a power-law decrease with the exponent $\eta(T)$ is observed. (Quoted from [164].)

The described measurement of the $g_1(\mathbf{r})$ correlation function [164] is based on the assumption that after the confinement is switched off, the cloud flies apart along the z axis without collisions [21]. The superfluid phase can fly apart according to a different scenario that follows from the hydrodynamic equations for superfluid gases [21]. This would make both the relation between $n_{2D}(\mathbf{k}, \tau/4)$ and the sought $\tilde{n}_{2D}(\mathbf{k}, 0)$ and the calculation of $g_1(\mathbf{r})$ using the measured $n_{2D}(\mathbf{r}, \tau/4)$ more involved. However, flying apart in the normal phase is supposed to occur almost without collisions due to small collision cross sections. Therefore, the measured power-law decrease in $g_1(\mathbf{r})$ cannot be obtained in the normal gas and is therefore evidence of superfluidity. Calculations of the η exponent performed recently take the inhomogeneity of the trapped gas [166, 168] and the contribution of the normal component [168] into account. The calculated results are close to the measured one [168], and this can be regarded as an argument against the hydrodynamic-expansion model.

6. Strongly interacting mixture of spinons and holons in high-temperature superconductors

There is another nice analogy between the physics of composite particles in the BCS–BEC crossover for quantum gases and the physics of composite holes (spin polarons or magnetic strings) in cuprate high-temperature superconductors (HTSCs) with a small concentration of holes. This analogy, suggested in review [33], is related to Laughlin's ideas [175, 176] regarding the confinement of spin and charge in strongly correlated 3D and 2D systems and the classic results of Bulaevskii–Nagaev–Khomskii [177] and Brinkman–Rice [178], who used the analogy with quark physics to predict the emergence of a linearly growing trace of wrongly oriented frustrated spins (string confinement potential) when a hole propagates on the antiferromagnetic background. Actually, following Laughlin's ideas, we can regard the hole as a composite object resembling a quark bag, containing a holon and a spinon connected with a string or confinement potential. It should be kept in mind that according to Anderson's suggestion [179], the physical hole $h_{i\sigma}$ at a site i with spin σ in the so-called adjoint representation can be represented as

$$h_{i\sigma} = f_{i\sigma} b_i \,, \tag{20}$$

where $f_{i\sigma}$ is the spin part of the composite hole, or spinon, with spin σ at the site i, and b_i is the charge part of the composite hole (or holon). Usually, the spinon is a fermionic excitation (fermion) with $S = 1/2$ and $Q = 0$, and the holon is a boson with spin $S = 0$ and charge $Q = e$. By solving the Schrödinger equation with a linear confinement potential, the binding energy E_b can be determined for the ground state of the string oscillator (spin polaron or composite hole), while taking the probability of quantum tunneling (actually, quantum fluctuations in the exchange interaction) into account yields a large but finite mass $m_{\text{eff}} \sim 1/J$ of the spin polaron. As a result, the composite-hole spectrum on a square 2D lattice characteristic of HTSC cuprates has the form [180]

$$E_h = E_b + J(\cos p_x d + \cos p_y d)^2 \,. \tag{21}$$

At the same time, the Cooper pair with a low hole density is a pair of composite holes $h_{i\sigma} h_{j-\sigma}$ with opposite spins at the sites i, j of the crystal lattice or a quadruple $(f_{i\sigma} b_i, f_{j-\sigma} b_j)$ consisting of two holons and two spinons. We note that the bound state of two composite holes (two strings) on a square 2D lattice can emerge due to a residual dipole–dipole interaction between them in the $d_{x^2-y^2}$ channel [181, 182]. This interaction in the 2D $t-J$ model has the form

$$V(r) \sim \frac{\lambda_d}{r^2} \,. \tag{22}$$

If the hole concentration is low, we can speak about the formation of local pairs from composite holes at the smooth crossover temperature $T_* \sim |E_b|$ and their subsequent Bose condensation at a (lower) critical temperature $T_c^{\text{BEC}} \sim Jx$, where x is the hole concentration in the 2D system [33, 100]. We note that the linear dependence of the critical temperature on the hole concentration agrees with Uemura's scaling results [183] based on the boson superconductivity scenario in weakly doped HTSC systems. At the same time, if the hole density is higher (and hence the electron density is lower), extended Cooper pairing of two composite holes (two spin polarons) is shown to occur in the $t-J$ model [184, 185]. Therefore, we can conclude with some caution that the BCS–BEC crossover occurs for the pairing of two composite holes (two spin polarons or two strings) in the d-wave channel for a weakly doped HTSC system. However, this crossover seems not to be smooth and must contain a quantum critical point or even intermediate phases on the boundary between the BCS and BEC regions [100, 186, 187].

7. Composite fermions and bosons, trios and quartets in resonance gases and mixtures

We can actually say that in the HTSC systems we are dealing with a strongly interacting Fermi–Bose mixture of spinons and holons, with a linearly increasing repulsive confinement potential acting between the fermions and bosons. We note that a short-range repulsive (or van der Waals) potential between fermionic He-3 and bosonic He-4 atoms is usually observed in solutions of He-3 in He-4. At the same time, both short-rage repulsion and short-range attraction can emerge in resonance fermion–boson mixtures. We consider in more detail how bound complexes consisting of three and four elementary particles are created. We also explore the amplitude of dimer scattering on an elementary particle and on another dimer in the resonance approximation when the two-particle scattering length is much larger than the potential radius $a \gg r_0$. We recall that the amplitude of the $(f_\sigma f_{-\sigma})$ dimer scattering on a dimer, a_{2-2}, determines the nontrivial correction to Einstein formula (3) for the critical temperature of Bose condensation in the BEC region for 3D resonance Fermi gases. The 2D amplitude of dimer scattering on the dimer, f_{2-2}, determines the mean-field critical temperature (10) in the BEC region for a weakly nonideal 2D resonance Fermi gases. Composite fermions $(f_\sigma b)$ and bound complexes consisting of three $(f_\sigma b, b)$ and four $(f_\sigma b, f_{-\sigma} b; f_\sigma b, bb)$ elementary particles emerge in a natural way in fermion–boson mixtures with attraction between fermions and bosons [29, 31–33]. Two-boson states $(b_1 b_2)$ consisting of bosons of different species can emerge in boson–boson mixtures under certain conditions and subsequently undergo Bose condensation; the same is true for three-particle $(b_1, b_1 b_2)$, four-particle $(b_1 b_2, b_1 b_2)$, and multiparticle boson droplets [18, 30–33]. Finally, the scattering length a_{2-1} of an elementary fermion f_σ on a dimer $(f_\sigma f_{-\sigma})$ plays an important

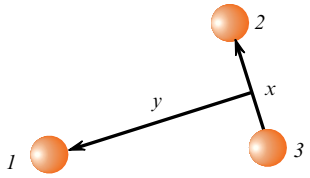

Figure 6. Coordinate y (which coincides with R in Eqn (25)) describes the distance between the elementary boson *1* and the center of mass of the molecule consisting of two bosons (*2* and *3*) [33, 100].

role in determining the lifetime of metastable quasiresonance states of a Fermi gas confined in a magnetic trap [188]. A crucial difference between 3D and 2D systems must be noted here. An important role in 3D systems is played by the so-called Efimov effect [189, 190], according to which, if $a \gg r_0$ in the 3D case, a large number

$$N \sim \frac{1}{\pi} \ln \frac{a}{r_0} \tag{23}$$

of three-particle levels emerge in the energy range

$$\frac{1}{ma^2} < |E_3| < \frac{1}{mr_0^2} \,. \tag{24}$$

This phenomenon, which occurs in space dimensions $2.3 < D < 3.8$ is related to the presence of an attractive part

$$V_{\text{eff}} = -\frac{\alpha}{R^2} < 0 \tag{25}$$

in the three-particle Schrödinger equation (Fig. 6), with the coefficient α in (5) depending on the space dimension D. As a result, the phenomenon of falling on the center occurs in the 3D system of three bosons, and three-particle complexes emerge whose binding can be arbitrarily strong. At the same time, the Efimov effect does not exist in 2D systems [191]. The reason is that in this case, the three-particle Schrödinger equation contains a repulsive term $V_{\text{eff}} \sim \beta/R^2 > 0$ instead of an attractive one. The number of three-particle levels with a negative energy $E_3 < 0$ becomes finite in the 2D case. The kernel of the Skorniakov–Ter-Martirosian integral equation [192] for the three-particle T-matrix in a 2D system also becomes finite. The exact solution of this equation in the 2D case shows that the system of three bosons interacting in a resonance way has only two levels, whose three-particle binding energies [193, 194] are

$$E_3^{(1)} = 16.4E_{\text{b}} \,, \quad E_3^{(2)} = 1.3E_{\text{b}} \,, \tag{26}$$

where $E_{\text{b}} < 0$, as before, is the two-particle binding energy (for two elementary bosons). Similarly, there is only one bound level [31] in the scattering of an elementary boson b on a composite fermion $f_\sigma b$ or scattering of an elementary boson b_1 of one species on a molecule $b_1 b_2$ (consisting of two elementary bosons of different species); the energy of this level is [31]

$$E_3 = 2.4E_{\text{b}} \tag{27}$$

for two identical boson and fermion masses $m_{\text{B}} = m_{\text{F}}$. We stress again that the binding energies of the three-particle complexes E_3 in (26) and (27) are functions of only the two-particle binding energy E_{b}.

In contrast to the situation with bosons, the Pauli principle plays a decisive role in analyzing the three-fermion problem: it results in an effective repulsion between the elementary fermion f_σ and the molecule $f_\sigma f_{-\sigma}$, irrespective of the space dimension. As a result, the exact solution of the Skorniakov–Ter-Martirosian equation (found for the first time in [192] for the scattering of a neutron on a deuteron) yields the classical result in the 3D case:

$$a_{2-1} = 1.18|a| > 0 \,. \tag{28}$$

We now proceed to the four-particle problem and first consider the scattering of an $f_\sigma f_{-\sigma}$ molecule on another molecule. In this case, owing to the Pauli principle, we also have repulsion in both 3D and 2D systems. The exact formula for the scattering amplitude in the 3D case,

$$a_{2-2} = 0.6|a| > 0 \,, \tag{29}$$

which takes into account the dynamics and possible existence of virtual intermediate states that contain not only two molecules (pairs or dimers) but also three particles and one particle, was obtained in [114] at the level of a correctly chosen ansatz for the four-particle Schrödinger equation and in [31] at the level of an exact diagram approach to solving a Skorniakov–Ter-Martirosian-type integral equation for the four-particle T-matrix. We note that in [195], the diagram approach in the so-called ladder approximation (which is related to multiple rescattering of pairs without losing their identity and does not take the possible formation of triplets and singlets in the intermediate state into account) yielded a somewhat larger value (compared to the exact one), $a_{2-2} = 0.75|a| > 0$. In the 2D case, similarly, Eqn (11) for the scattering amplitude f_{2-2} was obtained in [113].

In proceeding to the analysis of four-particle boson complexes, we note that in the 3D case we again observe an analog of the Efimov effect involving the fall on the center and the emergence of strongly bound four-particle complexes. At the same time, this effect is again absent in the 2D case, and we again obtain a finite number of bound states. For four elementary bosons $bbbb$ interacting in a resonance way, there are two bound states with the energies

$$E_4^{(1)} = 194E_{\text{b}} \,, \quad E_4^{(2)} = 24E_{\text{b}} \,. \tag{30}$$

The energies of these levels were first determined in [196]. For $f_\sigma b$, $f_{-\sigma} b$ complexes consisting of two elementary bosons and fermions or the $b_1 b_2, b_1 b_2$ complex consisting of bosons of different species, we again have two bound states with the energies [31]

$$E_4^{(1)} = 10.7E_{\text{b}} \,, \quad E_4^{(2)} = 2.9E_{\text{b}} \,. \tag{31}$$

Finally, for the complex $f_\sigma b, bb$ in the case of equal masses $m_{\text{B}} = m_{\text{F}}$, there is only one level [31]

$$E_4 = 4.1E_{\text{b}} \,. \tag{32}$$

We note that the energies of bound states of four-particle complexes in Eqns (30)–(32) in the 2D case are again expressed (similarly to three-particle complexes) in terms of the two-particle binding energy alone. The results obtained in the preceding section enable us to complete the construction of the phase diagrams of 3D and 2D resonance fermion–

boson mixtures with attraction between fermions and bosons and mixtures of bosons belonging to different species [18, 29, 30, 68]. We stress that in a fermion–boson mixture with equal densities of fermions and bosons, $n_F = n_B$, and strong (resonance) attraction between fermions and bosons, if the binding energy of a composite fermion is much larger than the fermion and boson degeneration temperatures, $|E_b| \gg \{T_{0B}, T_{0F}\}$, then all elementary particles can combine pairwise into composite fermions $f_\sigma b$ or (if relations (27) and (31) are satisfied) into quartets $f_\sigma b, f_{-\sigma} b$ containing two fermions and two bosons or into large droplets with the number of particles $N > 4$ [18].

8. s-wave and p-wave pairing in solutions of He-3 in He-4. Kohn–Luttinger mechanism

One of the most challenging problems in low-temperature physics that has yet to find an experimental resolution is the search for superfluidity in 3D and especially 2D (thin films, submonolayers) solutions of He-3 in He-4. The solution of He-3 in He-4 is known to be the simplest diluted Fermi system of He-3 atoms (the maximum He-3 concentration in an unpolarized solution is $x = 9.5\%$ under the pressure $P = 10$ atm) placed into inert superfluid He-4 condensate. The solutions are therefore an ideal subject for developing and testing various theoretical methods for low-density Fermi liquids, i.e., actually, the Fermi gas theory of Galitskii–Bloom [170, 171]. The first classical results in which Cooper pairing in the diluted fermion subsystem of He-3 atoms was predicted were published by Bardeen, Baym, and Pines [197]. Those results were obtained in the late 1960s shortly after the BCS theory had been formulated [4–6].

The theory of fermion superfluidity for He-3 atoms in solutions was further advanced by Bashkin and Meyerovich [198] and an author of this review [68]. We recall that the critical temperature of Cooper pairing in dense superfluid He-3 (with the He-3 concentration $x = 100\%$) is 2.5 mK (under the pressure $P = 34$ atm) and corresponds to the transition of this dense Fermi liquid into a superfluid state with triplet p-wave pairing (the state with the total Cooper-pair spin $S = 1$ and relative orbital momentum of the pair $l = 1$) [50, 51]. Only two of 18 possible superfluid phases of 3D He-3 have been observed in experiment: the so-called isotropic triplet B phase and anisotropic triplet A-phase [199–203]. The isotropic B phase is paramagnetically suppressed in magnetic fields $H \geqslant 1$ T, as a result of which the phase diagram of superfluid He-3 becomes trivial. The normal He-3 phase transforms in strong magnetic fields into the superfluid triplet A1 phase with the Cooper pair spin projection $S_z = 1$, and afterwards, at lower temperatures, the global minimum of the Ginzburg–Landau functional corresponds to the A2 phase, which also contains Cooper pairs with the projection $S_z = -1$ [50, 51]. At the same time, it was predicted in [68, 198] that singlet s-wave pairing ($S = l = 0$) occurs in diluted solutions of He-3 in He-4 in both 3D and 2D situations (for submonolayers) at low He-3 concentrations ($x < x_0$), while at higher concentrations, triplet p-wave pairing occurs. In addition, it was shown in [67, 68, 204] that the critical temperature of the triplet pairing can be significantly increased in a spin-polarized solution or strong external magnetic fields.

We note that the critical temperature of s-wave pairing in 3D solutions is again determined by Gor'kov–Melik-Barkhudarov formula (2) for extended Cooper pairs. The Galitskii effective gas parameter (which is contained in the exponent for T_c) is now determined by the formula

$$\lambda = \frac{2ap_{F0}x^{1/3}}{\pi}, \tag{33}$$

where p_{F0} is the Fermi momentum of dense He-3 and x is the He-3 concentration in a diluted solution. In this approach, the scattering length a depends on the concentration and changes sign at $x = x_0$. It corresponds to attraction ($a < 0$) at $x < x_0$ and becomes repulsive ($a > 0$) at $x > x_0$. Spin diffusion experiments performed in the 3D case suggest that $x_0 \sim 4\%$ [204]. The estimates in [198] show that the critical temperature of s-wave pairing attains a maximum at the concentration $x \sim 1\%$ and is of the order of $T_{c0} \sim 10^{-4}$ K. However, according to the Frossati group's estimates [204], the maximum critical temperature corresponds to the He-3 concentration $x \sim 2\%$ and is an order of magnitude lower: $T_{c0} \sim (5 \times 10^{-6} - 10^{-5})$ K. For the concentration $x > 4\%$, the scattering length becomes positive, and s-wave pairing is no longer possible. However, superfluid p-wave pairing in the triplet channel is possible in this concentration range [68], being driven by the generalized Kohn–Luttinger mechanism [64–66]. The Kohn–Luttinger mechanism was initially suggested in the classic study [64] for d-wave pairing in the 3D case. It is related to the presence of the Kohn singularity of the form $(q - 2p_F)\ln|q - 2p_F|$ [205] (Friedel oscillations $\cos(2p_F r)/(2p_F r)^3$ [206]) in the effective interaction of two fermions via polarization of the fermionic background. These results were later generalized in [65, 66] to triplet p-wave pairing, where the Kohn singularity and Friedel oscillations play only a minor role in determining the critical temperature.

It was assumed in [207] that for the p-wave pairing to occur, it is sufficient that the effective interaction in the momentum space between two fermions via polarization of the Fermi background increases in the important interval from 0 to $2p_F$ (and afterward decreases in the case of a diluted Fermi gas at larger momenta $p \geqslant 1/r_0$, where r_0 is the effective radius of the potential and $p_F r_0 \ll 1$). The critical temperature of p-wave pairing then has the form [65, 66]

$$T_{c1} \sim \varepsilon_F \exp\left(-\frac{13}{\lambda^2}\right), \tag{34}$$

where the effective gas parameter λ follows from Eqn (33) and the Fermi energy in a 3D solution is $\varepsilon_F = \varepsilon_{F0}x^{2/3}$ (where ε_{F0} is the Fermi energy of pure He-3). Importantly, the critical temperature of p-wave pairing is determined by the second order in the effective gas parameter, in contrast to s-wave pairing, where $T_{c0} \sim \varepsilon_F \exp(-1/|\lambda|)$. We note that the pre-exponential in Eqn (34) is determined by the third- and fourth-order diagrams in the gas parameter and retardation effects. It was calculated exactly in [208].

Kagan and Chubukov [66] have also shown that the critical temperature of p-wave pairing can be significantly increased in a spin-polarized Fermi gas and in a two-band situation [209]. These results were generalized in a later study [69] to the Fermi gas of neutral particles at ultralow temperatures in a restricted geometry of magnetic traps and, in [174], to an increase in the critical temperature in the charged electron layer in a magnetic field parallel to the layer. The main underlying idea is that the channels are separated: two 'up'-spin fermions (of the same species) create a Cooper

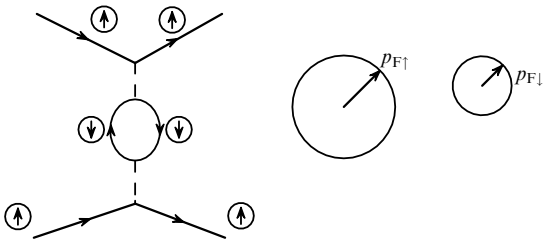

Figure 7. Separation of channels with Cooper pairing and effective interaction in a spin-polarized Fermi gas. The effective interaction is related to two 'down' spins, while the Cooper pairing in the triplet channel is related to two 'up' spins.

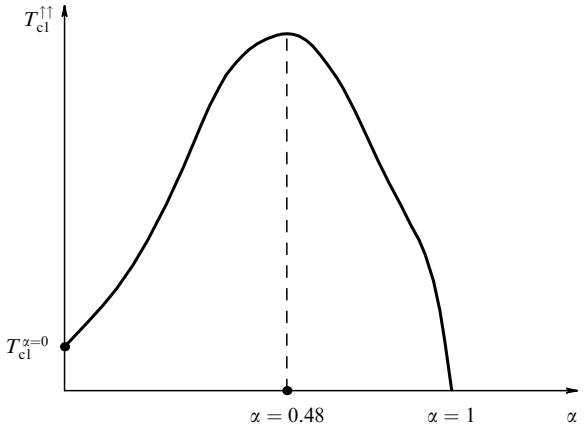

Figure 8. Critical temperature $T_{c1}^{\uparrow\uparrow}$ of triplet p-wave pairing in the A1 phase as a function of the polarization degree α in the 3D case [33, 67, 68].

pair, while their effective interaction is generated by two 'down'-spin fermions (belonging to another species) (Fig. 7). This mechanism enhances the role of the Kohn singularity, which now acquires the form $(q_\uparrow - 2p_{F\downarrow}) \ln|q_\uparrow - 2p_{F\downarrow}|$, which leads to the emergence of the anisotropic triplet A1 phase. The critical temperature of p-wave pairing for this phase is an essentially nonmonotonic function of spin-polarization degree

$$\alpha = \frac{n_\uparrow - n_\downarrow}{n_\uparrow + n_\downarrow} \tag{35}$$

whose maximum is attained at the polarization degree $\alpha = 48\%$. The p-wave pairing temperature at the maximum can be significantly higher than the critical temperature in the absence of spin polarization [66] (Fig. 8):

$$\max T_{c1}^{\uparrow\uparrow} = T_{c1}^{\uparrow\uparrow}(\alpha = 0.48) \sim \varepsilon_{F\uparrow} \exp\left(-\frac{7}{\lambda^2}\right). \tag{36}$$

The maximum temperature for superfluid He-3 is [18, 66]

$$T_{c1}^{\uparrow\uparrow}(\alpha = 48\%) = 6.41\, T_{c1}\,. \tag{37}$$

Similar estimates for $T_{c1}^{\uparrow\uparrow}$ have been obtained in [204] using a more phenomenological approach based of the Landau Fermi-liquid theory for the A1 phase of superfluid He-3. We stress that $\lambda \sim 1.4$ for dense He-3, and therefore our theory is more of a qualitative nature. Nevertheless, it yields reasonable estimates for both pure He-3 in the absence of an external magnetic field and the A1 phase width in experimentally available magnetic fields $H \leqslant 15$ T. We note that Frossati et al. [210, 211] observed a 20% increase in the critical temperature of triplet p-wave pairing in the A1 phase of superfluid He-3 in the magnetic field $H = 15$ T (and polarization degree $\alpha = 7\%$). Estimates in [68] show that the maximum temperature of p-wave pairing in 3D solutions can be attained at the maximum permissible concentration of He-3 atoms $x \sim 9.5\%$ and for the optimum spin polarization can reach the values $T_{c1}^{\uparrow\uparrow} \sim (10^{-5} - 10^{-4})$ K.

Another important observation reported in [212, 213] that may result in an increase in $T_{c1}^{\uparrow\uparrow}$ is that the maximum solubility in highly polarized solutions can exceed the maximum solubility concentration at $\alpha = 0$ by a factor of 3 to 4. We note that hopes to create a highly spin-polarized solution of He-3 in He-4 in experiment, as in the case of pure He-3, are related to the elegant technique of fast melting of spin-polarized quantum He-3 crystals proposed in [214].

We next consider the phase diagram of superfluid 2D solutions. The s-wave pairing region in these solutions is divided into two subregions. If the He-3 concentration is very low ($x \leqslant 1\%$ and $|E_b| > 2\varepsilon_F$), then, first, dimers consisting of two He-3 atoms emerge at a higher temperature of smooth crossover $T_* \sim |E_b|$ [215] and, second, they undergo Bose condensation at a lower critical temperature determined by Eqn (10), which in this case contains the 2D-solution Fermi energy $\varepsilon_F = \varepsilon_{F0} x$. A subregion of Cooper pairing emerges at higher concentrations ($1\% \leqslant x \leqslant 3\%$), where the critical temperature is determined by Miyake formula (8). Finally, if $x > 3\%$ in the 2D case, triplet p-wave pairing occurs whose critical temperature can again be significantly increased by applying an external magnetic field. This strong increase in the critical temperature is related to a strong 2D Kohn singularity having a one-sided nature, $\mathrm{Re}\sqrt{q - 2p_F}$, and being not effective for the Cooper pairing problem (where momentum transfers $q \leqslant 2p_F$ are of importance). But if an external magnetic field is applied or spin polarization occurs, the character of the Kohn singularity changes to $\mathrm{Re}\sqrt{q_\uparrow - 2p_{F\downarrow}}$, as a result of which (because $p_{F\uparrow} > p_{F\downarrow}$) the strong 2D Kohn singularity becomes effective in the Cooper pairing problem, and therefore $T_{c1}^{\uparrow\uparrow}$ significantly increases in the second order in the gas parameter f_0. The maximum critical temperature corresponds to the polarization degree $\alpha = 60\%$ but in the 2D case, in contrast to the 3D case, the maximum is very broad and effectively spans the spin polarization range from 10% to 90% (Fig. 9).

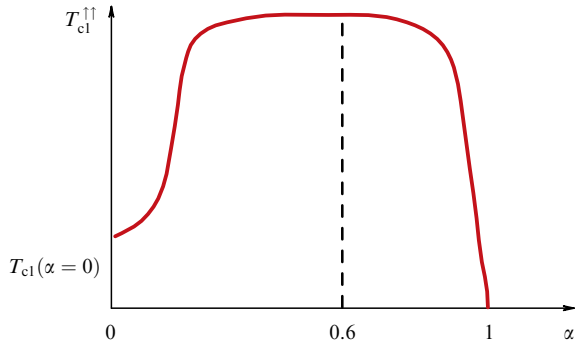

Figure 9. Critical temperature $T_{c1}^{\uparrow\uparrow}$ as a function of the polarization degree α in the 2D case [33, 67, 68, 87, 88].

The critical temperature at the maximum is given by the formula

$$\max T_{c1}^{\uparrow\uparrow} = T_{c1}^{\uparrow\uparrow}(\alpha = 0.6) \sim \varepsilon_F \exp\left(-\frac{1}{2f_0^2}\right), \qquad (38)$$

where the Bloom effective gas parameter in the 2D case $f_0 = 1/\ln(1/p_F^2 a^2)$ is determined by Eqn (12) and the Fermi momentum is $p_F = p_{F0} x^{1/2}$. Estimates in [68] show that if the magnetic field is $H = 15$ T and the 2D density of He-3 atoms is of the order of $n_3 \sim 0.05$ monolayer (the spin polarization degree is then $\alpha \sim 10\%$), we can expect experimentally measurable critical temperatures $T_{c1}^{\uparrow\uparrow} \sim 1$ mK [68, 208].

In concluding this section, we repeat that experimental observation of fermionic superfluidity of He-3 atoms in 3D and 2D solutions of He-3 in He-4 remains one of the most serious challenges in the physics of low and ultralow temperatures. It is worth mentioning the progress in experimental exploration of 2D He-3 submonolayers in the degenerate (Pauli) regime at low 2D densities and ultralow temperatures and search for the superfluidity by the Saunders group [216, 217]. We note that a mixture of ^{7}Li–^{6}Li boson and fermion isotopes [218] and a ^{40}K–^{87}Rb mixture of a bosonic Rb isotope and a fermionic K isotope [29, 33, 219, 220] are now explored in experimental and theoretical studies of ultra-cold quantum gases. We stress that these mixtures contain both a diluted fermion subsystem (Fermi gas) and a diluted Bose gas. If a short-range repulsion between all mixture components is in effect (for $\{U_{FF}, U_{BB}, U_{FB}\} > 0$), then, according to theoretical results reported in [218], Cooper pairing in the triplet p-wave channel is possible in the fermion subsystem via the Kohn–Luttinger mechanism enhanced owing to density fluctuations in the bosonic component. Attractive resonance interactions between a fermion and a boson and between two bosons can be realized in a mixture of potassium and rubidium isotopes. In this case, experimental [220] and theoretical [33] studies suggest that for $n_B \gg n_F$, large droplets can emerge and the boson component collapses.

9. Imbalanced Fermi gas. Phase separation

The ideology of Cooper pairing driven by the enhanced Kohn–Luttinger mechanism was generalized in [69] to the imbalanced ultra-cold Fermi gas of neutral particles in a restricted geometry of optical dipole traps. We note that Stoof et al. [221] predicted that singlet Cooper s-wave pairing occurs in the Fermi gas of ^{6}Li atoms with equal densities of trapped hyperfine components in the case of an attractive scattering length $a < 0$ according to the Gor'kov–Melik-Barkhudarov formula (2). The critical temperature for the maximum possible densities of the trapped fermion gas and resonance scattering lengths $|a| \sim (2-3) \times 10^3$ Å (for which $\lambda \leqslant 1$) can be as high as 10^{-6} K. We note that if $\lambda > 1$, the system compressibility $\kappa^{-1} \sim C_s^2 < 0$ becomes negative (the speed of sound squared becomes negative), and the system becomes unstable with respect to clustering or phase separation.

The authors of [69] noted an important circumstance: in the case of even a small imbalance between the hyperfine component densities (if, for example, for two components $p_{F1} - p_{F2} \geqslant T_{c0}/v_F$, where $v_F = p_F/m$ is the Fermi velocity and T_{c0} is the critical temperature in the absence of imbalance), Cooper pairs acquire a finite center-of-mass momentum owing to the Landau superfluidity criterion, to become unpaired at larger imbalance values. Strictly speaking, first, a narrow strip of the Larkin–Ovchinnikov–Fulde–Ferrel inhomogeneous superfluid phase appears in the phase diagram [70, 71] in the case of a small imbalance, and, next, s-wave pairing is fully suppressed. The trapped Fermi gas can nevertheless become superfluid in this case as well, owing to possible triplet p-wave pairing with the A1-phase symmetry. As shown in Section 8, the most efficient pairing occurs in this case between fermionic particles with larger p_{F1} (or density $n_1 = p_{F1}^3/6\pi^2$) via polarization of the components with lower densities. The polarization diagrams that contribute to the effective interaction V_{eff} in the second order in the gas parameter are shown in Fig. 10. Summing those diagrams in the case of v trapped hyperfine components yields the triplet p-wave pairing temperature in the absence of imbalance [69]

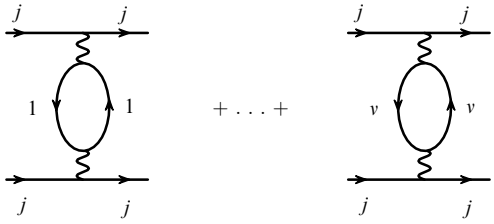

Figure 10. Loop diagrams that in the second order of the perturbation theory in the gas parameter determine the effective interaction between atoms belonging to the same component via excitation of virtual pairs of the particle–hole type of the other component [69]. This sum does not include the $i = j$ term.

$$T_{c1} \sim \varepsilon_F \exp\left(-\frac{13}{(v-1)\lambda^2}\right), \qquad (39)$$

where the gas parameter λ depends on the density of individual components. If $v = 2$, we naturally reproduce the result for He-3 in (34). The optimal imbalance that is needed to obtain the maximum critical temperature corresponds to the density ratio $n_j/n_i \approx 3$ (or the Fermi momentum ratio $p_{Fj}/p_{Fi} \sim 1.4$). We note that the critical temperature in the optimal situation is

$$T_{c1} \sim \varepsilon_{Fj} \exp\left(-\frac{7}{(v-1)\lambda_{eff}^2}\right), \qquad (40)$$

where $\lambda_{eff}^2 = (2a/\pi)^2 p_{Fj} p_{Fi}$. As a result, for the 3D imbalanced ^{6}Li gas (with the number of components $v = 2I + 1 = 3$, where $I = 1$ is the nucleus spin) and densities at which $\lambda_{eff} \leqslant 1$, we obtain the optimal critical p-wave pairing temperature of the order of $T_{c1} \sim 10^{-8}$ K. As follows from Eqn (38), if the relation between the hyperfine component densities in a quasi-two-dimensional imbalanced gas is optimal, the maximum value of T_{c1} is supposed to be significantly higher. Based on this result, one may hope that Cooper pairing driven by the enhanced Kohn–Luttinger mechanism can be observed experimentally in quasi-two-dimensional imbalanced gases. If $\lambda_{eff} > 1$, the partial compressibility and the speed of sound in each (or one) of the subsystems is $C_{si}^2 \sim \partial^2 E/\partial n_i^2 \sim \partial \mu_i/\partial n_i < 0$, and the system is again unstable with respect to phase separation. We also note that following [222], a prerequisite for recalculating the formulas for critical s-wave and p-wave pairing temperatures for a trap is that the semiclassical approximation criterion be satisfied (which requires the Cooper pair coherence length to be less than the characteristic radius of the trap at the energy

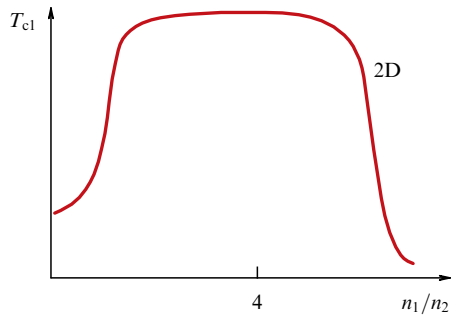

Figure 11. Triplet-pairing temperature as a function of the relative density n_1/n_2 in a 2D fermion–fermion mixture with two particle species [209].

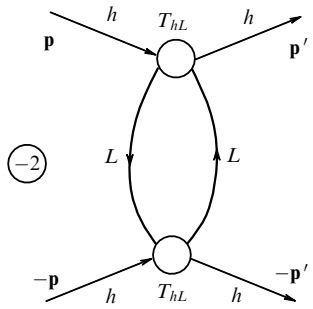

Figure 12. Leading contribution to the effective interaction for Cooper pairing of heavy particles via polarization of light particles. Unfilled circles show the vacuum T-matrix T_{hL} [223–226].

equal to the Fermi energy):

$$\xi_0 \sim \frac{v_F}{T_c} < R(\varepsilon_F)\,, \tag{41}$$

where $R \sim v_F/\omega$ in the Thomas–Fermi approximation.

The condition for the validity of the semiclassical approximation can be represented as

$$\varepsilon_F \gg T_c \gg \hbar\omega\,, \tag{42}$$

where the estimated characteristic frequency of the harmonic potential of a 3D spherically symmetric trap is

$$\omega \sim \frac{\varepsilon_F}{N^{1/3}}\,. \tag{43}$$

Here, N is the characteristic number of particles in the trap:

$$N \sim \left(\frac{\varepsilon_F}{\hbar\omega}\right)^3 \sim 10^6\,. \tag{44}$$

Similarly, the maximum critical temperatures are to be attained in quasi-two-dimensional gases at the optimum ratio of the 2D densities of hyperfine components $n_j/n_i = 4$ or the ratio of their Fermi momenta $p_{Fj}/p_{Fi} = 2$ (Fig. 11). We note that all the results quoted above refer to the case where the masses of different components are the same: $m_i = m_j$. For a mixture of fermions of two different species with unequal masses $m_1 > m_2$, we can see that new exciting phenomena related to polaron effects occur in the system [223, 224]. In particular, the larger mass m_1 can be additionally (and significantly) increased as a result of 'dressing' the heavier particle with a coat of soft (low-energy) virtual particle–antiparticle pairs of light particles [223]. The additional increase in the 'heavy' mass is effectively controlled by the parameter $\lambda_{\rm eff}^2 \ln(m_1/m_2) \gg 1$ related to the potential U_{hL} of interaction between the light and heavy particles.

A similar phenomenon in electron systems in metals, which is referred to as the electron polaron effect, is observed in the mixed-valence regime in narrow-gap multiband systems, such as uranium heavy-fermion compounds. In such systems in the so-called unitary limit of the Hubbard interaction between the heavy and light particles, starting from the bare-mass ratio $m_1/m_2 \sim 10$, one-particle calculations based on the local-density LDA method allow obtaining the effective mass of the heavy particle $m_1^*/m_2 \sim 100$ if polaron-type collective effects are taken into account. It was shown in [223–226] that the maximum temperature of the superfluid transition corresponds to the Cooper pairing of heavy particles occurring via polarization of light particles (Fig. 12). We note that the large effective masses of heavy particles are characteristic of many heavy-fermion compounds. We also note that if the bare imbalance of the initial densities and masses is very large (at $\lambda_{\rm eff}^2 m_1 p_{F1}/m_2 p_{F2} \geqslant 1$), then phase separation can occur in the mixture [223, 224]. The Ketterle group was the first to experimentally observe phase separation in imbalanced ultracold Fermi gases [73].

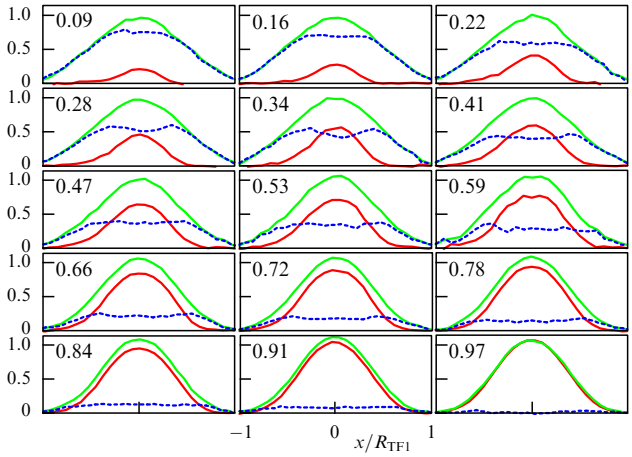

Figure 13. (Color online.) Linear concentration profiles measured in units N_1/R_{TF1} in a field of 775 G for $\varepsilon_{F1}/E_b = 0.75$ ($R_{TF1} \equiv \sqrt{2\varepsilon_{F1}/(m\omega_\perp^2)}$ is the Thomas–Fermi radius for the spin majority and E_b is the binding energy of two atoms in the trap). Green curves are plotted for the majority (*1*), red for the minority (*2*), and dotted blue lines show the difference between the profiles. Each plot is labeled with the corresponding imbalance N_2/N_1 value. The presence of a flat center part flanked by two peaks in the difference plots is in agreement with complete pairing in the core. (Quoted from [74].)

Ketterle and coauthors detected a pairwise state (Bose condensate of composite bosons with equal densities of components $n_\uparrow = n_\downarrow$) in the center of a 3D trap, while excessive 'up' spins were primarily concentrated at the trap periphery. The situation is reversed in kinematically 1D gases: balanced paired fermions are located at the periphery, while excessive 'up' spins are concentrated in the trap center [227].

The first experimental results for phase separation in quasi-two-dimensional gases were obtained by the Thomas group [74]. The experimental data show that the situation in the quasi-two-dimensional geometry is similar in qualitative terms to that in the 3D case: balanced paired fermions are located in the trap center. The concentration profiles of atoms in two spin states are shown in Fig. 13. The images are made along the motion plane, and therefore the profiles show an

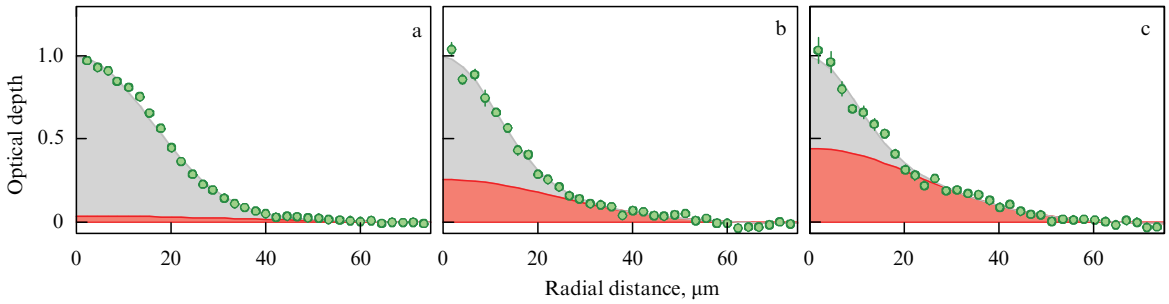

Figure 14. (Color online.) Optical depth profiles of spin-majority atoms after 3 ms of flying apart, normalized to the maximum value, and the result of fitting with two Gauss functions for the polarization values (a) $(N_1 - N_2)/(N_1 + N_2) = 0.25$, (b) 0.55, and (c) 0.75 in the 780 G field. The thermal part is shown in red, and the condensed one in grey. The error ranges show the standard deviation of the mean in averaging by azimuth. Each image corresponds to averaging over 30 iterations of the experiment. (Quoted from [75].)

integral over the concentration distribution along one direction. The flat central parts of the plots of the difference between the distributions (blue broken line) indicate that the spin concentrations in the center are the same.

Further explorations of phase separation [75] indicate the absence of discontinuities in spin polarization or concentration profiles near the phase transition line, in qualitative contrast to phase separation in 3D systems [228], where a first-order phase transition is observed. It is assumed in [75] that the absence of discontinuities is related to fluctuations, whose the role is enhanced if the dimension decreases.

Motion along the z axis can be of importance for imbalanced quasi-two-dimensional gases. A spin-minority atom moving in the majority's field can be in a superposition of states that include excited states of the oscillator along z.

Images of a spin-imbalanced gas made after the trap is disabled and the gas flies apart in free space [75] are shown in Fig. 14. The bimodal structure of the concentration distribution is clearly seen. The gas was initially prepared on the Bose side of a 3D Feshbach resonance, owing to which the disabling of tight confinement does not result in the rupture of dimer molecules. The dimer concentration profile can be closely related to the velocity distribution prior to flying apart, while the bimodal structure is interpreted as a signature of Bose condensation of dimer molecules [75]. It is noteworthy that the bimodal distribution is seen in expanded-gas images, regardless of whether phase separation occurs. The bimodal structure has been observed in a 2D Bose gas with weak repulsion without Bose condensation [229].

In the case of an external harmonic potential effective in the xy plane, the tendency of gas to form a spin-balanced core prevents other interesting phenomena — Fulde–Ferrell–Larkin–Ovchinnikov superfluidity [70, 71] and p-wave pairing driven by the Kohn–Luttinger mechanism [64–66], which require concentration imbalance — from being observed. A trap with rigid walls and a flat interior is needed for obtaining these effects. Confinement of a 2D Fermi gas in such a trap was recently reported in [150].

10. BCS – BEC crossover in the 100% polarized superfluid A1 phase

We note that new ways of studying triplet p-wave pairing in a 100% polarized superfluid Fermi gas have been provided by recent experiments related to Feshbach resonance in ultracold ^{6}Li and ^{40}K gases in the p-wave channel [230–232]. These experiments bring studies of resonance quantum gases closer to the physics of superfluid He-3 and of anomalous complex superconductors, for example, Sr_2RuO_4, $U_{1-x}Th_xBe_{13}$, and UNi_2Al_3 [233]. We note that in studying the p-wave Feshbach resonance, we are dealing with the BCS–BEC crossover between local and extended pairs for the triplet A1 phase, in which particles with the total spin projection $S_z = 1$ pair. A detailed description of the Feshbach resonance for the p-wave channel is contained in the first part of [25]. We only note here that the p-wave pairing occurs in a 100% polarized gas in the third order in the gas parameter (in the Fermi momentum) for the effective interaction in accordance with the Pauli principle (absence of 'down' spins) and general quantum mechanical results for the scattering amplitude of slow particles in a channel with the orbital momentum l [25, 102]. As a result, according to [18, 25, 66], the critical temperature T_{cp} in the dilute BCS region is

$$T_{cp} \simeq 0.1\varepsilon_F \exp\left(-\frac{\pi}{2|\lambda_p|}\right), \tag{45}$$

with the coupling constant (effective gas parameter)

$$\lambda_p \sim a_p r_0^2 p_F^3 < 0, \tag{46}$$

where r_0 is the effective radius of the potential and a_p is the negative p-wave scattering length. We stress that in the p-wave Feshbach resonance, it is the scattering length a_p (or more precisely, the scattering volume $V_p = r_0^2 a_p$) that changes sign in passing through the resonance field B_0. A qualitative scheme of the p-wave Feshbach resonance is shown in Fig. 15 [18, 25]. The Einstein formula for the gas of composite bosons with the spin $S = S_z = 1$ is again valid in the dilute BEC region. According to that formula,

$$T_{cp} \simeq \frac{3.31(n_\uparrow/2)^{2/3}}{2m}, \tag{47}$$

where $n_\uparrow = p_{F\uparrow}^3/6\pi^2$ is the density of 'up' spin particles. We note that the binding energy of composite bosons (bipolarons with the spin $S = S_z = 1$) for the p-wave Feshbach resonance is

$$|E_b| = \frac{\pi}{2mr_0 a_p}. \tag{48}$$

In the unitary limit, $1/\lambda_p = 0$ and $T_{cp} \simeq 0.1\varepsilon_F$ still corresponds to the BCS region. The dotted line in Fig. 16 shows the effective boundary between the BCS and BEC regions that is set by the line of zero chemical potential $\mu(T) = 0$. Also indicated is the important quantum phase transition point [234, 235] where $\mu(T = 0) = 0$. In accordance with

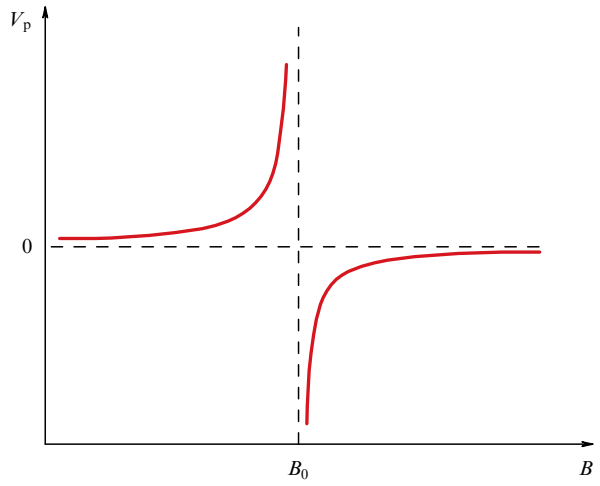

Figure 15. Qualitative scheme of the p-wave channel Feshbach resonance. The scattering volume V_p diverges at $B = B_0$ [25].

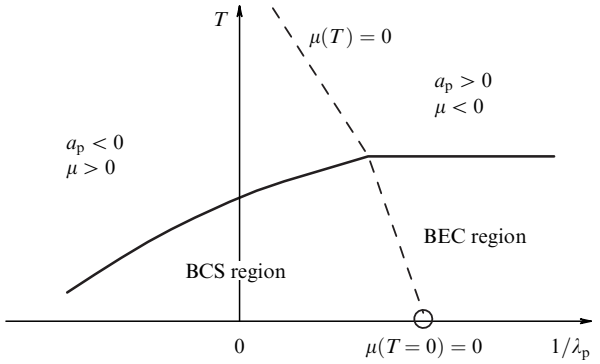

Figure 16. Qualitative diagram of the p-wave channel BCS–BEC crossover for the 100% polarized superfluid A1 phase represented as a dependence of the temperature T on $1/\lambda_p$, where $\lambda_p = V_p p_F^3 = r_0^2 a_p p_F^3$ is the effective gas parameter. The phase diagram displays a (dotted) line where the chemical potential $\mu(T) = 0$ and the important quantum phase transition point where $\mu(T = 0) = 0$ [234, 235].

general theoretical concepts [18, 25, 50, 234, 235], the result of calculating the quasiparticle contribution to the thermal capacity and normal density near a quantum critical point depends on the path the point is approached as $\mu \to 0$ and $T \to 0$, which means that the limits $|\mu|/T \to 0$ and $T/|\mu| \to 0$ are not equivalent [25]. We now consider this interesting aspect in more detail. We know that points or lines emerge for anomalous p-wave and d-wave pairing superconductors where the superconducting gap vanishes. For example, in the 3D A1 phase of superfluid He-3, the gap squared $\Delta^2 = \Delta_0^2 \sin^2\theta$ as a function of the polar angle θ (with respect to the z axis of orbital momentum quantization) vanishes at two points on the Fermi surface: the north and south poles $\theta = 0$ and $\theta = \pi$. As a result, the energy spectrum of quasiparticles in the superfluid A1 phase at low temperatures $T \ll T_c$ has the form [50, 51]

$$E_p = \sqrt{\left(\frac{p^2}{2m} - \mu\right)^2 + \frac{|\Delta\,\mathbf{p}|^2}{p_F^2}}, \tag{49}$$

where

$$\boldsymbol{\Delta} = \Delta_0(\mathbf{e}_x + i\mathbf{e}_y) \tag{50}$$

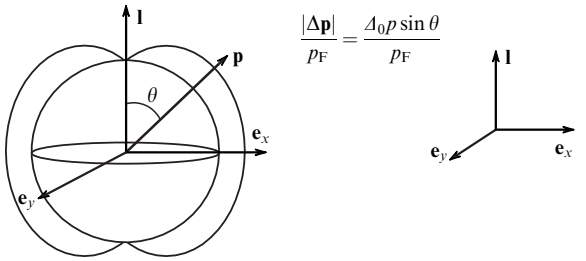

Figure 17. Superfluid gap topology in the A1 phase. Two points are distinguished that correspond to the north and south poles on the Fermi surface where the quasiparticle energy and superfluid gap vanish [25].

is the complex-valued order parameter in the A1 phase, and Δ_0 is the superfluid gap amplitude. It is easy to see that

$$|\Delta\mathbf{p}|^2 = \Delta_0^2 p^2 \sin^2\theta = \Delta_0^2[\mathbf{p} \times \mathbf{l}]^2, \tag{51}$$

where $\mathbf{l} = \mathbf{e}_x \times \mathbf{e}_y$ is the unit vector of the orbital momentum of a pair (Fig. 17). We note that the low-temperature quasiparticle spectrum for a normal s-wave pairing superconductor has the form

$$E_s = \sqrt{\left(\frac{p^2}{2m} - \mu\right)^2 + \Delta_0^2}. \tag{52}$$

We also note that the quasiparticle energy in the (bosonic) BEC region at negative chemical potential values $\mu = -|\mu| < 0$ for both s-wave and p-wave pairing is nonvanishing everywhere because $p^2/2m - \mu = p^2/2m + |\mu| > 0$. At the same time, the quasiparticle energy in the dilute BCS region with p-paring vanishes at two points: $p^2/2m = \mu$ and $\theta = 0; \pi$. As a result, a nontrivial quasiparticle contribution to the thermal capacity emerges at small $|\mu|$ and low temperatures T in the classical limit $|\mu|/T \to 0$ (more precisely, if $|\mu| \ll T \ll \Delta_0^2/\varepsilon_F$):

$$C_V \sim \frac{(2mT)^{3/2}}{2\pi^2}\frac{\varepsilon_F T}{\Delta_0^2} \propto T^{5/2}. \tag{53}$$

But the quasiparticle contribution to the thermal capacity in the quantum limit $T/|\mu| \to 0$ (if $T \ll |\mu| \ll \Delta_0^2/\varepsilon_F$) behaves differently in the BCS ($\mu > 0$) and BEC ($\mu < 0$) regions. The quasiparticle contribution in the BCS region is described as before by a power-law function, but the exponent is different:

$$C_V \sim \frac{1}{2\pi^2}\frac{m^{3/2}}{\mu^{1/2}}\frac{\varepsilon_F T}{\Delta_0^2}T^2 \propto T^3. \tag{54}$$

At the same time, this contribution is exponentially small in the BEC region:

$$C_V \sim \frac{(2mT)^{3/2}}{2\pi^2}\left(\frac{|\mu|}{T}\right)^3\frac{\varepsilon_F T}{\Delta_0^2}\exp\left(-\frac{|\mu|}{T}\right) \propto \frac{1}{\sqrt{T}}\exp\left(-\frac{|\mu|}{T}\right). \tag{55}$$

We note that the order of magnitude of all three formulas (52)–(54) becomes the same at $|\mu| \sim T$. The normal density ρ_n behaves similarly in the classical and quantum limits. We obtain a more expectable result for the quasiparticle contribution to the thermal capacity for small values of $|\mu|$ and

intermediate temperatures $|\mu| \ll \Delta_0^2/\varepsilon_F \ll T \ll \Delta_0$:

$$C_V \sim \frac{(2mT)^{3/2}}{2\pi^2} \propto T^{3/2}. \tag{56}$$

It is noteworthy that the fermionic (quasiparticle) contribution to the thermal capacity can easily be separated from the bosonic contribution related to sound oscillations using the exponential in the temperature dependence. The phonon contribution to the A1-phase thermal capacity is

$$C_V^{\mathrm{B}} \sim \frac{1}{2\pi^2}\frac{T^3}{C_s^3} \propto T^3, \tag{57}$$

where C_s is the speed of sound in the BCS–BEC crossover for the A1 phase. The speed of sound in the BCS regions is

$$C_{\mathrm{BCS}} \approx \frac{v_F}{\sqrt{3}}, \tag{58}$$

in accordance with the thermodynamic identity $C_s^2 = \partial P/\partial\rho$ for the derivative of the pressure P with respect to the mass density $\rho = mn$ in a normal (nonsuperfluid) Fermi gas at low temperatures $T \ll \varepsilon_F$ [28]. The speed of sound in the dilute BEC region is given by the thermodynamic identity

$$C_{\mathrm{BEC}} = \left(\frac{n_B}{m_B}\frac{\mathrm{d}\mu_{\mathrm{Bose}}}{\mathrm{d}n_B}\right)^{1/2}, \tag{59}$$

where $n_B = n_\uparrow/2$, $m_B = 2m$, and $\mu_{\mathrm{Bose}} = 2\mu + |E_b|$. The solution of the self-consistent Leggett system of equations shows that $C_{\mathrm{BEC}} \propto v_F(p_F r_0) \ll v_F$ in the dilute BEC system. It is shown in [25] that the phonon contribution to thermal capacity (57) and a similar contribution to the normal density near the quantum critical point,

$$\rho_n^{\mathrm{B}} \sim \frac{T^4}{C_s^5}, \tag{60}$$

exceed the fermion contribution near the quantum critical point and are the dominant ones.

We outline the specific features of the BCS–BEC crossover in the 100% polarized 2D A1 phase. Using the terminology adopted for thin films of superfluid He-3, it is referred to as the axial phase [18, 50, 236]. The order parameter in this phase again has the form

$$E_p = \left[\left(\frac{p^2}{2m} - \mu\right)^2 + \frac{\Delta_0^2 p^2}{p_F^2}\right]^{1/2}, \tag{61}$$

where $p^2 = p_x^2 + p_y^2$. Quasiparticle energy spectrum (61) vanishes at a single point $p = \mu = 0$. The results in [237] show that this point is the point of a topological phase transition that separates the gapped region of the quasiparticle spectrum from the gapless region, while the axial phase itself is characterized by the presence of a nonzero topological invariant (topological charge) [50, 103]

$$Q = \frac{\pi}{2}\varepsilon_{\alpha\beta}\int\frac{\mathrm{d}^2 p}{(2\pi)^2}\,\mathbf{n}[\partial_\alpha\mathbf{n}, \partial_\beta\mathbf{n}], \tag{62}$$

where $\mathbf{n}$ is the unit vector with the components

$$\mathbf{n} = \frac{1}{E_p}(-\Delta_0 p_x, \Delta_0 p_y, \xi_p) \tag{63}$$

and $\xi_p = p^2/2m - \mu$. This invariant, introduced in the physics of quantum gases and superfluid He-3, was taken from the physics of the quantum Hall effect, where it controls quantization of the Hall conductivity. According to Pokrovskii, the nontrivial topology in lower-dimension spaces is controlled in qualitative terms by the sites in the crossing of nearby paths in the approach based on Feynman path integrals. At the same time, nearby paths can 'bypass' each other in the 3D space without linking, and the nontrivial topology is not so evident in the 3D case. Formula (62), taking conditions (63) into consideration, can be transformed for the 100% polarized axial phase into the easily comprehensible form

$$Q = \frac{1}{2}\left(1 + \frac{\mu}{|\mu|}\right). \tag{64}$$

Formula (64) obviously shows that $Q = 0$ in the BEC region (for negative values of the chemical potential) and $Q = 1$ in the BCS region (for positive values of the chemical potential).Thus, we conclude that the BCS region for the 2D axial phase is topologically nontrivial. The quantum critical point $p = \mu = 0$ is actually a boundary between the topologically trivial and topologically nontrivial phases. We note that the results for thermal capacity and normal density near the quantum critical point differ in the classical and quantum limits in the 2D case just as in the 3D A1 phase. We stress that in both the 3D and 2D cases, we always effectively use the classical limit $|\mu|/T \to 0$ because the chemical potential is always continuous near $\mu = 0$. Therefore, the real (quantum) phase transition only occurs at $T = 0$ [234, 235]. Finally, it is worth noting a kink in compressibility in the 100% polarized axial phase at the point $\mu = 0$. This kink, which can be deduced using both analytic [25, 57] and numerical [238, 239] methods, is given by the formula

$$\frac{\partial n_\uparrow}{\partial\mu} \propto 1 + \frac{\mu\varepsilon_F}{\Delta_0^2}[1 - \operatorname{sign}\mu], \tag{65}$$

where $\operatorname{sign}\mu = 1$ if $\mu \geqslant 0$ and $\operatorname{sign}\mu = -1$ if $\mu < 0$. Consequently, we have the compressibility $\partial n_\uparrow/\partial\mu \simeq 1$ as $\mu \to +0$ and $\partial n_\uparrow/\partial\mu \simeq 1 + 2\mu\varepsilon_F/\Delta_0^2$ as $\mu \to -0$.

In concluding this section, we note that according to [240], the existence of a nonzero topological invariant $Q \neq 0$ causes the existence of anomalous spin current in thin films of the superfluid A1 phase in He-3 (in the BCS region) in the presence of a nonuniform magnetic field $\mathbf{H}(\mathbf{r})$:

$$j_{\alpha i}^{\mathrm{spin}} \sim \varepsilon_{izk} l_z \partial_k H_\alpha^\perp. \tag{66}$$

Here, $l = l_z$ is the unit quantization vector of the orbital momentum of the pair and $\mathbf{H}_\perp\mathbf{d} = 0$, where $\mathbf{d}$ is the spin vector in the 2D (thin) film of the He-3 superfluid A1 phase. Another possible manifestation of the nontrivial topology in the 2D case can be related to attempts to find so-called Majorana fermions [241] in experiment, for example, in boundary states on the interface of superfluid He-3B and a rough wall or on the surface of a wire oscillating in superfluid He-3 in Lancaster experiments [242].

11. Critical velocities and spectrum of collective excitations in the BCS – BEC crossover for s-wave and p-wave pairing

In this section, we briefly discuss the spectrum of collective excitations in the BCS–BEC crossover for s-wave and p-wave

pairing. We note that the main collective mode in the BCS region in the case of resonance s-wave pairing in the Fermi gas of neutral (uncharged) particles is Bogoliubov–Anderson sound oscillations [243–246], while in the BEC region, Bogoliubov's results for a weakly nonideal Bose gas with repulsion (in this case, the gas of composite bosons with mass $2m$ and density $n/2$) hold. However, both spin and orbital waves can also be excited in the case of triplet p-wave pairing [25, 50–53, 57].

The spectra of collective excitations for s-wave pairing in gases and high-temperature superconductors have been theoretically explored in many studies [24, 247–251]. We first outline the results reported in [24]. The speed of sound and the critical velocity of the breakup of superfluidity have been calculated in this work, not only in dilute-gas BCS and BEC regions but also in the involved transition regime. The spectrum of collective excitations for a negative scattering length $a < 0$ and positive chemical potential $\mu \approx \varepsilon_F$ (deep in the BCS region) is linear, in agreement with the Anderson–Bogoliubov theory:

$$\Omega^2 = C_{BCS}^2 q^2, \tag{67}$$

where the speed of sound is again $C_{BCS} \approx v_F/\sqrt{3}$. At the same time, if the scattering length is positive, $a > 0$, and the chemical potential is negative, $\mu < 0$ (deep in the BEC region), the spectrum of collective excitations is described by the Bogoliubov formula

$$\Omega^2 = C_{BEC}^2 q^2 + \left(\frac{q^2}{4m}\right)^2, \tag{68}$$

where

$$C_{BEC} = \sqrt{\frac{\mu_{Bose}}{m_B}} \tag{69}$$

is the Bogoliubov speed of sound and the boson chemical potential in the 3D case is represented as

$$\mu_{Bose} = \frac{4\pi a_{2-2} n_B}{m_B}. \tag{70}$$

The scattering length in Eqn (70), $a_{2-2} = 0.6|a| > 0$, is the length of repulsive dimer–dimer scattering, $n_B = n/2$ is the boson density, and $m_B = 2m$ is the composite boson mass. For the absolute value of the gas parameter $|a|p_F \ll 1$, we can easily show that $C_{BEC} \ll C_{BCS}$. The speeds of sound only become comparable in the intermediate region where $|a|p_F \geqslant 1$. We note the speed of sound $C_s \approx 0.4 v_F$, as shown in [24] in the unitary limit $1/a \to 0$ by solving the self-consistent Leggett system of equations for the superfluid gap and the superfluid density. Figure 18 shows the behavior of the dimensionless speed of sound C_s/v_F and the dimensionless critical velocity at which the superfluid flow is suppressed as a result of spontaneous generation of normal excitations according to the Landau criterion [13, 28]. We note that the critical velocity in a superfluid Fermi liquid or Fermi gas can be found from the formula [24]

$$v_c = \min\left\{C_s, \left(\frac{\sqrt{\Delta_0^2 + \mu^2} - \mu}{m}\right)^{1/2}\right\}, \tag{71}$$

where Δ_0 is the superfluid gap amplitude (for Cooper pairing). The speed of sound deep in the dilute BCS region at small

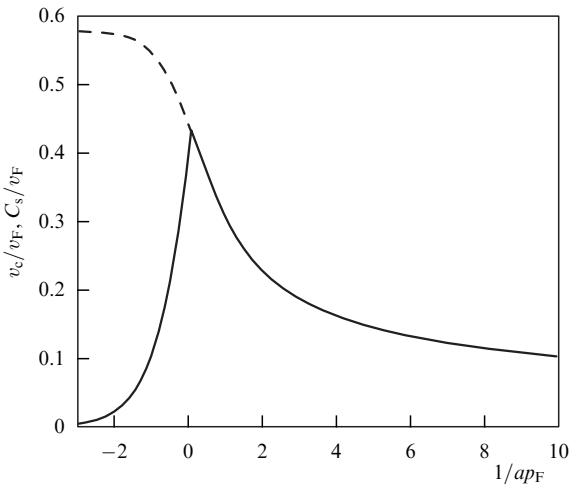

Figure 18. Dimensionless speed of sound C_s/v_F and the dimensionless critical velocity v_c/v_F (in units of the Fermi velocity v_F) in the 3D BCS–BEC crossover for standard s-wave pairing as a function of the inverse gas parameter $1/ap_F$ [24].

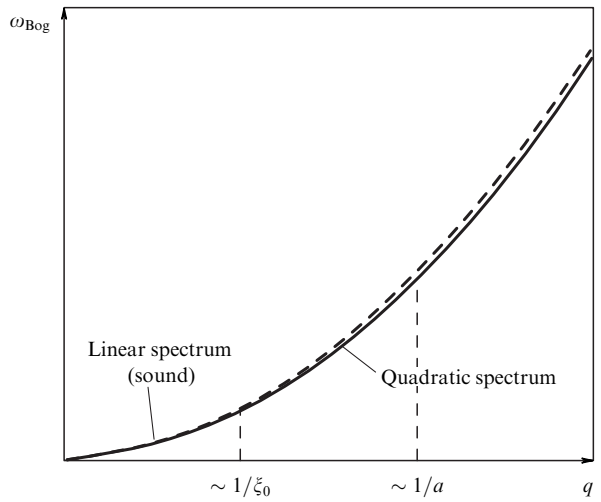

Figure 19. Collective excitation spectrum in the dilute BEC region. The solid curve shows the Bogoliubov spectrum for pointlike bosons. The dashed curve shows corrections to the Bogoliubov spectrum at large wave vectors $q \gg 1/a \gg 1/\xi_0$ [24].

values of the gas parameter $|a|p_F \ll 1$ is $C_s = v_F/\sqrt{3}$, while $v_c = \Delta/p_F \ll C_s$ as a result of Cooper pairs being unpaired. It is natural that the critical velocity coincides in the dilute BEC region with the speed of sound, $v_c = C_s$. It is noteworthy that there are nontrivial corrections to Bogoliubov spectrum (68) and (69) due to the composite character of bosons in the resonance Fermi gas in the BEC region. Those corrections are shown in Fig. 19 [24]. They are most significant at large wave vectors $q \geqslant 1/a \gg 1/\xi_0$, where

$$\xi_0 = \frac{1}{\sqrt{n_B a_{2-2}}} \tag{72}$$

is the Bogoliubov-gas coherence length [28, 252, 253] whence

$$\frac{\xi_0}{a} \sim (na^3)^{-1/2} \gg 1. \tag{73}$$

The speed of sound in an ultracold Fermi gas has been measured in [27]. The sound is excited in a spindle-shaped gas

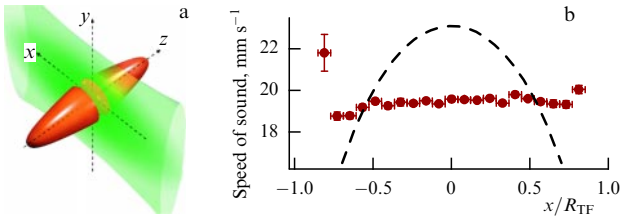

Figure 20. (Color online.) (a) Green beam, whose short-time activation excites a sound wave in the atomic cloud (shown in red). (b) Speed of sound as a function of the transverse coordinate x (dots) showing that the wave front is flat. For comparison, the dashed line shows the values obtained in the isotropic model (74) by averaging over y. The coordinate x is normalized to the Thomas–Fermi radius. (Quoted from [27].)

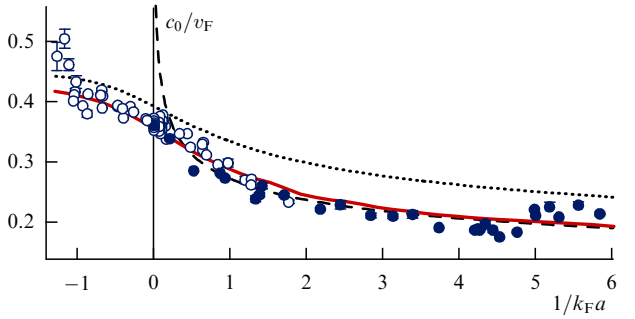

Figure 21. (Color online.) Normalized speed of sound c_0/v_F as a function of the interaction parameter $1/k_Fa$. The respective filled and open circles correspond to measurements in a trap whose depths are 140–500 nK and 0.6–80 μK. The solid red lines shows calculations done using the Monte Carlo method. The dashed line is plotted using the mean-field method. The dotted line corresponds to Eqn (76) for BEC molecules at $a_{2-2} = 0.6\,a$. (Quoted from [27].)

cloud of lithium-6 atoms confined in an optical dipole trap. The atoms are uniformly distributed between two internal states with the minimum energy. The interaction parameter $1/k_Fa$ is varied by changing the s-wave scattering length a and the wave vector $k_F \equiv \sqrt{2m\varepsilon_F}/\hbar$, where $\varepsilon_F \equiv \hbar(3N\omega_x\omega_y\omega_z)^{1/3}$ is the Fermi energy of a noninteracting Fermi gas in the same trap. The length a is in turn controlled using the magnetic field B, the strength of which is selected in the range 700–1100 G, spanning both sides of the Feshbach resonance located at $B_{res} = 832$ G [107] (it was believed at the time of measurement that the resonance occurred at $B_{res} = 834$ G [254], but this circumstance weakly affects the interpretation of the results). The Fermi wave vector k_F depends on the variable frequencies of the trap and the total number of atoms N, which varies from 6×10^4 for molecular BEC to 5×10^5 near and above the Feshbach resonance. Temperatures that are close to the lowest values attainable in such experiments are estimated to be $\simeq 0.1\varepsilon_F$. Sound waves are excited using a green-light beam (Fig. 20a), which is switched on for a short time. The green beam creates a repulsive potential because its wavelength 532 nm is shorter than 671 nm, the wavelength that corresponds to the strongest electric dipole transition in lithium. A similar excitation method was used earlier for the BEC of atoms [255]. The sound waves propagate from the excitation plane to the edges along the long direction z. The waves were detected by variations in density.

The sound wave front is flat despite the nonuniformity of the cloud in radial directions, as can be seen in Fig. 20b, which shows the distribution of the speed of sound along the transverse coordinate. The calculated function obtained in an isotropic propagation model, shown for comparison in the same figure,

$$c_{\text{local}}\bigl(n(x,y,z)\bigr) = \sqrt{\frac{n}{m}\frac{\mathrm{d}\mu}{\mathrm{d}n}}, \tag{74}$$

predicts that the wave front is curved. The isotropic approximation obviously disagrees with the data. The sound propagation is therefore close to the narrow cylindrical channel approximation, owing to which the measured speed of sound can be related to the equation of state for the chemical potential of an atom at zero temperature $\mu = \mu(n)$ [256]:

$$c(z) = \sqrt{\frac{\int n(x,y,z)\,\mathrm{d}x\,\mathrm{d}y}{m\int(\mathrm{d}\mu/\mathrm{d}n)^{-1}\mathrm{d}x\,\mathrm{d}y}}. \tag{75}$$

The speed of sound was measured in an experiment in a larger part of the BCS–BEC crossover. Figure 21 shows results of the measurements: the normalized speed of sound c_0/v_F ($v_F \equiv \hbar k_F/m$) plotted as a function of the interaction parameter $1/k_Fa$. The speed of sound in the central cross section of the cloud $z = 0$ is plotted.

The only parameter of the system in the $T = 0$ approximation is the interaction parameter $1/k_Fa$. If $|1/k_Fa| \ll 1$, the gas is in the strong-coupling regime; if $1/k_Fa < -1$, the gas is a weakly coupled Fermi system; and if $1/k_Fa > 1$, it is a Bose–Einstein condensate of molecules. Using the mean-field approximation [10] and the quantum Monte Carlo method [127], we can derive the equation of state for all coupling regimes. The mean-field approximation yields the speed of sound (the dotted curve in Fig. 21), which is systematically higher than the speed measured for virtually all values of $1/k_Fa$. Calculations based on the quantum Monte Carlo algorithm [127, 257], which are shown with the solid red line, agree much better with the measured results.

The state of the system in the BEC regime, at $1/k_Fa > 1$, can be regarded as a BEC of pointlike molecules interacting with the s-scattering length a_{2-2}. Using equation of state (70) in formula (75) for c_0, we find

$$\frac{c_0}{v_F} = \frac{1}{4}\left(\frac{5}{2}\,k_Fa_{2-2}\right)^{1/5}. \tag{76}$$

The model that exactly takes the scattering of four fermions into account predicts $a_{2-2} = 0.6\,a$ [114]. Formula (76), where this scattering length is used, yields a speed of sound that coincides with the measurements (shown in Fig. 21 with a dotted line). The mean-field theory [10] where the ground state in the form of a direct product of Cooper pairs is used predicts in contrast $a_{2-2} = 2a$, a value that yields a speed of sound 27% higher than that observed in the BEC regime. The results obtained using the quantum Monte Carlo method [127, 257] are still higher than the measured speeds in the larger part of the BEC region, although being closer to the measured data.

The lower speed observed in the larger part of the BEC regime at $1 < 1/k_Fa < 5$ can be a consequence of mixing of the first and second sounds [258]. The speed of the second sound is lower, as a result of which the excitation propagation speed can become smaller. The nonzero temperature can hardly be a reason for the sound being slowed down: first, the thermal component has not been detected in the BEC of

molecules and, second, an opposite effect is observed in the Feshbach resonance: an increase in temperature results in the growth of c_0.

Measurements at the Bose asymptote of the crossover have been made for the largest values of the $1/k_F a$ parameter attainable in the experiment. To reach the value $1/k_F a > 5$, both the magnetic field and the trap depth were tuned in such a way that both k_F and a were concurrently minimized. If $1/k_F a > 5$, the measurements show that the ratio c_0/v_F grows. Taking images in this regime is complicated by insufficient expansion of the cloud after its release from the optical trap: the chemical potential is not large enough in comparison with the magnetic field potential for the cloud to fly apart to the extent that would enable accurate measurement of the sound-wave front position.

Sound propagation is not observed in the furthermost Fermi part of the resonance, at $1/k_F a < -1.3$. In this case, the dip in density is simply filled in as in an ideal Fermi gas. The gas is not necessarily in the superfluid phase for the lowest temperatures attained in the weak-coupling region. Hydrodynamic propagation of sound is maintained in this case due to collisions rather than the superfluid component.

The vibrational modes of an ultracold gas confined in a spindle-shaped potential can be a source of information about the gas properties [259–270]. The breathing mode in the radial direction has been studied in depth in experiments [26, 111, 271–273]. The behavior of the mode frequency and decrement evidence the occurrence of superfluidity in the Fermi-atom gas in the strong s-coupling regime [111, 272] and the breakup of the superfluid state if the interaction becomes weaker [26, 271]. The dependence of the frequency on the interaction parameter was used to verify the equation of state of the gas [26, 273], to discover a deviation from the mean-field model [273].

The breathing mode is excited if the spindle-shaped potential of the trap is switched off for a short time $\ll 1/\omega_\perp$. After the potential is restored, the gas oscillates in the trap for a time t_{hold}. Then, to observe small-amplitude oscillations, the trap is fully disabled, and the cloud flies apart in free space in a fixed time $\gg 1/\omega_\perp$. Images of the gas after expansion, which correspond to various oscillation phases, are shown in Fig. 22. To find the oscillation frequency ω and the decrement $1/\tau$, the cloud size as a function of the oscillation duration was fitted using a damped sinusoid,

$$A \exp\left(-\frac{t_{\text{hold}}}{\tau}\right) \cos\left(\omega t_{\text{hold}} + \varphi\right), \tag{77}$$

as shown in Fig. 23.

The frequency ω of the radial breathing mode can be calculated under the assumption that the system is a superfluid liquid. The particle motion is described in this case by Euler's equation without rotation and the continuity equation:

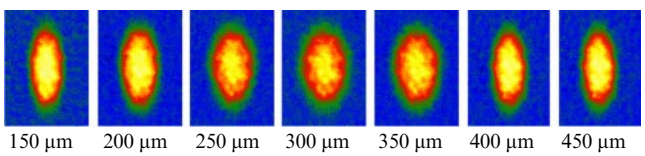

Figure 22. (Color online.) Transverse breathing mode. A cloud of atoms after oscillations in a trap during a variable time t_{hold} (indicated below the images) and subsequently flying apart for 1 ms. Experiment parameters [272]: $N = 2 \times 10^5$, $\omega_\perp/(2\pi) = 1700$ Hz, and $\omega_z/(2\pi) = 70$ Hz.

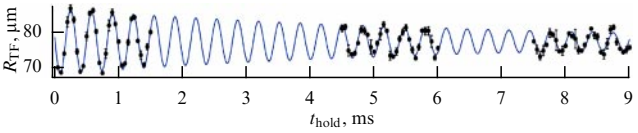

Figure 23. Transverse breathing mode [272]. The Thomas–Fermi radius of the dissipated cloud as a function of the oscillation duration t_{hold}. Data are shown as dots, and the fitting sinusoid as a solid line. (Quoted from thesis [274].)

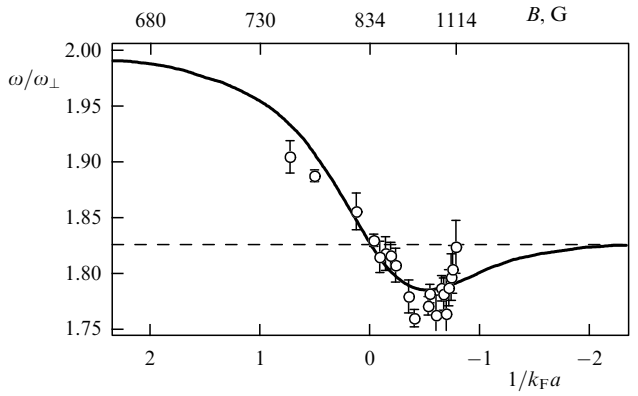

Figure 24. Normalized frequency of the transverse breathing mode for different values of detuning from the Feshbach resonance. Data are shown as dots, and the results of simulation in the mean-field approximation [264, 267] as a solid line. The broken line corresponds to the hydrodynamic frequency at the resonance $\omega = \sqrt{10/3}\,\omega_\perp$. The detuning is set on the lower horizontal axis in units of $1/k_F a$, and the corresponding magnetic field on the upper axis with a nonlinear scale. (Quoted from [26].)

$$m \frac{\partial \mathbf{u}}{\partial t} = -\nabla V - \frac{\nabla P}{n} - \nabla \frac{m\mathbf{u}^2}{2}, \tag{78}$$

$$\frac{\partial n}{\partial t} + \operatorname{div} \mathbf{u} n = 0, \tag{79}$$

where $n(\mathbf{x}, t)$ is the total concentration of atoms, $\mathbf{u}(\mathbf{x}, t)$ is the velocity field of atom pairs, P is the total pressure, and $V(\mathbf{x})$ is the confining potential. Assuming that the equation of state is

$$P = \text{const}\, n^{\gamma+1}, \tag{80}$$

we can deduce that the breathing-mode frequency in the elongated cylindrically symmetric field depends only on the exponent γ and the transverse frequency [264, 266]:

$$\omega = \sqrt{2(\gamma+1)}\,\omega_\perp. \tag{81}$$

The breathing-mode frequency for the exponent γ calculated in the mean-field approximation of Cooper pairs [264, 267] is shown in Fig. 24. Approximation (80) arises in a natural way in at least three cases:

— P is equal to the pressure of a noninteracting Fermi gas on the fermion asymptote of the BCS–BEC crossover with weak attraction between atoms; this yields $\gamma = 2/3$ and $\omega = \sqrt{10/3}\,\omega_\perp$;

— the leading contribution to the pressure at the boson asymptote comes from the mean field of molecules (70) and hence the mean-field approximation yields $\gamma = 1$ and $\omega = 2\omega_\perp$; and

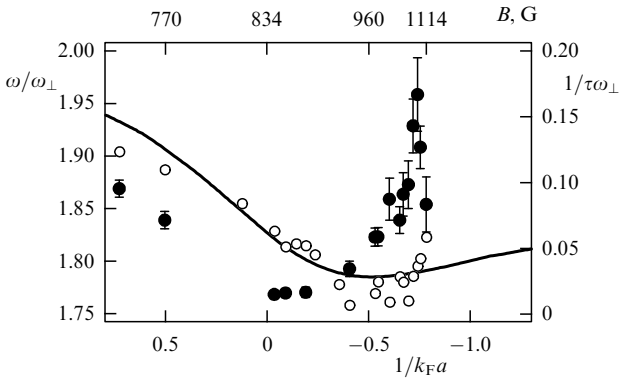

Figure 25. Normalized decrement and frequency of the transverse breathing mode for different values of detuning from the Feshbach resonance. Data for decrements are shown with filled circles. Data (open circles) and calculations done in the mean-field approximation [264, 267] (solid curve) are displayed for the frequency. The detuning value is set to the lower horizontal axis in units of $1/k_{\mathrm{F}}a$, and the corresponding magnetic field to the upper axis with a nonlinear scale. (Quoted from [26].)

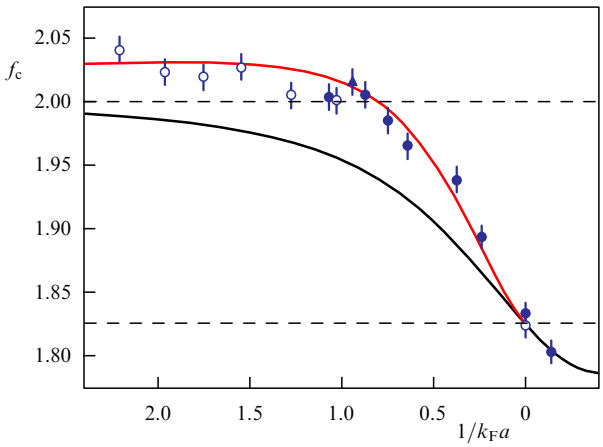

Figure 26. Normalized breathing mode frequency $f_{\mathrm{c}} \equiv \omega/\omega_{\perp}$ as a function of the interaction parameter $1/k_{\mathrm{F}}a$. Data are shown by filled and open circles. The calculated curves that refer to the mean-field BCS theory (lower curve) and the calculations done using the quantum Monte Carlo method (upper curve) are based on the result in [268]. Horizontal lines show the values in the BEC limit ($f_{\mathrm{c}} = 2$) and the unitary limit ($f_{\mathrm{c}} = \sqrt{10/3}$). (Quoted from [273].)

— in the unitary limit, $\gamma = 2/3$, as is the case of weak attraction, because the pressure has the form [275, 276]

$$P(n) = (1+\beta)\frac{2}{5}\,n\,\varepsilon_{\mathrm{F}} = (1+\beta)\,\frac{2}{5}\,\frac{\hbar^2}{2m}\,(3\pi^2)^{2/3}\,n^{5/3}\,, \qquad (82)$$

where $\beta = -0.63$ [107, 277].

For the gas of noninteracting particles, $\omega = 2\omega_{\perp}$, which coincides with the boson limit in the case of hydrodynamic oscillations.

Measured frequencies [26] of the radial breathing mode are also shown in Fig. 24. The experimental setup was similar to that of the experiment where the speed of sound was measured, as described above in this section [27]. The coupling between two Fermi atoms in two spin states is varied by tuning the magnetic field in the range 700–1100 G. The estimated temperature is $\simeq 0.1\varepsilon_{\mathrm{F}}$. The measured frequencies agree as a whole with the mean-field calculation results; we can also see the agreement in the unitary limit $1/k_{\mathrm{F}}a = 0$.

Deviations of the breathing-mode frequency from the frequency that follows from the mean-field theory are also of interest. Figure 25 displays the enlarged central part of the plot in Fig. 24, where measured decrements are added. In moving away from the resonance to the Fermi side, $B > 832$ G, we can see that the frequency values systematically deviate from the predictions of the simple hydrodynamic model. First, in the range $0 > 1/k_{\mathrm{F}}a > -0.7$, the frequency is systematically lower than the theoretical curve, and the frequency rapidly increases in the range $1/k_{\mathrm{F}}a < -0.7$ ($B > 1050$ G). Located at the parameter value where the frequency starts rapidly growing, $1/k_{\mathrm{F}}a = -0.74$ ($B = 1080$ G), is the damping decrement peak. The width of the peak as a function of the magnetic field is much smaller than the Feshbach resonance width; therefore, the decrement peak values cannot originate from a process related to the mean field or the particle collision rate. The only process that features a steep dependence on changes in B is the resonance between the breathing mode oscillations and the Cooper pair binding energy. Therefore, the damping peak near $B = 1080$ G is most probably related to the breakup of Cooper pairs by phonons. It was found in a similar experiment performed earlier [271] that the peaking of the decrement is accompanied by the rapid growth of the breathing mode frequency. It was not possible in [271] to relate the decrement peak to the deviation from the frequency predicted in the superfluid-gas hydrodynamics because of an unaccounted systematic shift in trap frequency measurements. The rapid growth of collective mode damping near the phase transition from the superfluid state to the normal one was predicted in [260].

In shifting away from the Feshbach resonance to the Bose side ($1/k_{\mathrm{F}}a > 0$), we can see in Figs 24 and 25 that the breathing frequency mode goes down with respect to the prediction of the mean-field model at $T = 0$. It was shown in [273] that the breathing mode frequency decreases if the temperature is not zero. The authors of the experiment in [273], having decreased the temperature relative to the experiment in [26], have shown that the breathing mode frequency in the Bose region lies higher than the mean-field model predictions (Fig. 26). The upward deviation of the frequency from the mean-field model is due to the Lee–Huang–Yang fluctuation corrections [278, 279]. For comparison, Fig. 26 shows the calculations done using the quantum Monte Carlo method including the fluctuation corrections.

12. Orbital wave spectrum and orbital momentum paradox in the hydrodynamics of the superfluid A1 phase

There is another interesting branch that is observed in the collective excitation spectrum in the superfluid A phase of He-3 and resonance Fermi gas if the anisotropic A phase is realized (or, more precisely, for the A1 and A2 phases in strong magnetic fields or in the case of strong imbalance): the so-called orbital waves related to the rotation of the quantization vector of the Cooper pair orbital momentum $\mathbf{l}$ about the axis perpendicular to that vector. The spectrum of this mode is quadratic for small wave vectors (the A phase of superfluid He-3 is often referred to as an orbital ferromagnet; the A1 phase is also a spin ferromagnet) and in the bosonic limit (BEC) $\Omega \sim q_z^2/m$, where z is the quantization axis of orbital momentum $\mathbf{l}$. The situation becomes much less trivial

in the BCS region, where the orbital wave spectrum for small wave vectors has the form [36, 50, 53]

$$(\rho - C_0)\Omega \simeq \rho\,\frac{q_z^2}{m}\ln\frac{\Delta_0}{v_{\mathrm{F}}|q_z|}\,. \tag{83}$$

The conclusions on the values of the C_0 factor at low frequencies and small wave vectors that are reported in the literature are very controversial. The relative difference between density and this coefficient in the single-particle approximation in the dilute BCS region $C_0 \approx \rho$ and, moreover, in the weakly coupled theory (at $T_{\mathrm{c1}} \ll \varepsilon_{\mathrm{F}}$) is

$$\frac{\rho - C_0}{\rho} \sim \frac{\Delta_0^2}{\varepsilon_{\mathrm{F}}^2} \ll 1\,. \tag{84}$$

We have the value $\Delta_0 \sim T_{\mathrm{c1}} \sim 1$ mK in the A phase of He-3 in the weak-coupling approximation while $\varepsilon_{\mathrm{F}} \sim 1$ K, whence $\Delta_0^2/\varepsilon_{\mathrm{F}}^2 \sim 10^{-6}$. A matter of discussion is whether this conclusion persists in the hydrodynamic limit with multiparticle interactions taken into account. We note that all researchers agree that the coefficient

$$C_0 \simeq \frac{N(0)}{2}\int \mathrm{d}\xi_p\left(1 - \frac{\xi_p}{|\xi_p|}\right), \tag{85}$$

where $N(0)$ denotes the density of states on the Fermi surface, vanishes in the BEC region: $C_0 = 0$ at $\xi_p = p^2/2m + |\mu| > 0$. At the same time, formula (85) determines the full density in the BCS region at negative values $\xi_p < 0$, whence $C_0 \approx \rho$. Therefore, the orbital wave spectrum in the BEC region has the form

$$\Omega \simeq \frac{q_z^2}{m}\ln\left(\frac{\Delta_0}{v_{\mathrm{F}}|q_z|}\right). \tag{86}$$

Using spectrum (83), we can obtain a similar estimate for the internal orbital momentum density in the BCS region:

$$\mathbf{L} = \frac{\hbar}{2m}(\rho - C_0)\,\mathbf{l}\,, \tag{87}$$

while in the BEC region we have a more natural expression:

$$\mathbf{L} = \frac{\hbar}{2m}\,\rho\mathbf{l}\,. \tag{88}$$

It is of importance that in the BCS region, as we see below, the C_0 coefficient also determines the anomalous term in the mass current, and therefore for $C_0 \neq 0$ the conservation law for the total momentum is not satisfied at zero temperature, and hence the hydrodynamic description fails. The nature of the anomalous term in the current is often related to the chiral anomaly that is responsible for the axial current nonconservation in quantum electrodynamics [54–56], and the factor C_0 (by analogy with the topological charge in 2D systems) is often referred to as the topological coefficient.

We note that the value of the coefficient C_0 was determined in the well-known experiments [50, 280] using measurements of the nondissipative-friction factor $d_\perp$ in the scattering of quasiparticles on vortices. The measurements were performed in the ballistic collisionless regime at low temperatures in He-3B and the hydrodynamic regime at high temperatures, $T > 0.82T_{\mathrm{c}}$, in He-3A (we discuss this in more detail in Section 14). However, the collisional region at very low temperatures in the anisotropic A phase remained unexplored. It is specifically this region that has led to discussions regarding the value of C_0. We stress that the problems related to the emergence of the chiral anomaly and the applicability of the hydrodynamic description at nonzero temperatures are actually nonexistent; the reason is that the normal (temperature) component is in this case an independent hydrodynamic variable in the scheme for deriving quantum hydrodynamic equations developed by Landau. It is owing to the presence of this independent variable that the conservation law for the total momentum of the system is restored at nonzero temperatures.

We stress that the anisotropic A-phase is only realized (being the global extremum) in the absence of an external magnetic field in the phase diagram of superfluid He-3 at temperatures close to the critical temperature T_{c}. If there is no magnetic field, the isotropic B phase alone is realized at zero temperature. For the A phase to 'sprout' to zero temperature in the phase diagram of superfluid He-3 (in the form of the so-called A2 phase), rather strong magnetic fields are needed, $H \geqslant 1$ T, which paramagnetically suppress the B phase.

Moreover, in order to pass to the hydrodynamic region of large wavelengths, large experimental cells 0.5 to 1 cm in size are needed to ensure that in any event the wavelength is shorter than the sample size in measuring the collective excitation spectrum and damping

It would be of interest to extend the results measured in [280] to very low temperatures $T \ll T_{\mathrm{c}}$ and the collisional regime for the A2 phase of superfluid He-3 in strong magnetic fields and to explore whether the topological coefficient C_0 experiences a significant change in passing to the hydrodynamic limit of very long wavelengths at temperatures tending to zero.

Another very important aspect in understanding experimental data is the so-called Mermin–Ho identity in the hydrodynamics of superfluid He-3A,

$$\nabla_i v_{sj} - \nabla_j v_{si} = \frac{\hbar}{2m}\,\mathbf{l}\,(\partial_i\mathbf{l} \times \partial_j\mathbf{l})\,, \tag{89}$$

which relates the local vorticity of the superfluid component to nonsingular textures (gradients) of the local orbital momentum $\mathbf{l}$.

We note that as a consequence of the Mermin–Ho identity, the setup for rapid rotation of cells containing superfluid He-3A (the ROTA facility at the Helsinki-based low-temperature laboratory) can be used to create orbital textures nonuniform in space and time, which can be further used for measuring the nondissipative friction coefficient $d_\perp$ and the topological coefficient C_0 in the experiments in [50, 280].

Finally, an additional proposal by the authors of this review that may be of significant interest for experimental exploration is to measure the coefficient C_0 in the anomalous current term in moderately pure superfluid He-3A. We note that the role of impurities is played in superfluid He-3 by an aerogel that consists of interwoven quasi-one-dimensional filaments.

It would be of interest in this context to check the predictions in [52] and [25, 57] regarding suppression of the chiral anomaly and restoration of the hydrodynamics at low frequencies and to measure the orbital wave spectrum and damping in an aerogel. This would make it possible to use these data to directly extract the frequency dispersion and the value of the coefficient C_0 in the anomalous term in the 'dirty' (hydrodynamic) limit of small frequencies $\Omega\tau \ll 1$ (at large

aerogel concentrations), to gradually decrease its concentration afterwards, thus making the system increasingly pure and passing to the ballistic region of high frequencies, $\Omega\tau \gg 1$, i.e., to the ultra-pure limit in the concentration of impurities.

It will be necessary to take into account the changes that occur in the global phase diagram of superfluid He-3 in the presence of large amounts of aerogel [281]. We note that Volovik and Stone adhere in this case to the opposite opinion and believe that the larger the concentration of impurities, the easier (in the $\Omega\tau \ll 1$ regime) the chiral anomaly is restored in accordance with the spectral flow concept (see Section 13).

We note that calculations done by different groups for the orbital momentum density disagree even in the BCS region. The calculations done in [282, 283] for $\mathbf{l} = \text{const}$ yield Eqn (88) without the coefficient C_0 even in the BCS limit. If nonuniform textures of the $\mathbf{l}$ vector are included, Eqn (87) is recovered, however. Based on the results in [282, 283], we note the paradox of internal orbital momentum in the A phase of superfluid He-3. We stress that according to Leggett [284], the N-particle Hamiltonian $\hat{H}$ exactly commutes with the z projection of the orbital momentum $\hat{L}_z = \hbar\hat{N}/2$. This circumstance favors Eqn (88). We note that similar calculations of the internal orbital momentum in superfluid He-3A, the BCS phase for 2D superfluid Fermi gases, and topological superconductors with anomalous p-wave and f-wave pairing have been performed in Volovik's earlier [285] and later [286] studies, in papers by Japanese theoreticians [287, 288], and by Sauls [289].

Volovik [285, 286] explored the BCS phase of superfluid liquid or gas with a Cooper pair orbital momentum $\boldsymbol{\nu}$ at the level of eigenvalues of the combined orbital–gauge symmetry operator $\hat{Q} = \hat{L}_z - \boldsymbol{\nu}\hat{N}/2$, where $\hat{L}_z$ is the operator of the z projection of the orbital momentum corresponding to SO(2) rotations and $\hat{N}$ is the gauge symmetry operator related to the global U(1) symmetry, which ensures conservation of the total number of particles.

In [285], Volovik studied the so-called adiabatic transition from the BEC phase to the BCS phase, i.e., actually, the transition from negative values of the chemical potential μ to positive values. We return to analyzing this transition in subsequent sections.

We stress that an interesting discussion occurred based on calculations by Sauls [289] and Tada [287] and Volovik's comments [286] on those results; the matter of that discussion was the internal orbital momentum in the BCS phase for p-wave pairing in the restricted 2D disc geometry.

We note that all of these results [286–288] for the 2D disc show a significant decrease (in the Δ/ε_F parameter) in the total momentum with respect to $\hbar N/2$ values due to the particle–hole asymmetry of boundary conditions at large orbital momenta $\nu = 3$ (for f-wave pairing). However, according to Tada's results [287] for a more essential case $\nu = 1$ (p-wave pairing), the intuitively expected result of Leggett, $\hbar N/2$, is reproduced in the BCS phase.

We stress that the orbital momentum density was determined in Sauls's studies [289] by the boundary condition type. Leggett's result [289] persists in the case of mirror scattering on the boundary and fails for diffuse scattering.

Volovik disagreed in 2015 [286] with Tada's result [287] for p-wave pairing. He noted, in agreement with Sauls, that the result depends on the boundary conditions. Boundary conditions for the disc geometry were chosen in Volovik's study [286] such that axial symmetry was not violated, while parity was. The parity violation in the boundary conditions is controlled by the phase α. It is noteworthy that if $\alpha = 0$, Leggett's result is recovered, while if $\alpha = \pi/2$, a result is obtained for $l = 1$ that is similar to Tada's result for $l = 3$ but with a significantly smaller total momentum. Generically, the decrease in the total momentum is controlled in [286] by the $\sin^2\alpha$ parameter.

We stress that all the calculations in [285–288] were done at the level of solving single-particle Bogoliubov–de Gennes equations without consideration for strong many-body correlations (residual interactions) and quasiparticle damping. We return to discussing those results in subsequent sections when considering the spectral flow concept.

As was briefly noted above, the paradox of internal orbital momentum in the A-phase is closely related to another difficult problem: nonconservation of the anomalous current (chiral anomaly) in the quantum hydrodynamics of the superfluid A phase at low temperatures $T \to 0$. We note that the hydrodynamics that assumes the conditions of local thermodynamic equilibrium to be satisfied describes all low-frequency (Goldstone) collective modes for which $\omega \to 0$ as $q \to 0$. The applicability area of the hydrodynamic equations is actually restricted by the conditions $\omega\tau \ll 1$ and $ql_{MF} \ll 1$, where $l_{MF} \sim v_F\tau$ is the mean free path and τ is the free propagation time. We note that the hydrodynamic description involves a limited set of hydrodynamic variables in a way proposed by Landau, where the left-hand side of the hydrodynamic equations usually contains a partial time derivative of the density of a conserved hydrodynamic variable, while the right-hand side contains a generalized divergence of the corresponding flow (mass, momentum, energy, etc.).

We note that as $T \to 0$, according to general symmetry considerations, the total mass–current density in the BCS region has the form

$$\mathbf{j}_{tot} = \mathbf{j}_B + \mathbf{j}_{an}\,, \tag{90}$$

where the anomalous current is

$$\mathbf{j}_{an} = -\frac{\hbar}{4m}\, C_0(\mathbf{l}\,\mathrm{rot}\,\mathbf{l})\,\mathbf{l}\,. \tag{91}$$

In (91), the coefficient is $C_0 = 0$ in the BEC region for composite bosons with $S = l = 1$, and there is no anomalous current. The full mass current is then equal to the bosonic current

$$\mathbf{j}_B = \rho\mathbf{v}_s + \frac{\hbar}{2m}\,\mathrm{rot}\,\frac{\rho\mathbf{l}}{2}\,, \tag{92}$$

where $\rho = mn$ is the total density, $\mathbf{L} = (\hbar/2m)\rho\mathbf{l}$ is the orbital momentum density, and $\mathbf{v}_s$ is the superfluid velocity. However, $C_0 \approx \rho$ in the single-particle approximation in the BCS region, and therefore the presence of anomalous current (91) in formula (90) results in nonconservation of the total mass current (or total momentum) $\mathbf{j}_{tot}$ at $T = 0$. This observation implies that it is not possible to represent the partial time derivative of the total current as a generalized divergence of the momentum flow tensor,

$$\frac{\partial j^i_{tot}}{\partial t} \neq -\frac{\partial}{\partial x_k}(\Pi_{ik})\,. \tag{93}$$

Thus, the momentum conservation law is not satisfied. This implies that the presence of the anomalous term destroys the hydrodynamics of superfluid liquid in the A phase as $T \to 0$.

The contribution of the time derivative of the anomalous current in Eqn (93) can only be compensated by adding a term with the normal density and the relative normal velocity $\rho_n(T=0)(v_n - v_s)$ to the total current already at $T=0$ [53, 58, 59, 290]. Adding this term is in disagreement with our intuitive understanding that the hydrodynamics of a quantum superfluid liquid at zero temperature can be described in terms of the superfluid component alone (without involving the normal component). However, if it were possible to show that $C_0 \approx \rho$ in the high-frequency (collisionless) region, while in passing to low frequencies (collisional frequency range) this coefficient experiences strong dispersion and becomes very small, $C_0(\omega\tau \ll 1) \to 0$, we would recover the hydrodynamics at $T=0$ in terms of the superfluid component alone.

This concept has been suggested by Andreev and an author of this report in [52] and later studies and monographs [18, 25, 57]. An approach has been developed in [52] that involves incorporating the fermionic Goldstone mode (which is due to the presence of zeros in the superfluid gap for the A phase) in the general scheme of hydrodynamic equations. As a result, superhydrodynamics of superfluid He-3A was developed in [52]. At the same time, Volovik and coauthors asserted in [53] that the coefficient C_0 in the anomalous current term is always of the order of the total density ρ due to important topological factors related to the existence of a zero mode in the solutions of Bogoliubov–de Gennes equations for the quasiparticle spectrum in the nonuniform texture of the vector $\mathbf{l}$. If $\mathbf{l} \parallel \operatorname{rot}\mathbf{l}$, these equations are equivalent to the Dirac equation in the magnetic field $\mathbf{B} = \operatorname{rot}\mathbf{l}$ for massless particles. Consequently, the authors of [53] relate the nature of the anomalous current in (91) to the chiral anomaly in quantum electrodynamics [291].

13. Two approaches to the involved problem of chiral anomaly in the A phase of superfluid He-3

We now consider two elegant approaches to the involved problem of chiral anomaly in the superfluid A-phase of He-3 in more detail. In the first approach, the authors of [25, 52, 57] described the total hydrodynamic action $S_{\rm tot}$ at small frequencies and wave vectors as a sum of bosonic and fermionic parts:

$$S_{\rm tot} = S_{\rm B} + S_{\rm F}\,, \tag{94}$$

where $S_{\rm B}(\rho, \mathbf{v}_s, \mathbf{l})$ is the bosonic part of the action and $S_{\rm F}$ is the fermionic part, related to the superfluid gap zeros (Fig. 27). The main idea in [25, 52, 57] was to check whether the chiral anomaly (or, more precisely, the term $\mathbf{j}_{\rm an}\mathbf{v}_s$ in the formula for the total energy) is directly related to superfluid gap zeros. The authors of [25, 52, 57] assumed that the only reason for the occurrence of the anomaly in a condensed system at low frequencies can be related to the presence of infrared singularities. We note that unlike quantum electrodynamics, condensed matter physics does not contain ultraviolet singularities. Strong (critical) fluctuations are also suppressed in 3D systems. Thus, the main idea in [25, 52, 57] was to explore dangerous infrared regions where the superfluid gap could practically vanish.

We can say in more general terms that the main idea in [25, 52, 57] was to develop supersymmetric hydrodynamics that describes all gapless Goldstone modes, including the fermionic Goldstone mode related to gap zeros. The authors of [52] were inspired by the elegant study by Volkov and Akulov [292], who were the first to include the massless neutrino in the effective infrared Lagrangian of the weak interaction. Having integrated over fermionic variables, the authors of [25, 52, 57] derived the effective bosonic interaction and explored the infrared singularities that it contained. As a result, they obtained

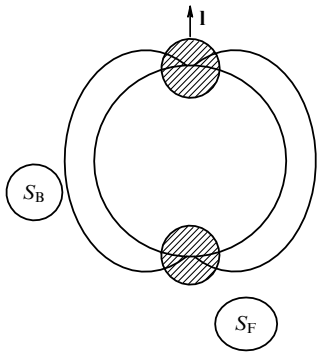

Figure 27. Qualitative illustration of two contributions to the fermionic ($S_{\rm F}$) and bosonic ($S_{\rm B}$) parts of the total hydrodynamic action $S_{\rm tot}$ for the A phase as $T \to 0$ [25, 52, 57].

$$S_{\rm B}^{\rm eff} = S_{\rm B} + \Delta S_{\rm B}\,, \tag{95}$$

where the contribution from the hazardous regions near the gap zeros to the 'liquid crystal' part of the effective action [293], which is related to the gradient orbital energy, has a form characteristic of the zero-charge situation in quantum electrodynamics:

$$\Delta S_{\rm B} = -\frac{p_{\rm F}^2 v_{\rm l}}{32\pi^2}\int {\rm d}^4x \left\{ [\mathbf{l}\times\operatorname{rot}\mathbf{l}]^2 + \frac{v_{\rm t}^2}{v_{\rm l}^2}\,(\mathbf{l}\operatorname{rot}\mathbf{l})^2 \right\} \left(\ln\frac{l_{\rm MF}^2}{r^2} \right). \tag{96}$$

Here, $x = (\mathbf{r}, t)$, and the radius vector r varies within the range $\xi_0 < r < l_{\rm MF}$, where $\xi_0 \sim v_{\rm F}/\Delta_0$ is the coherence length and $l_{\rm MF}$ is the mean free path. Formula (96) has a general character and holds in both the weak and strong coupling regimes. We emphasize that the transverse velocity $v_{\rm t} \sim v_{\rm F}\Delta_0/\varepsilon_{\rm F} \ll v_{\rm F}$ in Eqn (96) while the longitudinal velocity is $v_{\rm l} \sim v_{\rm F}$ in the weak-coupling regime. We see that the expression for $\Delta S_{\rm B}$ contains only weak logarithmic divergences. At the same time, in (96), we do not observe any traces of strong divergences, which should have a δ-function character, because the fermionic density $\rho_{\rm F}$ that is contained in formula (95) for $S_{\rm F}$ and related to the regions near gap zeros is small in comparison to the total density: $\rho_{\rm F} \ll \rho$. In other words, we do not see any traces of the anomalous contribution

$$\mathbf{j}_{\rm an}\mathbf{v}_s = -\frac{\hbar}{4m}\,C_0(\mathbf{l}\operatorname{rot}\mathbf{l})(\mathbf{l}\,\mathbf{v}_s) \tag{97}$$

to $\Delta S_{\rm B}$. Thus, even if there is a chiral anomaly in the BCS region for the superfluid A phase, it is not directly related to the hazardous regions in the momentum space close to the gap zeros. Therefore, the nature of the chiral anomaly is not an infrared one.

We stress that the authors of [53, 58, 59, 290] suggested another very nice approach based on the formal similarity between the anomalous current problem in the A phase of He-3 and the chiral anomaly problem in quantum electrodynamics. They assume that the anomalous current with the

large coefficient $C_0 \sim \rho$ in the BCS region for the superfluid A phase is not directly related to gap zeros and therefore does not exist, even in superhydrodynamics [25, 52, 57]. In their opinion, the anomalous current is related to global topological factors, and therefore the topological term should be added by hand to the scheme of supersymmetric hydrodynamics. To illustrate this approach, the authors of [53, 290] solve microscopic Bogoliubov–de Gennes equations for fermionic quasiparticles in a nonuniform orbital texture of the vector $\mathbf{l}$ with $\mathbf{l} \parallel \operatorname{rot}\mathbf{l}$. More specifically, they consider the case where

$$\mathbf{l} = \mathbf{l}_0 + \delta\mathbf{l}\,, \tag{98}$$

and

$$l_z = l_{0z} = e_z\,, \quad l_y = \delta l_y = Bx\,, \quad l_x = 0\,, \tag{99}$$

where $\mathbf{e}_z$ is the direction of the unperturbed vector $\mathbf{l}$. In this case,

$$\mathbf{l}\operatorname{rot}\mathbf{l} = l_z\,\frac{\partial l_y}{\partial x} = B = \text{const}\,, \tag{100}$$

whence

$$\mathbf{j}_{\text{an}} = -\frac{\hbar}{4m}\,C_0 B\mathbf{e}_z\,. \tag{101}$$

After being linearized, the Bogoliubov–de Gennes equations become equivalent to the Dirac equation in a uniform magnetic field $B = \mathbf{l}\operatorname{rot}\mathbf{l}$. A solution of the Dirac equation determines the structure of energy levels for fermionic quasiparticles:

$$E_n(p_z) = \pm\sqrt{\xi^2(p_z) + \tilde{\Delta}_n^2}\,, \tag{102}$$

where $\xi(p_z) = p_z^2/2m - \mu$, $e = p_z/p_{\text{F}} = \pm 1$ is the electric charge,

$$\tilde{\Delta}_n^2 = 2nv_{\text{t}}^2 p_{\text{F}}|e|B \tag{103}$$

is the gap squared, and the transverse velocity is $v_{\text{t}} \sim v_{\text{F}}\Delta_0/\varepsilon_{\text{F}}$. All energy levels in (102) corresponding to the principal quantum number $n \neq 0$ (Fig. 28) have a gap $\tilde{\Delta}_n \neq 0$ and are doubly degenerated with respect to $p_z \to -p_z$. Thus, their contribution to the total current is zero at $T \to 0$. However, if $n = 0$, the gap vanishes ($\tilde{\Delta}_0 = 0$), and we have an asymmetric chiral branch that exists only if $p_z < 0$ or, more precisely, for only one sign of eB (see [53]). The energy spectrum for $n = 0$ has the form

$$E_0 = \xi(p_z)\,. \tag{104}$$

We can conclude that there is no gap in the spectrum for the zeroth Landau level and, moreover, in the BCS region, $E_0 = 0$ at $|p_z| = p_{\text{F}}$. This implies that the chiral branch passes through the origin (see Fig. 28), and we have the zero mode.

We note that $E_0 \geqslant |\mu|$ in the BEC region, and the zeroth Landau level does not pass through the origin. The absence of the zero mode in the BEC region is the physical reason explaining why $C_0 = 0$ there. The zeroth Landau level makes an anomalous contribution to the total mass current in the BCS region:

$$\mathbf{j}_{\text{an}}(\mathbf{r} = 0) = -\mathbf{e}_z(\mathbf{l}\operatorname{rot}\mathbf{l})\int_{p_z<0}\frac{p_z}{2\pi^2}\,\mathrm{d}\xi(p_z) = -\frac{\hbar C_0}{4m}(\mathbf{l}\operatorname{rot}\mathbf{l})\mathbf{e}_z\,, \tag{105}$$

where

$$\frac{(\mathbf{l}\operatorname{rot}\mathbf{l})\,p_z}{2\pi^2 p_{\text{F}}} = \frac{eB}{2\pi^2} = \int |f_0|^2\,\frac{\mathrm{d}p_y}{2\pi}\,, \tag{106}$$

and hence $C_0 \approx \rho$ in the BCS region. We note that f_0 in (106) is the wave function of the zeroth Landau level. We can easily see that the leading contribution to integrals (105) and (106) comes from a narrow cylindrical tube inside the Fermi sphere of the length p_{F} directed parallel to the z axis and the cylinder radius squared equal to (Fig. 29)

$$\langle p_y^2\rangle \sim p_{\text{F}}|eB|\,. \tag{107}$$

In accordance with the ideas in [53, 58, 59, 285, 290], this tube plays the role of an effective vortex in the six-dimensional $\mathbf{k}-\mathbf{r}$ space, in this way ensuring the emergence of a normal core that at $T = 0$ connects the north and south poles on the Fermi sphere (see Fig. 29), where the superfluid gap in He-3A vanishes.

We stress that according to the results obtained by Volovik, Stone, and Combescot [53, 58, 59, 283, 290], it is along this normal core of the vortex that the spectral weight is transferred from the normal component to the superfluid one (from negative to positive energy values) in the effective electric field $\mathbf{E} \propto \dot{\mathbf{l}}$ directed along the vortex axis. This momentum transfer is needed in order to cancel the chiral anomaly by adding a Schwinger term proportional to

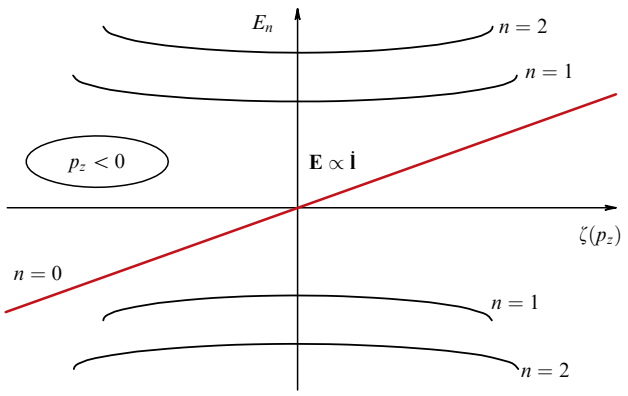

Figure 28. Energy level structure for the Dirac equation in the magnetic field $B = \mathbf{l}\operatorname{rot}\mathbf{l}$. All levels with quantum numbers $n \neq 0$ are doubly degenerate. The zeroth level is a chiral one. It passes through the origin at $|p_z| = p_{\text{F}}$ in the BCS region. This figure also illustrates the concept of the spectral flow, which is briefly discussed at the end of this section [53].

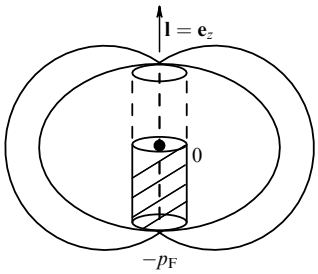

Figure 29. The leading contribution to the anomalous coefficient C_0 is due to a narrow cylindrical tube whose length is p_{F} and width $\langle p_y^2\rangle \sim p_{\text{F}}|eB|$ inside the Fermi sphere [25, 52, 57].

$\mathbf{E}\,\mathbf{B} \propto \dot{\mathbf{l}}\,\mathrm{rot}\,\mathbf{l}$ and recovering the conservation law for the total momentum.

The approach proposed by Andreev and Kagan is in a sense more pragmatic. There is no problem in the hydrodynamic description of He-3A at $T = 0$ at the level of the first two terms in the total momentum. It is therefore more practical and easier to ensure the vanishing of the coefficient at the third anomalous term in the current at low frequencies than to salvage the situation by adding an artificial fourth term, at the same time violating the Landau hydrodynamic scheme for a superfluid liquid.

It is important that according to Kagan and Efremov [25, 57], the exact cancelation of the anomalies in the nonconserving terms of the equations for time derivatives of the anomalous current and the normal component current at $T = 0$ must be explicitly demonstrated in superfluid He-3A via exact derivation and solution of nonlinear kinetic equations for the dynamics of gapless fermionic quasiparticles in a nonequilibrium texture of the orbital momentum vector $\mathbf{l}$.

Kopnin [294, 295], who shared this approach, tried to implement it by analyzing another important problem with the zero chiral mode for the energy levels of quasiparticles localized in vortex cores and an additional nondissipative friction force (the so-called Kopnin spectral friction force [58]). We consider this problem in more detail in Section 14 below.

We note that as was briefly discussed above, an attempt to explicitly demonstrate the cancelation of anomalies owing to the spectral flow was made by Volovik [285] in exploring an adiabatic transition from the state that does not have gap zeros and whose chemical potential is negative ($\mu < 0$) in the BEC phase to the state with a positive value ($\mu > 0$) in the BCS phase. However, Volovik assumed in this approach that only the chemical potential changes with time while considering nonuniform but stationary textures of the vector $\mathbf{l}$. In our opinion, this treatment violates self-consistency in the derivation of hydrodynamic equations, with its coupling of time derivatives of various hydrodynamic variables, including the time derivative of the variable that is of critical importance for the chiral anomaly problem, the orbital momentum vector $\mathbf{l}$.

We note that the main results in [53, 290] related to the absence of a gap for the zeroth Landau level are very persistent with respect to small variations of the vector $\mathbf{l}$ texture in Eqn (99). The analysis that we have performed shows that the account of small bending corrections that results in the emergence of the transverse projection of the magnetic field $[\mathbf{l} \times \mathrm{rot}\,\mathbf{l}] \neq 0$ or small nonuniformity of the magnetic field (as a result of which a two-well potential is formed) do not suppress the zero mode in the Bogoliubov–de Gennes equation, i.e., do not result in the emergence of a gap for the zeroth Landau level. Despite the stability of the zero mode, the authors of [25, 52, 57] expressed doubts regarding the calculation of the anomalous coefficient C_0 based on solving the Dirac equation in a uniform magnetic field $B = \mathbf{l}\,\mathrm{rot}\,\mathbf{l}$. In their opinion, the calculation of C_0 based on Eqns (105) and (106) is too strong a simplification of the involved multiparticle problem. They especially emphasize the role of finite damping $\gamma = 1/\tau$ and other residual interactions in the suppression of chiral anomaly (related to the states inside the Fermi sphere in Fig. 29) and restoration of the superfluid hydrodynamics without additional contributions (containing the normal velocity $\mathbf{v}_\mathrm{n}$ and the normal density ρ_n). Indeed, if, for example, the damping γ (or another residual interaction) is much larger than the distance between Landau levels $\omega_0 = v_\mathrm{t}\, p_\mathrm{F} (\mathbf{l}\,\mathrm{rot}\,\mathbf{l}/p_\mathrm{F})^{1/2}$ in the case $\xi(p_z) = 0$, the zeroth Landau level would be washed out by damping, and the hydrodynamic regime at low frequencies would be recovered (Fig. 30). These arguments are considered in more detail in [25, 52, 57]. We invite experimentalists to actively participate in resolving this very difficult problem. It would be very interesting from the experimental perspective to measure the spectrum and damping of orbital waves at low temperatures $T \ll T_\mathrm{c}$ both in pure superfluid He-3A and in the presence of impurities (the role of impurities in superfluid He-3 is played by aerogel).

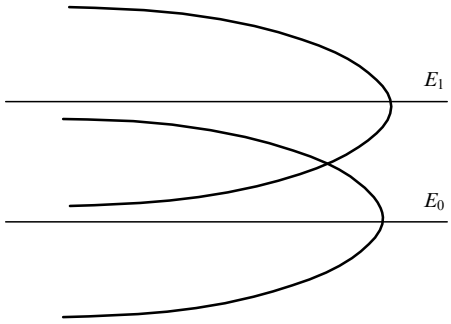

Figure 30. Possible role of damping (and other residual interactions) in washing out the zeroth Landau level and recovering superfluid hydrodynamics at low frequencies [25, 52, 57].

We stress again that while the authors of [25, 52, 57] use damping as an argument in favor of the possible suppression of chiral anomaly at low frequencies, in the approach developed by Volovik [53, 58, 59], Combescot [290], and Stone [283], the damping plays quite the opposite role of ensuring the spectral flow along the vortex core (see Fig. 28). Similarly, the hopes of various groups of theorists are opposite as regards using the Ward identities in the infrared region for possible suppression or stabilization of the chiral anomaly in going beyond the one-particle problem and accounting for many-body correlations and quasiparticle damping in superfluid He-3 and other systems discussed in this review (see [25, 57, 296]).

14. Hydrodynamics of superfluid quantum liquids and gases. Collective modes in rotating He and Bose–Einstein condensates of quantum gases

The discussion in the preceding section was primarily focused on the specific features of orbital hydrodynamics in superfluid Fermi systems with Cooper pairing. Here, in contrast, we concentrate on collective modes (related to the presence of vortex lattices) and the friction force between normal excitations and vortices in the superfluid Bose liquid of He-4 [15–18, 36–48] (see also the classic result [49] for bending oscillations of the vortex line in a normal liquid) and Bose–Einstein condensates of quantum gases [297–301]. We note that vortex lattices in He-3A and He-3B superfluid Fermi liquids [50, 51, 280, 294, 302] and in resonance Fermi gases in the BCS–BEC crossover regime [303, 304] have been studied in detail using experimental (in the case of He-3) and theoretical methods owing to the nontrivial topology and wealth of vortex phases and topological excitations in these systems, especially in the case of anisotropic p-wave pairing.

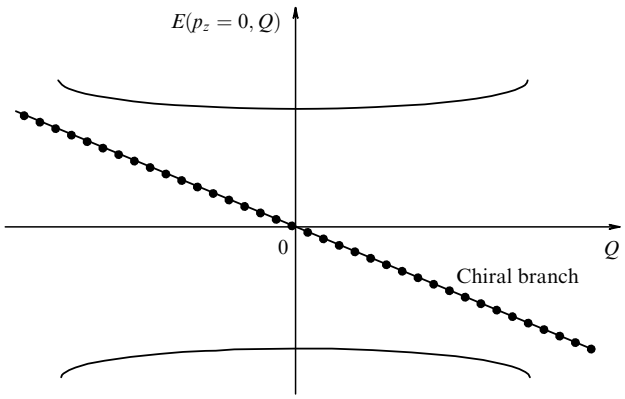

Figure 31. Level structure in the He-3A vortex core [25, 57]. All branches are even functions with respect to the generalized angular momentum Q, the only exception being the branch $E(p_z = 0, Q) = -\omega_0 Q$ that crosses 0 at $Q = 0$. This branch is chiral (an odd function of Q). According to [50, 302], this branch is involved in the momentum exchange between the vortex core fermions and the thermal reservoir.

Our understanding of the physics of various topologically nontrivial vortex states and vortex lattice structures and the structure of extended cores of vortices (whose radius is large compared with the interatomic distance, $\xi_0 \gg d$) with possible various transformations of the order parameter inside the cores in the A and B phases of superfluid He-3 was considerably enriched by Volovik (see, in particular, a presentation of this set of problems in monographs [50, 302]).

We note that an interesting problem of superfluid systems with a complex order parameter in the fermionic BCS phase, such as superfluid He-3, is connected with the energy spectrum of the quasiparticles localized inside vortex cores.

The results obtained by Volovik and Kopnin for a vortex with a cylindrical geometry in He-3A show that the energy level structure is very similar to the level structure of quasiparticles in the field of nonuniform textures of the orbital momentum vector **l** (see Section 13). The vortex core has only one asymmetric (chiral) level that crosses the zero-energy line. Being a function of the generalized angular momentum Q, this energy level crosses the horizontal axis at $Q = 0$ at zero temperature and corresponds to a discrete set of points with integer momenta $Q = 1, 2, \ldots$, separated from each other with a mini-gap $\Omega_0 = \Delta^2/\varepsilon_F$ (Fig. 31).

This result is of utmost importance because of the following reasons. As was briefly noted in previous sections, in the mid-1990s, Kopnin, Thouless, and Stone extended the discussion about the existence of chiral anomaly in condensed matter physics, shifting it to the problem of the possible contribution of the chiral zero mode in vortex cores to the so-called Kopnin spectral (nondissipative) friction force, which, along with Iordanskii and Magnus forces that are standard for rotating Bose systems, can emerge in the vortex dynamics of fermionic He-3A in the scattering of quasiparticles on vortices. In that discussion, Stone supported Volovik's stance, while Thouless and Ao did not believe in the emergence of the spectral force, and Kopnin was somewhere in between, relying on specific results of his own calculations.

We note that Kopnin's friction force is again fully determined by the transfer of spectral weight from the zero mode ($Q = 0$) to states with $Q > 0$ along the vortex core. Thus, a certain difficulty occurs here in justifying the results at strictly zero temperature $T = 0$ and in the absence of impurities when the scattering of quasiparticles is completely absent. Therefore, we are again in the ballistic region in the parameter $\Omega_0\tau(T = 0) \gg 1$, where we have a discrete set of points corresponding to the quantum number $Q = 0, 1, 2, \ldots$, and, in accordance with Volovik's and Stone's ideology, the spectral flow is in this case fully suppressed. Thouless and Ao's result [305] regarding the suppression of the spectral friction forces is thus recovered (Thouless and Ao call this situation the Berry phase).

The spectral flow is restored only at finite temperatures, $\Omega_0\tau(T) \ll 1$, when the variable Q again becomes continuous.

We note that the presence of spectral friction forces was theoretically demonstrated in Kopnin's and Stone's calculations at $\Omega_0\tau \ll 1$ for high temperatures close to the critical temperature T_c in the A phase of He-3. As we emphasized in Section 12, this result has been confirmed by measurements of the nondissipative friction coefficient $d_\perp$ in He-3A experiments performed by Bevan et al. (see [280] and Fig. 18.5 in monograph [50], where $d_\perp \to 1$ with $T \to T_c$ in the $\Omega_0\tau \ll 1$ regime for the case of He-3A).

We also note that in his calculations, Kopnin explored along with He-3A, the problem of the spectral weight transfer due to zero modes in vortex cores in both superfluid isotropic He-3B and normal type-II superconductors. The superconducting gap in these systems does not have zeros but the role of topological points (gap zeros) in the fermionic quasiparticle spectrum is played by the presence of vortices with quantized circulation that create an Aharonov–Bohm-type potential.

For these systems (in particular, singular vortices in He-3B), Kopnin suggested an interpolation formula in the parameters $\Omega_0\tau(T)$ and $\Delta(T)/T$ to discover that the nondissipative friction coefficient $d_\perp(T)$ changes its sign in passing from the collisionless regime $\Omega_0\tau(T) \gg 1$ to the collisional regime $\Omega_0\tau(T) \ll 1$ (see Eqn (25.17) in [50]).

Kopnin's results in the collisionless region of very low temperatures coincide again with the experimental results of Bevan at al. [280], who measured $d_\perp$ for superfluid He-3B ($d_\perp \to 0$ at $\Omega_0\tau \gg 1$ and $T \to 0$; see Fig. 25.1 in [50]).

Another interpolation result of Kopnin is related to studying the damping $\gamma = 1/\tau$ that is due to impurities in type-II superconductors. The value of γ is not zero, even at $T = 0$ in the 'moderately clean' limit.

In our opinion, it is of great interest to derive an interpolation formula for C_0 in the parameter $\Omega\tau$ (where Ω is now not a constant minigap but a running frequency of the orbital wave $\Omega(q) \to 0$ at $q \to 0$) based on the correct infrared Ward identities for the vertex $\Gamma(\Omega, q)$ and the self-energy $\Sigma(\Omega, q) = \mathrm{Re}\,\Sigma(\Omega, q) + \mathrm{i}\,\mathrm{Im}\,\Sigma(\Omega, q)$. The Ward identities should be derived so as to include strong many-body correlations (residual interactions) and quasiparticle damping in passing to the hydrodynamic limit of low frequencies $\Omega(q)\tau \ll 1$ and wave vectors $ql_{MF} \ll 1$ (l_{MF} is the mean free path) for the orbital wave spectrum in superfluid He-3A at very low temperatures.

Here, according to Andreev and Kagan's ideology, if strong many-body correlations (residual interactions) and various damping mechanisms and collective excitations are taken into account, an intermediate frequency range $\Omega\tau \sim 1$ is possible where the orbital momentum spectrum is over-damped or, in a more general case, an essential re-expansion of the real or imaginary part of the spectrum starts. It is noteworthy that over-damped spectrum branches in superfluid He-3A occur in the calculations in [306] performed using the Feynman path integral technique.

A similar scenario, in which a transition occurs from a propagation-type linear spectrum of antiferromagnetic spin waves at high frequencies to an over-damped and diffusion-type spectrum at low frequencies (actually, a scenario of essential re-expansion in the equation for the spectrum in the parameter $\Omega\tau$), was also realized at $T = 0$ in Chubukov's diagram calculations, where the spin wave spectrum and damping in weakly doped HTSC cuprates were explored using the impurity diagram technique.

We note that quite recently (2014–2016), Haldane, Spivak et al. [296, 308–310] initiated a discussion about the possible contribution of the chiral anomaly to longitudinal magnetoresistance in currently popular Dirac semimetals based on bismuth, including topological insulators $Bi_{1-x}Sb_x$ (near the critical point in the Sb concentration x [311, 312]) and nematic superconductors Bi_2Se_3 doped with Cu, Sr, or Nb [313].

Theoretical studies of this class of materials are complemented with very interesting experimental work [311, 312], where longitudinal magnetoconductivity and the anomalous contribution to it were measured at helium temperatures of 2–4 K. This is not only of great importance for the development of basic condensed matter physics but also very promising for nanoelectronics and spintronics applications. We discuss this class of materials in more detail in the concluding section.

We stress that vortex lattices in superfluid He-4 and Bose–Einstein condensates (for composite bosons with spin $S = 0$) are significantly simpler from the topological perspective. This is due to the scalar nature of the order parameter for this class of systems (in contrast to the tensor order parameter for superfluid He-3 with the pair spin $S = 1$). The basics of the vortex lattice theory for rotating superfluid He-4 and key experimental results in this area are presented in Khalatnikov's classic monograph [16], the well-known paper by Bekarevich and Khalatnikov [40], and Andronikashvili and Mamaladze's [41] and Sonin's [42] reviews. We recall that the first vortex emerges in superfluid He-4 at the angular frequencies of rotation of a cylindrical helium-filled vessel $\Omega \geqslant \Omega_{c1}$; the vortex emerges in the vessel center (on the cylinder axis), while at the frequencies

$$\Omega_{c1} \ll \Omega \ll \Omega_{c2}\,, \tag{108}$$

where Ω_{c1} and Ω_{c2} are the first and second critical rotation frequencies, a triangular lattice of quantum vortices emerges in the system. The quantum vortices were predicted in superfluid He-4 by Feynman and Onsager [37–39]. A theory of the vortex state in type-II superconductors has been developed by Abrikosov [314]. We note that the first critical frequency in a dense Bose liquid (for He-4) is $\Omega_{c1} \sim 0.1\ \mathrm{s}^{-1}$, while the second critical frequency (related to overlapping of vortex cores) is very large, $\Omega_{c2} \sim 10^{11}\ \mathrm{s}^{-1}$, and cannot be attained in experiment. The size of the vortex core in dilute Bose gases is significantly larger (see Eqn (72)), and hence the frequency Ω_{c2} is not very high. We also note that in deriving hydrodynamic equations for rotating helium with a large number of vortices, so-called supermacroscopic averaging [16, 36, 43] over scales much larger than the average distance between vortices is used in [40–42]. As a result, not only the dissipative velocity of the normal component but also the nondissipative velocity of the superfluid component mimics solid-state motion, $\mathbf{v}_s \approx [\mathbf{\Omega} \times \mathbf{r}]$, with small corrections related to the elasticity of the vortex lattice and friction force between normal excitations (phonons and rotons in superfluid helium) and vortices [40, 41, 315–317]. Therefore, the average vorticity becomes of the order of

$$\boldsymbol{\omega} = \mathrm{rot}\,\mathbf{v}_s \approx 2\mathbf{\Omega}\,, \tag{109}$$

where the direction of $\mathbf{\Omega}$ coincides with the z axis in the cylindrical geometry. Consequently, $\mathbf{v} = \boldsymbol{\omega}/|\boldsymbol{\omega}|$ is the unit vector along the local direction (deformed in the general case) of the vortex lattice. Related to the average vorticity is the vortex density per cm^2:

$$\frac{\hbar}{m_B}\, n_v = 2\Omega\,, \tag{110}$$

where $\hbar/m_B = \Gamma$ is the circulation quantum. In the case of the He-4 Bose liquid, m_B is the mass of the He-4 atom and in a superfluid fermionic liquid or gas, $m_B = 2m$. In constructing a nonlinear theory of vortex lattice elasticity in a general form, it is convenient to use field-theory variables for a curved space (such as the metric tensor) and the number of lattice sites; the last variable is actually a topological invariant in the absence of lattice discontinuities (dislocations) [36, 45, 46]. As a result, from the Euler equation for superfluid velocity, we can derive the general form of the conservation law for the number of vortices:

$$\frac{\partial \boldsymbol{\omega}}{\partial t} = \mathrm{rot}\,[\mathbf{v}_L, \boldsymbol{\omega}]\,, \tag{111}$$

where $\mathbf{v}_L$ is the vortex lattice velocity. The difference between this velocity and the superfluid velocity in the direction perpendicular to the vortex axes, $\mathbf{v}_L - \mathbf{v}_{s\perp}$, receives contributions not only from the terms related to vortex lattice elasticity [18, 36] but also from the friction force between normal excitations and vortices, which is proportional to the relative velocity $\mathbf{w}_\perp = \mathbf{v}_{n\perp} - \mathbf{v}_{s\perp}$ of the normal and superfluid components in the direction perpendicular to the vortices and is determined by the Hall–Vinen coefficients B and B' [16, 316, 317]. We note that one of the coefficients, B, has a dissipative nature, while the other coefficient, B', is of a Hall type and is nondissipative. Andreev and an author of this review hypothesized in [36] that in the limit of a large number of vortices (and high rate of umklapp processes in the scattering of normal excitations on vortices that result in the relaxation of quasiparticle momentum), we can pass to the limit of the hydrodynamics of rapid rotation. In this limit, there is a common velocity of the normal and superfluid components in the direction perpendicular to the vortex axis, $\mathbf{v}_{n\perp} = \mathbf{v}_{s\perp}$, and two different velocities, $\mathbf{v}_{n\parallel} \neq \mathbf{v}_{s\parallel}$, in the direction along the vortex axis. It may be asserted that we have a crystal in the direction perpendicular to the vortex axis and free superfluid liquid in the longitudinal direction. We note that this limit is attained at low frequencies, when not only the condition $\omega\tau_N \ll 1$, standard for hydrodynamics, is satisfied (where τ_N is the normal time of relaxation of excitations related to their scattering on each other) but also

$$\omega\tau_U \ll 1 \tag{112}$$

holds, where the inverse time of scattering of normal excitations on vortices with umklapp processes is

$$\frac{1}{\tau_U} \sim B\Omega\,. \tag{113}$$

The dimensionless Hall–Vinen coefficient at temperatures $T \sim 1$ K in superfluid He-4 is $B \sim 1$, and to have the hydrodynamics of rapid rotations realized, it is sufficient to have the condition $\omega \ll (1/\tau_{\rm U} \sim \Omega)$ satisfied, regardless of the relation between the times $\tau_{\rm N}$ and $\tau_{\rm U}$ of the scattering of excitations on each other and the vortex lattice with umklapp processes. We note that the second sound (related to the relative velocity of normal and superfluid components $\mathbf{w} \neq 0$) in the hydrodynamics of rapid rotations only propagates along the vortex axis, while there is a dissipative thermal conductive mode in the perpendicular direction. In the limit of rapid rotations, the spectrum of this mode acquires the following form that replaces the relation $\omega = u_{\rm II} q$ standard for the second sound:

$$\omega = \mathrm{i}\,\frac{\kappa_\perp q_\perp^2}{2C_p\rho} \pm \sqrt{u_{\rm II}^2 q_z^2 - \left(\frac{\kappa_\perp q_\perp^2}{2C_p\rho}\right)^2}\,, \tag{114}$$

where C_p is the thermal capacity under constant pressure, $\kappa_\perp$ is the coefficient of thermal conductivity of vortices in the direction perpendicular to the vortex axis, and $u_{\rm II}$ is the speed of the second sound. It is noteworthy that the terms with the normal components fully disappear in the limit of low temperatures $T \to 0$ in the hydrodynamics of superfluid He-4, and the difference between the hydrodynamics of slow and rapid rotations is blurred. The vortex lattice velocity $\mathbf{v}_{\rm L}$ differs from the superfluid velocity $\mathbf{v}_{{\rm s}\perp}$ in the direction perpendicular to the vortices by the terms that are related to vortex lattice elasticity. Linearizing the nonlinear elasticity theory developed in [36] allows finding the vortex lattice oscillation spectrum. Tkachenko's results [47, 48] show that collective excitations of the vortex lattice correspond to the compression mode and the shear mode, and the shear mode has a nontrivial dispersion

$$\omega_{\rm t}^2 = c_{\rm t}^2\,\frac{C_{\rm s}^2 q_\perp^4}{4\Omega^2 + C_{\rm s}^2 q_\perp^2}\,, \tag{115}$$

where

$$c_{\rm t}^2 = \frac{\hbar\Omega}{8m} \tag{116}$$

is the transverse sound velocity in the vortex lattice squared and $C_{\rm s}^2$ is the speed of the first sound squared. Thus, the spectrum of Tkachenko shear waves at the smallest wave vectors $q_\perp \ll 2\Omega/c_{\rm t}$ is quadratic:

$$\omega_{\rm t} = \frac{c_{\rm t} C_{\rm s} q_\perp^2}{2\Omega}\,. \tag{117}$$

In the case of large wave vectors $q_\perp > 2\Omega/c_{\rm t}$, the Tkachenko wave spectrum becomes linear: $\omega_{\rm t} = c_{\rm t} q_\perp$. We stress that according to Baym [297], the quadratic character of the Tkachenko mode spectrum in the presence of small wave vectors in a superfluid gas and Bose–Einstein condensates can have dramatic consequences for purely 2D flows with $q_z = 0$. It results in a logarithmic divergence of the average shift squared of the deviation of the unit vortex line from the equilibrium position as a result of excitation of long-wave Tkachenko modes:

$$\frac{\langle \mathbf{u}^2\rangle}{b^2} \sim \frac{T}{\Omega}\,\frac{n_v}{nL}\,\ln\frac{q_{\max}}{q_{\min}}\,, \tag{118}$$

where $b = (\hbar/2\pi m\Omega)^{1/2}$ is the average distance between the vortices, L is the height of the vessel containing helium (or the size of the effective third dimension in quasi-two-dimensional magnetic traps), n_v and n are the densities of vortices and particles such that the ratio $p = nL/n_v$ is dimensionless, $q_{\max} = 2\Omega/c_{\rm t}$, $q_{\min} = 2\pi/R$, and R is the radius of the helium-containing vessel. If $\langle \mathbf{u}^2\rangle/b^2 \sim 1$, the vortex lattice in the system melts and the vortex-crystal–vortex-liquid phase transition occurs [300, 318, 319]. We note that the melted vortex lattice regime is practically unattainable in dense superfluid He-4 with the filling factor $p \gg 1$ and hence $\langle \mathbf{u}^2\rangle/b^2 \ll 1$. Also, it is very difficult to create purely 2D flows in superfluid He-4. Nevertheless, Gifford and Baym [320] also predict a logarithmic divergence of the displacement correlator in this case:

$$\frac{\left\langle \left|\mathbf{u}(\mathbf{r}) - \mathbf{u}(\mathbf{r}')\right|^2\right\rangle}{b^2} \propto T \ln R_\perp\,, \tag{119}$$

at low temperatures and very large distances $R_\perp^2 \gg Lb$, where $\mathbf{R} = \mathbf{r} - \mathbf{r}' = \{\mathbf{R}_\perp, R_z\}$. At the same time, this criterion can be satisfied much more easily in dilute Bose gases. The vortex-crystal–vortex-liquid phase transition is also possible at the temperature $T = 0$ due to quantum melting of the vortex crystal. According to Baym [297], for a dilute Bose gas at $T = 0$, instead of Eqn (118), we obtain

$$\frac{\langle \mathbf{u}^2\rangle}{b^2} \propto \frac{1}{p}\,\frac{b}{\xi_0}\,, \tag{120}$$

where ξ_0 is, as before, the coherence length or vortex core radius (72). Therefore, for quasi-two-dimensional traps with a very small third dimension L, the limit $p \geqslant 1$ can be attained and the Lindeman melting criterion can be satisfied [321]. We stress that apart from the compression and shear modes, there is another excitation branch in the vortex lattice and even for an individual vortex line, namely, bending oscillations of the vortex line. Their spectrum was determined by Thomson (Lord Kelvin) in 1880. It has quadratic behavior $\omega_b \propto q_z^2 \ln(1/q_z)$. It seems at first glance that at small q_z and low temperatures, such a quasi-one-dimensional quadratic spectrum should result in a strongly diverging infrared displacement of the vortex line $\langle \mathbf{u}^2\rangle \propto T\int \mathrm{d}q_z/q_z^2$ and, analogously to polymers, to folding of the vortex line into a globule. However, as was shown in [36], this oscillation branch does not actually correspond to bending but is related to rotation of the deformed line about its axis in such a way that the vector product of the vortex displacement and the displacement velocity is $[\mathbf{u} \times \dot{\mathbf{u}}] \neq 0$. As a result, the quanta of the vortex line bending oscillations acquire their own momentum $\hbar$ (diamagnetic situation), and the gap $\hbar\Omega$ emerges in the bending oscillation spectrum, which acquires the form [36]

$$\hbar\omega_b = \hbar\Omega + \frac{q_z^2}{2m}\,\ln\frac{1}{q_z d}\,, \tag{121}$$

where d is the interatomic distance in superfluid He-4. The presence of the gap in spectrum (121) stabilizes the bending oscillations of the individual vortex line in a helium-containing vessel and at low temperatures yields a finite vortex line displacement squared:

$$\frac{\langle \mathbf{u}^2\rangle}{R^2} \propto \frac{Tmd^2}{\hbar^2}\,\frac{d}{R}\,\frac{1}{\ln(R^2/d^2)}\,. \tag{122}$$

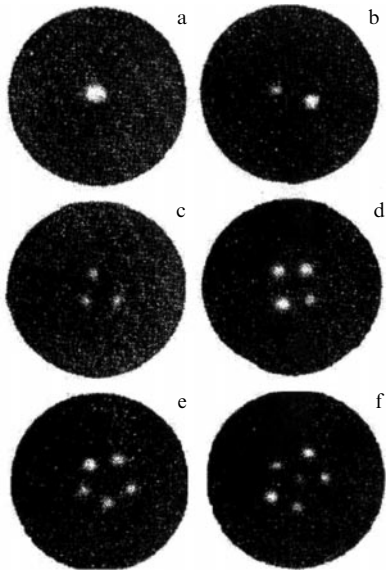

Figure 32. Emergence of a vortex lattice in superfluid He-4 as observed in experiments by Hall and Vinen [316, 317] and Yarmchuk, Packard, and Gordon [322–324]. Figures a–f show how the number of vortices increases from one to six.

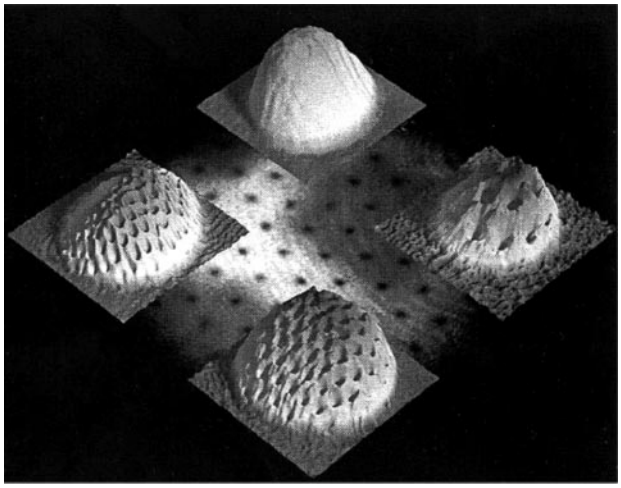

Figure 33. Vortex lattice in a rotating dilute ^{23}Na Bose gas [329].

It is owing to this circumstance that Packard et al. [322–324] managed to observe a vortex lattice in superfluid He-4 (actually, they were taking images; see Fig. 32). The vortex lattice was observed later in dilute Bose gases of alkali elements (^{23}Na and ^{87}Rb [325–329]; see Fig. 33) and in the BCS–BEC crossover regime for composite bosons ($^6Li_2$ molecules) in the Feshbach resonance [330].

15. Conclusion

Despite the rapid growth in the number of publications over the last 10 to 15 years and apparent progress in theoretical and experimental studies, the problem of the BCS–BEC crossover and the hydrodynamics of superfluid resonance Fermi–Bose gases and mixtures are still unresolved. We have discussed a number of interesting problems that are awaiting resolution by theoretical and experimental methods. In this context, we can single out the intriguing problem of quantum viscosity limit [122, 331, 332], which is of importance not only for ultracold quantum gases but also for cosmology and elementary particle physics. There are other aspects related, for example, to the rotation of vortex lattices in neutron stars, various versions of separation into phases ('lasagna' or 'spaghetti' type) and the emergence of fermionic and bosonic (pion) condensates in nuclear physics, multiparticle fermionic and bosonic complexes in the physics of nonrelativistic quarks and nucleons [333–337], and the thermodynamics and behavior of quasiparticles in the unitary limit, which are of interest for researchers in various areas of physics. Those problems are waiting to be resolved are a challenge for both experienced scientists and young researchers, whose activities in science are at the very beginning.

Finally, we note the recent experimental discovery [90] of anomalous superconductivity (which seems to be of the chiral $d + id$ type) with the critical temperature $T_c \simeq 1.7$ K and strong coupling (large T_c/ε_F ratio) in the limit of a very low 2D density $n_{2D} \sim 10^{12}$ cm^{-2} in graphene bilayers that are created as a result of twisting by a small ('magic') angle $\theta \simeq 1.2^\circ$ the layered graphene superstructure. The separation into phases [72] that occurs as a result seems to cause fragmentation of multilayer graphene, accompanied by the formation of a kind of AB$-$AA$-\ldots-$AB-type superlattice consisting of graphene bilayers with the AA and AB structure.

We note that owing to the large ratio of the critical temperature T_c and the Fermi energy ε_F, we can assert that bilayer graphene is similar to the BCS–BEC crossover situation between local and extended pairs in the d-wave channel (see Section 6 of this review). A bridge is established in this way between the physics and phase diagrams of the BCS–BEC crossover in superfluid quantum gases that we review here (see Sections 3–5) and similar phenomena and superconducting phase diagrams in the physics of high-temperature superconductors and Dirac semimetals.

We note that quite recently Spivak et al. [308–310] and Haldane [296] extended the discussion about the possible contribution of the chiral anomaly proportional to the **EB** scalar product in the presence of (often parallel) magnetic (**B**) and electric (**E**) fields to intervalley transitions of charge carriers and longitudinal magnetoresistance in 3D Dirac semimetals and $Bi_{1-x}Sb_x$ topological insulators (with topologically protected Dirac points) in the vicinity of the critical quantum point in the Sb concentration x (see also experimental study [311] in Dirac and Weil semimetals and a paper on the chiral anomaly in graphene [312]).

We note that in 3D Dirac semimetals and topological insulators in the presence of a magnetic field, the role of the collective mode can be played by magnetoplasmons. The electron spectrum in strong quantizing magnetic fields and in the so-called superquantum limit becomes quasi-one-dimensional if only one (lower) Landau level is filled. Therefore, it is possible to decrease the effective dimensionality of the collective mode and obtain a gapless magnetoplasmon spectrum even in 3D semimetals.

We recall that the plasmon spectrum in 3D metal systems in the absence of a magnetic field usually has a plasmon gap due to the presence of an ionic crystal lattice and the condition of local electro-neutrality. At the same time, the plasmon spectrum in 2D systems (in particular, such as a graphene mono- or bilayer) features a characteristic square-root

dependence of the wave vector [338] and is gapless (Goldstone) in a finite frequency window (range).

Consequently, the main experimental task in 3D Dirac semimetals is, on the one hand, to measure magnetoconductivity values $\sigma_{zz}(B)$ at zero frequency and at low frequencies (DC transport measurements) and, on the other hand, to determine the magnetoplasmon spectrum $\omega(q, B)$ in the microwave and terahertz ranges for various frequency ranges in the parameter $\omega\tau$. The last spectrum should be measured both for the semiclassical regime of weak magnetic fields and in strong quantizing magnetic fields in the range 1–10 T. Such measurements may be conducted both in Russia and in a number of leading laboratories located in the Netherlands, France, and the USA. The main tasks for the theory are to determine the analog of the important topological coefficient C_0 (see Section 12 and 13) in Dirac semimetals and to identify its behavior at high and low frequencies determined by the parameter $\omega\tau$.

We note that in some sense, according to Laughlin's ideology [339], the Larmor orbit center for strongly correlated electrons in Dirac semimetals placed into strong quantizing magnetic fields can form a kind of Wigner crystal in the plane perpendicular to the magnetic field. The longitudinal magnetoplasmon lattice oscillations in that crystal can preserve the gap due to the condition of electro-neutrality and have a finite plasmon gap at low frequencies and wave vectors (it is for this reason that the electron subsystem in the regime of a fractional quantum Hall effect is considered to be incompressible [339, 340]). At the same time, transverse (shear) magnetoplasmon oscillations in the electron subsystem may correspond to gapless Goldstone modes or have a very small gap.

These modes may exhibit a linear (magnetoacoustic) spectrum similar to Alfven waves in plasma hydrodynamics [13] or even a quadratic spectrum similar to the helical waves of Konstantinov and Perel [341], which emerge already in the semiclassical description of uncompensated metals in a magnetic field.

As we have noted, such waves may be truly gapless or have a small gap of a relativistic nature, similar to magnons in a ferromagnet [28]. In any event, the physics of these waves is very similar to the physics of orbital waves in He-3A, because they always correspond to a small rotating transverse component of the magnetic field in the background of a large invariable longitudinal component. Owing to this, the spectral equation for waves of that type is very similar to the Landau–Lifshitz equation for magnons in a ferromagnet and hence (as has been shown, for example, in [18]) to the spectral equation of orbital waves in He-3A.

We note that already in the semiclassical limit of small magnetic fields, we can extract important and relevant information regarding the value of the topological coefficient C_0 from the measurements of longitudinal magnetoplasmon modes with a gap in parallel electric and magnetic fields. This can be done using sum rules [309] that relate the gap squared and the longitudinal magnetoconductivity $\sigma_{zz} \propto \omega_{\rm pl}^2\tau$.

We stress that both the longitudinal magnetoconductivity σ_{zz} (in parallel electric and magnetic fields) and the magnetoplasmon gap squared $\omega_{\rm pl}^2$ are linear functions of C_0. The coefficient C_0 itself that can be determined in the single-particle approximation is directly proportional to the product of universal constants such as the number of valleys $N_{\rm v}$ in a Dirac semimetal, the Dirac velocity v, the electron charge e, and the fine structure constant $\alpha = e^2/\hbar c = 1/137$.

A task for the nearest future, of interest for both theorists and experimentalists, is to generalize the calculated and measured results for the plasmon gap and the longitudinal magnetoconductivity to the quantum case of very strong magnetic fields, very low temperatures, and very low carrier densities (ultra-quantum limit). According to Spivak, this limit is described by the chain of inequalities

$$\gamma = \frac{1}{\tau} < vL_B < \{\Omega_{\rm c}, \mu, T\}\,, \tag{123}$$

where $L_B = \sqrt{\hbar c/eB}$ is the magnetic length and the inequality $\Omega_{\rm c}\tau \gg 1$ corresponds to weakly broadened Landau levels in a strong quantizing magnetic field. These estimates correspond to magnetic fields whose strength is of the order of 10 T and temperatures that are significantly lower than those in Kim's experiments (in the millikelvin region).

In Spivak's opinion, very interesting infrared divergences can be observed in this limit both in the collisional case $\mu \gg T$ and in the collisionless case $\mu \ll T$ in expressions for the density of states, conductivity, and other characteristics of the system (such as a change in the number of particles in a valley in intervalley transitions.)

We reiterate that active experimental and theoretical studies of quantum hydrodynamics in ultra-pure graphene [342], the chiral anomaly in topological insulator $Bi_{1-x}Sb_x$ [311, 312], nematic anisotropic superconductivity in Bi_2Se_3 doped with Cu, Nb or Sr [313], and other Dirac semimetals that are being conducted now are of importance for the development of basic condensed matter physics and are very promising from the perspective of potential applications in nanoelectronics and spintronics.

Returning to anomalous superconductivity and the BCS–BEC crossover in a graphene bilayer, we stress again that the phase diagram of the superconducting and normal states of this system is very similar to the phase diagram of weakly doped HTSC cuprates (considered in Section 6 of this review). The BEC phase of the local pair with d-wave pairing is supposed to be realized in the limit of low carrier densities in the graphene bilayer (for small deviations from the half-filling that corresponds to the Mott insulator [90]), while at higher carrier densities, the BCS phase of extended Cooper pairs in the chiral d-wave channel is to be realized.

The superconductivity mechanism that dominates in the BCS phase seems again to be the Kohn–Luttinger mechanism discussed in Sections 8 and 9, enhanced due to the proximity to half-filling. We note that an author of this review (with collaborators) has theoretically predicted chiral d-wave pairing in an idealized ultra-pure (regarding impurities and structural defects) AB layer of graphene with the critical temperature $T_{\rm c} \sim 20-40$ K at the dimensionless 2D density $n_{\rm 2D} \sim 0.1$ of the monolayer [149, 343]. However, as was shown in [87, 88, 149, 343], a nonmagnetic impurity and structural defects decrease the critical temperatures of d-paring in the real graphene bilayer.

Lozovik et al. [344] have shown that another important factor responsible for decreasing $T_{\rm c}$ is the curvature of the real graphene monolayer surface. According to Lozovik's concept, it plays the role of an effective magnetic field in analyzing possible ('diamagnetic') suppression of superconductivity in real graphene. We note that an extended Hubbard model was used in the weak-coupling Born approximation in [149, 343] for exploring the graphene bilayer. The problem of

Coulomb correlation strength in graphene remains a matter of discussions.

Summarizing, we can assert that graphene and other Dirac semimetal systems can be used in some sense as reference systems that nicely combine all the effects discussed in this review regarding the realization of the BCS–BEC crossover scenario, the Berezinskii–Kosterlitz–Thouless fluctuation corrections, and the collective excitation spectrum, on the one hand, and Kohn–Luttinger anomalous superconductivity and the role of Dirac zero modes in the quasiparticle fermionic spectrum, on the other hand. We note that the role of the topological coefficient C_0 in 2D and layered systems being played by the topological charge Q [296] that controls the quantization of transverse Hall conductivity in the quantum Hall effect and anomalous spin current in thin films of the axial phase of superfluid He-3 [50].

We stress that graphene and other Dirac systems can be simulated in experiments in the physics of ultracold quantum gases using optical lattices, in particular, 2D hexagonal optical lattices with special (highly symmetric) Dirac points (see [86]).

The authors are grateful to A F Andreev, G E Volovik, Yu E Lozovik, N B Kopnin, G V Shlyapnikov, D V Efremov, A V Chubukov, M A Baranov, A A Golubov, V V Val'kov, A Brinkman, A Kimel, H W Capel, P Broussard, M S Mar'enko, I V Brodskii, A V Klaptsov, Ch van Weert, A Pruiskin, D Vollhardt, P Wölfle, B Spivak, A G Aronov, A I Larkin, D M Lee, G Frossati, I A Fomin, R Combescot, A S Aleksandrov, D E Khmel'nitskii, A V Balatskii, V V Dmitriev, D Ivanov, L P Pitaevskii, M Stone, and P N Brusov for the numerous useful discussions. M Yu K is grateful to the Russian Foundation for Basic Research (project no. 17-02-00135) and the Basic Research Program of the National Research University 'Higher School of Economics'. A V T is grateful to the Russian Science Foundation for the support provided as part of the project no. 18-12-00002.

References

1. Anderson M H et al. *Science* **269** 198 (1995)
2. Giorgini S, Pitaevskii L P, Stringari S *Rev. Mod. Phys.* **80** 1215 (2008)
3. Bloch I, Dalibard J, Zwerger W *Rev. Mod. Phys.* **80** 885 (2008)
4. Bardeen J, Cooper L N, Schrieffer J R *Phys. Rev.* **108** 1175 (1957)
5. Schrieffer J R *Theory of Superconductivity* (New York: W.A. Benjamin, 1964); Translated into Russian: *Teoriya Sverkhprovodimosti* (Moscow: Nauka, 1970)
6. Cooper L N *Phys. Rev.* **104** 1189 (1956)
7. Einstein A *Sitzungsber. Preuß. Akad. Wiss. Physi.-Math. Kl.* **1** 3 (1925)
8. Eagles D M *Phys. Rev.* **186** 456 (1969)
9. Leggett A J, in *Modern Trends in the Theory of Condensed Matter. Proc. of the XVI Karpacz Winter School of Theoretical Physics, February 19 – March 3, 1979 Karpacz, Poland* (Lecture Notes in Physics, Vol. 115, Eds A Pekalski, J A Przystawa) (Berlin: Springer-Verlag, 1980) p. 13
10. Nozières P, Schmitt-Rink S *J. Low Temp. Phys.* **59** 195 (1985)
11. Keldysh L V, Kozlov A N *Sov. Phys. JETP* **27** 521 (1968); *Zh. Eksp. Teor. Fiz.* **54** 978 (1968)
12. Gor'kov L P, Melik-Barkhudarov T K *Sov. Phys. JETP* **13** 1018 (1961); *Zh. Eksp. Teor. Fiz.* **40** 1452 (1961)
13. Landau L D, Lifshitz E M *Fluid Mechanics* (Oxford: Pergamon Press, 1987); Translated from Russian: *Gidrodinamika* 4th ed. (Moscow: Nauka, 1988)
14. Landau L *J. Phys. USSR* **5** 71 (1941); *Zh. Eksp. Teor. Fiz.* **11** 592 (1941)
15. Putterman S J *Superfluid Hydrodynamics* (Amsterdam: North-Holland, 1974); Translated into Russian: *Gidrodinamika Sverkhtekuchei Zhidkosti* (Moscow: Mir, 1978)
16. Khalatnikov I M *An Introduction to the Theory of Superfluidity* (CRC Press; 2018); Translated from Russian: *Teoriya Sverkhtekuchesti* (Moscow: Nauka, 1971)
17. Tilley D R, Tilley J *Superfluidity and Superconductivity* (New York: Wiley, 1974); Translated into Russian: *Sverkhtekuchest' i Sverkhprovodimost'* (Moscow: Mir, 1977)
18. Kagan M Yu *Modern Trends in Superconductivity and Superfluidity* (Lecture Notes in Physics, Vol. 874) (Dordrecht: Springer, 2013)
19. Combescot R, Leyronas X, Kagan M Yu *Phys. Rev. A* **73** 023618 (2006)
20. Kagan M Yu, Frésard R, Capezzali M, Beck H *Phys. Rev. B* **57** 5995 (1998)
21. Turlapov A V, Kagan M Yu *J. Phys. Condens. Matter* **29** 383004 (2017)
22. Barmashova T V, Martiyanov K A, Makhalov V B, Turlapov A V *Phys. Usp.* **59** 174 (2016); *Usp. Fiz. Nauk* **186** 183 (2016)
23. Feshbach H *Ann. Physics* **19** 287 (1962)
24. Combescot R, Kagan M Yu, Stringari S *Phys. Rev. A* **74** 042717 (2006)
25. Kagan M Yu, Efremov D V *JETP* **110** 426 (2010); *Zh. Eksp. Teor. Fiz.* **137** 483 (2010);
26. Kinast J, Turlapov A, Thomas J E *Phys. Rev. A* **70** 051401(R) (2004)
27. Joseph J et al. *Phys. Rev. Lett.* **98** 170401 (2007)
28. Lifshitz E M, Pitaevskii L P *Statistical Physics* Vol. 2 *Theory of the Condensed State* (Oxford: Pegramon Press, 1980); Translated from Russian: *Statisticheskaya Fizika* Pt. 2 *Teoriya Kondensirovannogo Sostoyaniya* 3rd ed. (Moscow: Fizmatlit, 2004)
29. Kagan M Yu et al. *Phys. Rev. A* **70** 023607 (2004)
30. Kagan M Yu, Efremov D V *Phys. Rev. B* **65** 195103 (2002)
31. Brodsky I V et al. *JETP Lett.* **82** 273 (2005); *Pis'ma Zh. Eksp. Teor. Fiz.* **82** 306 (2005)
32. Brodsky I V et al. *Phys. Rev. A* **73** 032724 (2006)
33. Kagan M Yu et al. *Phys. Usp.* **49** 1079 (2006); *Usp. Fiz. Nauk* **176** 1105 (2006)
34. Menushenkov A P, Klementev K V, Kuznetsov A V, Kagan M Yu *JETP* **93** 615 (2001); *Zh. Eksp. Teor. Fiz.* **120** 700 (2001)
35. Menushenkov A P, Kuznetsov A V, Klementiev K V, Kagan M Yu *J. Supercond. Nov. Magn.* **29** 701 (2016)
36. Andreev A F, Kagan M Yu *Sov. Phys. JETP* **59** 318 (1984); *Zh. Eksp. Teor. Fiz.* **86** 546 (1984)
37. Feynman R P *Prog. Low Temp. Phys.* **1** 17 (1955)
38. Feynman R P *Statistical Mechanics: a Set of Lectures* (Boulder: Westview Press, 1998); Translated into Russian: *Statisticheskaya Mekhanika. Kurs Lektsii* (Moscow: Platon, 2000)
39. Onsager L *Nuovo Cimento* **6** (Suppl. 2) 249 (1949)
40. Bekarevich I L, Khalatnikov I M *Sov. Phys. JETP* **13** 643 (1962); *Zh. Eksp. Teor. Fiz.* **40** 920 (1961)
41. Andronikashvili E L, Mamaladze Yu G *Rev. Mod. Phys.* **38** 567 (1966)
42. Sonin E B *Rev. Mod. Phys.* **59** 87 (1987)
43. Baym G, Chandler E *J. Low Temp. Phys.* **50** 57 (1983)
44. Andronikashvili E L *J. Phys. USSR* **10** 201 (1946); Andronikashvili E L *Zh. Eksp. Teor. Fiz.* **18** 424 (1948)
45. Volovik G E, Dotsenko V S (Jr.) *Sov. Phys. JETP* **51** 65 (1980); *Zh. Eksp. Teor. Fiz.* **78** 132 (1980)
46. Dzyaloshinskii I E, Volovick G E *Ann. Physics* **125** 67 (1980)
47. Tkachenko V K *Sov. Phys. JETP* **22** 1282 (1966); *Zh. Eksp. Teor. Fiz.* **49** 1875 (1966)
48. Tkachenko V K *Sov. Phys. JETP* **23** 1049 (1966); *Zh. Eksp. Teor. Fiz.* **50** 1573 (1966)
49. Thomson W (Lord Kelvin) *Phil. Mag.* **10** 155 (1880)
50. Volovik G E *The Universe in Helium Droplet* (Oxford: Oxford Univ. Press, 2002)
51. Vollhardt D, Woelfle P *The Superfluid Phases of Helium 3* (London: Taylor and Francis, 1990)
52. Andreev A F, Kagan M Yu *Sov. Phys. JETP* **66** 504 (1987); *Zh. Eksp. Teor. Fiz.* **93** 895 (1987)
53. Balatskii A V, Volovik G E, Konyshev G A *Sov. Phys. JETP* **63** 1194 (1986); *Zh. Eksp. Teor. Fiz.* **90** 2038 (1986)
54. Adler S L *Phys. Rev.* **177** 2426 (1969)

55. Bell J S, Jackiw R *Nuovo Cimento A* **60** 47 (1969)
56. Jackiw R *Lectures on Current Algebra and Its Applications* (Princeton, NJ: Princeton Univ. Press, 1972)
57. Kagan M Y, Efremov D V *J. Low Temp. Phys.* **158** 749 (2010)
58. Volovik G E *JETP Lett.* **98** 753 (2013); *Pis'ma Zh. Eksp. Teor. Fiz.* **98** 848 (2013)
59. Volovik G E *JETP Lett.* **103** 140 (2016); *Pis'ma Zh. Eksp. Teor. Fiz.* **103** 147 (2016)
60. de Gennes P G *Superconductivity of Metals and Alloys* (New York: W.A. Benjamin, 1966); Translated into Russian: *Sverkhprovodimost' Metallov i Splavov* (Moscow: Mir, 1968)
61. Bogoliubov N N, Tolmachev V V, Shirkov D V *A New Method in the Theory of Superconductivity* (New York: Consultants Bureau, 1959); Translated from Russian: *Novyi Metod v Teorii Sverkhprovodimosti* (Moscow: Izd. AN SSSR, 1958)
62. de Gennes P G *The Physics of Liquid Crystals* (Oxford: Clarendon Press, 1974); Translated into Russian: *Fizika Zhidkikh Kristallov* (Moscow: Mir, 1977)
63. Berestetskii V B, Lifshitz E M, Pitaevskii L P *Quantum Electrodynamics* (Oxford: Butterworth-Heinemann, 1999); Translated from Russian: *Kvantovaya Elektrodinamika* (Moscow: Nauka, 1980)
64. Kohn W, Luttinger J M *Phys. Rev. Lett.* **15** 524 (1965)
65. Fay D, Layzer A *Phys. Rev. Lett.* **20** 187 (1968)
66. Kagan M Yu, Chubukov A V *JETP Lett.* **47** 614 (1988); *Pis'ma Zh. Eksp. Teor. Fiz.* **47** 525 (1988)
67. Kagan M Yu, Chubukov A V *JETP Lett.* **50** 517 (1989); *Pis'ma Zh. Eksp. Teor. Fiz.* **50** 483 (1989)
68. Kagan M Yu *Phys. Usp.* **37** 69 (1994); *Usp. Fiz. Nauk* **164** 77 (1994)
69. Baranov M A, Kagan Yu, Kagan M Yu *JETP Lett.* **64** 301 (1996); Baranov M A, Kagan M Yu, Kagan Yu *Pis'ma Zh. Eksp. Teor. Fiz.* **64** 273 (1996)
70. Larkin A I, Ovchinnikov Yu N *Sov. Phys. JETP* **20** 762 (1965); *Zh. Eksp. Teor. Fiz.* **47** 1136 (1964)
71. Fulde P, Ferrell R A *Phys. Rev.* **135** A550 (1964)
72. Kagan M Yu, Kugel' K I *Phys. Usp.* **44** 553 (2001); *Usp. Fiz. Nauk* **171** 577 (2001)
73. Shin Y et al. *Phys. Rev. Lett.* **97** 030401 (2006)
74. Ong W et al. *Phys. Rev. Lett.* **114** 110403 (2015)
75. Mitra D et al. *Phys. Rev. Lett.* **117** 093601 (2016)
76. Berezinskii V L *Sov. Phys. JETP* **34** 610 (1972); *Zh. Eksp. Teor. Fiz.* **61** 1144 (1971)
77. Kosterlitz J M, Thouless D J *J. Phys. C* **6** 1181 (1973)
78. Fisher D S, Hohenberg P C *Phys. Rev. B* **37** 4936 (1988)
79. Beasley M R, Mooij J E, Orlando T P *Phys. Rev. Lett.* **42** 1165 (1979)
80. José J V (Ed.) *40 Years of Berezinskii – Kosterlitz – Thouless Theory* (Singapore: World Scientific, 2013)
81. Ryzhov V N *Phys. Usp.* **60** 114 (2017); *Usp. Fiz. Nauk* **187** 125 (2017)
82. Ryzhov V N et al. *Phys. Usp.* **60** 857 (2017); *Usp. Fiz. Nauk* **187** 921 (2017)
83. Miyake K *Prog. Theor. Phys.* **69** 1794 (1983)
84. Randeria M, Duan J-M, Shieh L-Y *Phys. Rev. Lett.* **62** 981 (1989)
85. Schmitt-Rink S, Varma C M, Ruckenstein A E *Phys. Rev. Lett.* **63** 445 (1989)
86. Tarruell L et al. *Nature* **483** 302 (2012)
87. Kagan M Yu, Mitskan V A, Korovushkin M M *Phys. Usp.* **58** 733 (2015); *Usp. Fiz. Nauk* **185** 785 (2015)
88. Kagan M Yu *JETP Lett.* **103** 728 (2016); *Pis'ma Zh. Eksp. Teor. Fiz.* **103** 822 (2016)
89. Di Bernardo A et al. *Nature Commun.* **8** 14024 (2017)
90. Cao Y et al. *Nature* **556** 43 (2018)
91. Bradley C C et al. *Phys. Rev. Lett.* **75** 1687 (1995)
92. Davis K B et al. *Phys. Rev. Lett.* **75** 3969 (1995)
93. Ketterle W, Durfee D S, Stamper-Kurn D M, in *Bose – Einstein Condensation in Atomic Gases* (Proc. of the Intern. School of Physics "Enrico Fermi", Course 140, Eds M Inguscio, S Stringari, C E Wieman) (Amsterdam: IOS Press, 1999) pp. 67 – 176
94. Greiner M, Regal C A, Jin D S *Nature* **426** 537 (2003)
95. Jochim S et al. *Science* **302** 2101 (2003)
96. Zwierlein M W et al. *Phys. Rev. Lett.* **91** 250401 (2003)
97. Bourdel T et al. *Phys. Rev. Lett.* **93** 050401 (2004)
98. Ni K-K et al. *Science* **322** 231 (2008)
99. Chin C et al. *Rev. Mod. Phys.* **82** 1225 (2010)
100. Kagan M Yu *Fizika Makroskopicheskikh Kvantovykh Sistem. Kurs Lektsii. Seminary* (Physics of Macroscopic Quantum Systems. A Set of Lectures) (Moscow: Izd. Dom MEI, 2014)
101. Pitaevskii L P *Phys. Usp.* **51** 603 (2008); *Usp. Fiz. Nauk* **178** 633 (2008)
102. Landau L D, Lifshitz E M *Quantum Mechanics. Non-Relativistic Theory* (Oxford: Pergamon Press, 1977); Translated from Russian: *Kvantovaya Mekhanika. Nerelyativistskaya Teoriya* 5th ed. (Moscow: Fizmatlit, 2002)
103. Gurarie V, Radzihovsky L *Ann. Physics* **322** 2 (2007)
104. Alexandrov A, Ranninger J *Phys. Rev. B* **23** 1796 (1981)
105. Ranninger J, Micnas R, Robaszkiewicz S *Ann. Phys. Fr.* **13** 455 (1988)
106. Hubbard J *Proc. R. Soc. Lond. A* **276** 238 (1963)
107. Zürn G et al. *Phys. Rev. Lett.* **110** 135301 (2013)
108. Fano U *Nuovo Cimento* **12** 154 (1935)
109. Fano U *Phys. Rev.* **124** 1866 (1961)
110. Kagan M Yu, Val'kov V V, Aksenov S V *Phys. Rev. B* **95** 035411 (2017)
111. Kinast J et al. *Phys. Rev. Lett.* **92** 150402 (2004)
112. Marsiglio F et al. *Phys. Rev. B* **91** 054509 (2015)
113. Petrov D S, Baranov M A, Shlyapnikov G V *Phys. Rev. A* **67** 031601(R) (2003)
114. Petrov D S, Salomon C, Shlyapnikov G V *Phys. Rev. Lett.* **93** 090404 (2004)
115. Prokof'ev N, Ruebenacker O, Svistunov B *Phys. Rev. Lett.* **87** 270402 (2001)
116. Kashurnikov V A, Prokof'ev N V, Svistunov B V *Phys. Rev. Lett.* **87** 120402 (2001)
117. Ngampruetikorn V, Levinsen J, Parish M M *Phys. Rev. Lett.* **111** 265301 (2013)
118. Liu X-J, Hu H, Drummond P D *Phys. Rev. B* **82** 054524 (2010)
119. Barth M, Hofmann J *Phys. Rev. A* **89** 013614 (2014)
120. Boettcher I et al. *Phys. Rev. Lett.* **116** 045303 (2016)
121. Fenech K et al. *Phys. Rev. Lett.* **116** 045302 (2016)
122. Vogt E et al. *Phys. Rev. Lett.* **108** 070404 (2012)
123. Chien C-C, Levin K *Phys. Rev. A* **82** 013603 (2010)
124. Bartenstein M et al. *Phys. Rev. Lett.* **92** 120401 (2004)
125. Heiselberg H *Phys. Rev. A* **63** 043606 (2001)
126. Pieri P, Pisani L, Strinati G C *Phys. Rev. B* **72** 012506 (2005)
127. Astrakharchik G E et al. *Phys. Rev. Lett.* **93** 200404 (2004)
128. Burovski E et al. *Phys. Rev. Lett.* **96** 160402 (2006)
129. Landau L D, Lifshitz E M *Statistical Physics* Vol. 1 (Oxford: Pergamon Press, 1980); Translated from Russian: *Statisticheskaya Fizika* Pt. 1, 5th ed. (Moscow: Fizmatlit, 2001)
130. Onofrio R *Phys. Usp.* **59** 1129 (2016); *Usp. Fiz. Nauk* **186** 1229 (2016)
131. Kolachevsky N N, Taichenachev A V *Quantum Electron.* **47** 393 (2017); *Kvantovaya Elektron.* **47** 393 (2017)
132. Martiyanov K, Makhalov V, Turlapov A *Phys. Rev. Lett.* **105** 030404 (2010)
133. Fröhlich B et al. *Phys. Rev. Lett.* **106** 105301 (2011)
134. Dyke P et al. *Phys. Rev. Lett.* **106** 105304 (2011)
135. Ando T, Fowler A B, Stern F *Rev. Mod. Phys.* **54** 437 (1982)
136. Dolgopolov V T *Phys. Usp.* **57** 105 (2014); *Usp. Fiz. Nauk* **184** 113 (2014)
137. Alikacem N, Sprague D T, Hallock R B *Phys. Rev. Lett.* **67** 2501 (1991)
138. Saunders J, Lusher C P, Cowan B P *Phys. Rev. Lett.* **64** 2523 (1990)
139. Østgaard E, Bashkin E P *Physica B* **178** 134 (1992)
140. Andreev A F *Sov. Phys. JETP* **23** 939 (1966); *Zh. Eksp. Teor. Fiz.* **50** 1415 (1966)
141. Pavloff N, Treiner J *J. Low Temp. Phys.* **83** 331 (1991)
142. Dalfovo F, Stringari S *Phys. Scripta* **38** 204 (1988)
143. Kurihara S *J. Phys. Soc. Jpn.* **52** 1311 (1983)
144. Novoselov K S et al. *Science* **306** 666 (2004)
145. Kotov V N et al. *Rev. Mod. Phys.* **84** 1067 (2012)
146. Castro Neto A H et al. *Rev. Mod. Phys.* **81** 109 (2009)
147. van der Marel D, van Mechelen J L M, Mazin I I *Phys. Rev. B* **84** 205111 (2011)
148. Smink A E M et al. *Phys. Rev. Lett.* **118** 106401 (2017)
149. Kagan M Yu et al. *Solid State Commun.* **188** 61 (2014)
150. Hueck K et al. *Phys. Rev. Lett.* **120** 060402 (2018)
151. Feld M et al. *Nature* **480** 75 (2011)

152. Savard T A, O'Hara K M, Thomas J E *Phys. Rev. A* **56** R1095 (1997)
153. Gehm M E et al. *Phys. Rev. A* **58** 3914 (1998)
154. Makhalov V, Martiyanov K, Turlapov A *Phys. Rev. Lett.* **112** 045301 (2014)
155. Dyke P et al. *Phys. Rev. A* **93** 011603(R) (2016)
156. Martiyanov K, Barmashova T, Makhalov V, Turlapov A *Phys. Rev. A* **93** 063622 (2016)
157. Cheng C et al. *Phys. Rev. A* **94** 031606(R) (2016)
158. Murthy P A et al. *Phys. Rev. A* **90** 043611 (2014)
159. Orel A A et al. *New J. Phys.* **13** 113032 (2011)
160. Mulkerin B C et al. *Phys. Rev. A* **96** 053608 (2017)
161. Salasnich L, Toigo F *Phys. Rev. A* **91** 011604(R) (2015)
162. He L et al. *Phys. Rev. A* **92** 023620 (2015)
163. Salasnich L, Bighin G *J. Supercond. Nov. Magn.* **29** 3103 (2016)
164. Murthy P A et al. *Phys. Rev. Lett.* **115** 010401 (2015)
165. Hadzibabic Z et al. *Nature* **441** 1118 (2006)
166. Wu C-T et al. *Phys. Rev. Lett.* **115** 240401 (2015)
167. Choi J, Seo S W, Shin Y *Phys. Rev. Lett.* **110** 175302 (2013)
168. Boettcher I, Holzmann M *Phys. Rev. A* **94** 011602(R) (2016)
169. Loktev V M, Quick R M, Sharapov S G *Phys. Rep.* **349** 1 (2001)
170. Galitskii V M *Sov. Phys. JETP* **7** 104 (1958); *Zh. Eksp. Teor. Fiz.* **34** 151 (1958)
171. Bloom P *Phys. Rev. B* **12** 125 (1975)
172. Josephson B D *Phys. Lett.* **1** 251 (1962)
173. Josephson B D *Adv. Phys.* **14** 419 (1965)
174. Baranov M A, Efremov D V, Kagan M Yu *Physica C* **218** 75 (1993)
175. Laughlin R B *Phys. Rev. Lett.* **60** 2677 (1988)
176. Fetter A L, Hanna C B, Laughlin R B *Phys. Rev. B* **39** 9679(R) (1989)
177. Bulaevskii L N, Nagaev E L, Khomskii D I *Sov. Phys. JETP* **27** 836 (1968); *Zh. Eksp. Teor. Fiz.* **54** 1562 (1968)
178. Brinkman W F, Rice T M *Phys. Rev. B* **2** 1324 (1970)
179. Anderson P W *Science* **235** 1196 (1987)
180. Fulde P *Electron Correlations in Molecules and Solids* (Springer Series in Solid-State Sciences, Vol. 100) (Berlin: Springer, 1993)
181. Belinicher V I, Chernyshev A L, Shubin V A *Phys. Rev. B* **56** 3381 (1997)
182. Shraiman B I, Siggia E D *Phys. Rev. B* **42** 2485 (1990)
183. Uemura Y J et al. *Phys. Rev. Lett.* **66** 2665 (1991)
184. Kagan M Yu, Rice T M *J. Phys. Condens. Matter* **6** 3771 (1994)
185. Plakida N M et al. *JETP* **97** 331 (2003); *Zh. Eksp. Teor. Fiz.* **124** 367 (2003)
186. Castellani C, Di Castro C, Grilli M *Phys. Rev. Lett.* **75** 4650 (1995)
187. Sachdev S *Phys. Status Solidi B* **247** 537 (2010)
188. Petrov D S, Salomon C, Shlyapnikov G V *Phys. Rev. A* **71** 012708 (2005)
189. Efimov V I *Sov. J. Nucl. Phys.* **12** 589 (1971); *Yad. Fiz.* **12** 1080 (1970)
190. Efimov V *Phys. Rev. C* **44** 2303 (1991)
191. Jensen A S et al. *Rev. Mod. Phys.* **76** 215 (2004)
192. Skorniakov G V, Ter-Martirosian K A *Sov. Phys. JETP* **4** 648 (1957); *Zh. Eksp. Teor. Fiz.* **31** 775 (1957)
193. Nielsen E et al. *Phys. Rep.* **347** 373 (2001)
194. Nielsen E, Fedorov D V, Jensen A S *Few-Body Syst.* **27** 15 (1999)
195. Pieri P, Strinati G C *Phys. Rev. B* **61** 15370 (2000)
196. Bruch L W, Tjon J A *Phys. Rev. A* **19** 425 (1979)
197. Bardeen J, Baym G, Pines D *Phys. Rev.* **156** 207 (1967)
198. Bashkin E P, Meyerovich A E *Adv. Phys.* **30** 1 (1981)
199. Leggett A J *Rev. Mod. Phys.* **47** 331 (1975)
200. Anderson P W, Morel P *Phys. Rev.* **123** 1911 (1961)
201. Brinkman W F, Anderson P W *Phys. Rev. A* **8** 2732 (1973)
202. Brinkman W F, Serene J W, Anderson P W *Phys. Rev. A* **10** 2386 (1974)
203. Rainer D, Serene J W *Phys. Rev. B* **13** 4745 (1976)
204. van de Haar P G, Frossati G, Bedell K S *J. Low Temp. Phys.* **77** (1) 35 (1989)
205. Kohn W *Phys. Rev. Lett.* **2** 393 (1959)
206. Friedel J *Adv. Phys.* **3** 446 (1954)
207. Noziéres P, private communication
208. Efremov D V, Mar'enko M S, Baranov M A, Kagan M Yu *JETP* **90** 861 (2000); *Zh. Eksp. Teor. Fiz.* **117** 990 (2000)
209. Kagan M Yu *Phys. Lett. A* **152** 303 (1991)
210. Frossati G et al. *Czech. J. Phys.* **40** 909 (1990)
211. Wiegers S A J et al. *Physica B* **165–166** 733 (1990)
212. Meyerovich A E *JETP Lett.* **37** 32 (1983); *Pis'ma Zh. Eksp. Teor. Fiz.* **37** 28 (1983)
213. Roobol L P et al. *Europhys. Lett.* **17** 219 (1992)
214. Castaing B, Nozières P *J. Phys. France* **40** 257 (1979)
215. Bashkin E P *Sov. Phys. JETP* **51** 181 (1980); *Zh. Eksp. Teor. Fiz.* **78** 360 (1980)
216. Saunders J et al. *Physica B* **280** 100 (2000)
217. Morley G W et al. *J. Low Temp. Phys.* **126** 557 (2002)
218. Efremov D V, Viverit L *Phys. Rev. B* **65** 134519 (2002)
219. Roati G et al. *Phys. Rev. Lett.* **89** 150403 (2002)
220. Modugno G et al. *Science* **297** 2240 (2002)
221. Stoof H T C et al. *Phys. Rev. Lett.* **76** 10 (1996)
222. Migdal A B *Qualitative Methods in Quantum Theory* (Cambridge, Mass.: Advanced Book Program, 2000); Migdal A B *Kachestvennye Metody v Kvantovoi Teorii* (Moscow: Nauka, 1975)
223. Kagan M Yu, Val'kov V V *JETP* **113** 156 (2011); *Zh. Eksp. Teor. Fiz.* **140** 179 (2011)
224. Kagan M Y, Val'kov V V *J. Supercond. Nov. Magn.* **25** 1379 (2012)
225. Baranov M A, Chubukov A V, Kagan M Yu *Int. J. Mod. Phys. B* **06** 2471 (1992)
226. Baranov M A, Kagan M Y *JETP* **75** 165 (1992); *Zh. Eksp. Teor. Fiz.* **102** 313 (1992)
227. Liao Y et al. *Nature* **467** 567 (2010)
228. Shin Y et al. *Nature* **451** 689 (2008)
229. Cladé P et al. *Phys. Rev. Lett.* **102** 170401 (2009)
230. Inada Y et al. *Phys. Rev. Lett.* **101** 100401 (2008)
231. Fuchs J et al. *Phys. Rev. A* **77** 053616 (2008)
232. Gaebler J P et al. *Phys. Rev. Lett.* **98** 200403 (2007)
233. Littlewood P B, Varelogiannes G (Eds) *Proc. of the First EuroConf. on Anomalous Complex Superconductors, Crete, Greece, September 1998* (Amsterdam: North-Holland, 1999)
234. Hertz J A *Phys. Rev. B* **14** 1165 (1976)
235. Millis A J *Phys. Rev. B* **48** 7183 (1993)
236. Kagan M Yu, Ogarkov S L *Laser Phys.* **18** 509 (2008)
237. Read N, Green D *Phys. Rev. B* **61** 10267 (2000)
238. Iskin M, Sá de Melo C A R *Phys. Rev. Lett.* **96** 040402 (2006)
239. Botelho S, Sá de Melo C A R *J. Low Temp. Phys.* **140** 409 (2005)
240. Volovik G E, Solov'ev A, Yakovenko V M *JETP Lett.* **49** 65 (1989); *Pis'ma Zh. Eksp. Teor. Fiz.* **49** 55 (1989)
241. Majorana E *Nuovo Cimento* **14** 171 (1937)
242. Volovik G E *JETP Lett.* **90** 398 (2009); *Pis'ma Zh. Eksp. Teor. Fiz.* **90** 440 (2009)
243. Bogoliubov N N *JETP* **7** 41 (1958); *Zh. Eksp. Teor. Fiz.* **34** 58 (1958)
244. Tolmachev V V, Tiablikov S V *Sov. Phys. JETP* **7** 46 (1958); *Zh. Eksp. Teor. Fiz.* **34** 66 (1958)
245. Bogoliubov N N *Sov. Phys. JETP* **7** 51 (1958); *Zh. Eksp. Teor. Fiz.* **34** 73 (1958)
246. Anderson P W *Phys. Rev.* **112** 1900 (1958)
247. Minguzzi A, Ferrari G, Castin Y *Eur. Phys. J. D* **17** 49 (2001)
248. Büchler H P, Zoller P, Zwerger W *Phys. Rev. Lett.* **93** 080401 (2004)
249. Pieri P, Pisani L, Strinati G C *Phys. Rev. B* **70** 094508 (2004)
250. Andrenacci N, Pieri P, Strinati G C *Phys. Rev. B* **68** 144507 (2003)
251. Kosztin I et al. *Phys. Rev. B* **61** 11662 (2000)
252. Abrikosov A A, Gorkov L P, Dzyaloshinski I E *Methods of Quantum Field Theory in Statistical Physics* (New York: Dover Publ., 1975); Translated from Russian: *Metody Kvantovoi Teorii Polya v Statitsticheskoi Fizike* (Moscow: Dobrosvet, 1998)
253. Pistolesi F, Strinati G C *Phys. Rev. B* **53** 15168 (1996)
254. Bartenstein M et al. *Phys. Rev. Lett.* **94** 103201 (2005)
255. Andrews M R et al. *Phys. Rev. Lett.* **79** 553 (1997)
256. Capuzzi P et al. *Phys. Rev. A* **73** 021603(R) (2006)
257. Astrakharchik G E, private correspondence (2006)
258. Heiselberg H *Phys. Rev. A* **73** 013607 (2006)
259. Guéry-Odelin D et al. *Phys. Rev. A* **60** 4851 (1999)
260. Baranov M A, Petrov D S *Phys. Rev. A* **62** 041601(R) (2000)
261. Vichi L *J. Low Temp. Phys.* **121** 177 (2000)
262. Pedri P, Guéry-Odelin D, Stringari S *Phys. Rev. A* **68** 043608 (2003)
263. Kim Y E, Zubarev A L *Phys. Lett. A* **327** 397 (2004)
264. Heiselberg H *Phys. Rev. Lett.* **93** 040402 (2004)
265. Kim Y E, Zubarev A L *Phys. Rev. A* **70** 033612 (2004)
266. Heiselberg H *New J. Phys.* **6** 137 (2004)
267. Hu H et al. *Phys. Rev. Lett.* **93** 190403 (2004)

268. Astrakharchik G E et al. *Phys. Rev. Lett.* **95** 030404 (2005)
269. Bruun G M, Smith H *Phys. Rev. A* **72** 043605 (2005)
270. Bruun G M, Smith H *Phys. Rev. A* **75** 043612 (2007)
271. Bartenstein M et al. *Phys. Rev. Lett.* **92** 203201 (2004)
272. Kinast J, Turlapov A, Thomas J E *Phys. Rev. Lett.* **94** 170404 (2005)
273. Altmeyer A et al. *Phys. Rev. Lett.* **98** 040401 (2007)
274. Kinast J M, PhD Thesis (Durham, NC: Duke Univ., 2006)
275. O'Hara K M et al. *Science* **298** 2179 (2002)
276. Thomas J E, Kinast J, Turlapov A *Phys. Rev. Lett.* **95** 120402 (2005)
277. Ku M J H et al. *Science* **335** 563 (2012)
278. Lee T D, Yang C N *Phys. Rev.* **105** 1119 (1957)
279. Lee T D, Huang K, Yang C N *Phys. Rev.* **106** 1135 (1957)
280. Bevan T D C et al. *Nature* **386** 689 (1997)
281. Dmitriev V V et al. *JETP Lett.* **86** 594 (2007); *Pis'ma Zh. Eksp. Teor. Fiz.* **86** 681 (2007)
282. Mermin N D, Muzikar P *Phys. Rev. B* **21** 980 (1980)
283. Stone M, Anduaga I *Ann. Physics* **323** 2 (2008)
284. Vakaryuk V, Leggett A J *Phys. Rev. Lett.* **103** 057003 (2009)
285. Volovik G E *JETP Lett.* **61** 958 (1995); *Pis'ma Zh. Eksp. Teor. Fiz.* **61** 935 (1995)
286. Volovik G E *JETP Lett.* **100** 742 (2015); *Pis'ma Zh. Eksp. Teor. Fiz.* **100** 843 (2015)
287. Tada Y, Nie W, Oshikawa M *Phys. Rev. Lett.* **114** 195301 (2015)
288. Shitade A, Nagai Y *Phys. Rev. B* **93** 174517 (2016)
289. Sauls J A *Phys. Rev. B* **84** 214509 (2011)
290. Combescot R, Dombre T *Phys. Rev. B* **33** 79 (1986)
291. Itzykson C, Zuber J-B *Quantum Field Theory* (New York: McGraw-Hill, 1980); Translated into Russian: *Kvantovaya Teoriya Polya* Vol. 2 (Novokuznetsk: Novokuznetsk. Fiz.-Mat. Inst., 2000)
292. Akulov V P, Volkov D V *JETP Lett.* **17** 261 (1973); *Pis'ma Zh. Eksp. Teor. Fiz.* **17** 367 (1973)
293. Cross M C *J. Low Temp. Phys.* **26** 165 (1977)
294. Kopnin N B, Soininen P I, Salomaa M M *Phys. Rev. B* **45** 5491 (1992)
295. Kopnin N B, Volovik G E, Parts Ü *Europhys. Lett.* **32** 651 (1995)
296. Haldane F D M *Phys. Rev. Lett.* **93** 206602 (2004)
297. Baym G *Phys. Rev. A* **69** 043618 (2004)
298. Fetter A L *Rev. Mod. Phys.* **81** 647 (2009)
299. Matveenko S I, Shlyapnikov G V *Phys. Rev. A* **83** 033604 (2011)
300. Cooper N R *Adv. Phys.* **57** 539 (2008)
301. Aftalion A, Blanc X, Dalibard J *Phys. Rev. A* **71** 023611 (2005)
302. Volovik G E *Exotic Properties of Superfluid He-3* (Singapore: World Scientific, 1992)
303. Simonucci S, Pieri P, Strinati G C *Nature Phys.* **11** 941 (2015)
304. Mizushima T, Machida K *Phys. Rev. A* **81** 053605 (2010)
305. Thouless D J, Ao P, Niu Q *Phys. Rev. Lett.* **76** 3758 (1996)
306. Brusov P N, Brusov P P *Collective Excitations in Unconventional Superconductors and Superfluids* (New Jersey: World Scientific, 2010)
307. Chubukov A V *Phys. Rev. B* **52** R3840 (1995)
308. Son D T, Spivak B Z *Phys. Rev. B* **88** 104412 (2013)
309. Spivak B Z, Andreev A V *Phys. Rev. B* **93** 085107 (2016)
310. Andreev A V, Spivak B Z *Phys. Rev. Lett.* **120** 026601 (2018)
311. Kim H-J et al. *Phys. Rev. Lett.* **111** 246603 (2013)
312. Shen S-Q, Li C-A, Niu Q *2D Mater.* **4** 035014 (2017)
313. Kuntsevich A Yu et al. *New J. Phys.* **20** 103022 (2018)
314. Abrikosov A A *Sov. Phys. JETP* **5** 1174 (1957); *Zh. Eksp. Teor. Fiz.* **32** 1442 (1957)
315. Iordanskii S V *Sov. Phys. JETP* **22** 160 (1966); *Zh. Eksp. Teor. Fiz.* **49** 225 (1966)
316. Hall H E *Adv. Phys.* **9** (33) 89 (1960)
317. Hall H E, Vinen W F *Proc. R. Soc. A* **238** 215 (1956)
318. Cooper N R, Wilkin N K, Gunn J M F *Phys. Rev. Lett.* **87** 120405 (2001)
319. Cooper N R, Komineas S, Read N *Phys. Rev. A* **70** 033604 (2004)
320. Gifford S A, Baym G *Phys. Rev. A* **70** 033602 (2004)
321. Kittel Ch *Quantum Theory of Solids* (New York: Wiley, 1963); Translated into Russian: *Kvantovaya Teoriya Tverdykh Tel* (Moscow: Nauka, 1967)
322. Packard R E *Physica B + C* **109 – 110** 1474 (1982)
323. Yarmchuk E J, Gordon M J V, Packard R E *Phys. Rev. Lett.* **43** 214 (1979)
324. Yarmchuk E J, Packard R E *J. Low Temp. Phys.* **46** 479 (1982)
325. Bretin V et al. *Phys. Rev. Lett.* **92** 050403 (2004)
326. Madison K W et al. *Phys. Rev. Lett.* **84** 806 (2000)
327. Chevy F, Madison K W, Dalibard J *Phys. Rev. Lett.* **85** 2223 (2000)
328. Madison K W et al. *Phys. Rev. Lett.* **86** 4443 (2001)
329. Abo-Shaeer J R et al. *Science* **292** 476 (2001)
330. Zwierlein M W et al. *Nature* **435** 1047 (2005)
331. Kovtun P K, Son D T, Starinets A O *Phys. Rev. Lett.* **94** 111601 (2005)
332. Turlapov A et al. *J. Low Temp. Phys.* **150** 567 (2008)
333. Ravenhall D G, Pethick C J, Wilson J R *Phys. Rev. Lett.* **50** 2066 (1983)
334. Maruyama T et al. *Phys. Rev. C* **72** 015802 (2005)
335. Maruyama T et al. *Phys. Rev. C* **73** 035802 (2006)
336. Pons J A, Viganò D, Rea N *Nature Phys.* **9** 431 (2013)
337. Kerbikov B *Surv. High Energy Phys.* **20** 47 (2006)
338. Hwang E H, Das Sarma S *Phys. Rev. B* **75** 205418 (2007)
339. Laughlin R B *Rev. Mod. Phys.* **71** 863 (1999)
340. Rezayi E H, Haldane F D M *Phys. Rev. B* **50** 17199 (1994)
341. Lifshitz E M, Pitaevskii L P *Physical Kinetics* (Oxford: Pergamon Press, 1981); Translated from Russian: *Fizicheskaya Kinetika* 2nd ed. (Moscow: Fizmatlit, 2001)
342. Bandurin D A et al. *Science* **351** 1055 (2016)
343. Kagan M Yu, Mitskan V A, Korovushkin M M *JETP* **119** 1140 (2014); *Zh. Eksp. Teor. Fiz.* **146** 1301 (2014)
344. Lozovik Yu E, Merkulova S P, Sokolik A A *Phys. Usp.* **51** 727 (2008); *Usp. Fiz. Nauk* **178** 757 (2008)